Doctoral School in Environmental Engineering

Modelling fine sediment transport over an immobile gravel bed

Corrado Pellachini

UNIVERSITÀ DEGLI STUDI DI TRENTO
Dipartimento di Ingegneria Civile e Ambientale

2011

Doctoral thesis in Environmental Engineering, XXII cycle

Faculty of Engineering, University of Trento

Academic year: 2010 - 2011

Supervisors: Zolezzi,Guido and Righetti,Maurizio

Part of the present research has been funded by the Fondazione Cassa di Risparmio di Trento e Rovereto under the call 2009 for young researchers/doctoral candidates.

FONDAZIONE
CASSA DI RISPARMIO
DI TRENTO E ROVERETO

Cover photograph: Castelvecchio bridge over Adige river, Verona-Italy

Università degli Studi di Trento

Trento, Italy

April 2011

There are idiots who define my work as abstract; yet what they call abstract is what is most realistic. What is real is not the appearance, but the idea, the essence of things.

Constantin Brâncuşi

Acknowledgements

Ho deciso di scrivere i ringraziamenti per questo lavoro di tesi nella lingua italiana, perché per me rappresenta la lingua del cuore e poiché questi ringraziamenti vogliono essere una certificazione di profonda gratitudine per quelle persone che mi hanno seguito in questo periodo della mia vita "dottorale", be' allora, ecco che il cuore fa spazio a qualunque altra regola istituzionale che avrebbe, forse, preteso che li scrivessi in inglese. Ma io pretendo il cuore nelle cose, e così voglio che il cuore ne sia protagonista. Dunque, per cominciare, e come è mia abitudine fare nelle cose, vorrei chiarire il motivo di questi miei ringraziamenti, insomma, inizio con una questione filosofica:

- la gratitudine implica una relazione per mezzo della quale alcuni hanno vissuto con me quelle faccende della vita che più mi hanno fatto tribolare, ma anche quelle più felici, e di tutto questo compartecipare, io voglio essere grato. Non sto scrivendo di quell'essere grato che in qualche misura lo si deve perché l'altro ricopre un ruolo sistemico-istituzionale suo malgrado, per cui il ruolo di ciascuno prescinde dalla specifica umanità, sto scrivendo di quella gratitudine che si ha quando l'altro da noi si percepisce aperto all'accoglienza, perché di animo buono nel pensiero e gentile nei modi; intendo scrivere, dunque, di quelle persone che sono anche miei amici e avventurieri con me nella vita. Accade, infatti, che mentre i ruoli potrebbero valere per sé, le relazioni valgono in loro, e io voglio, appunto, scrivere di queste relazioni, in primis, che mi hanno, poi, fatto scoprire di quanto l'altro sia per me importante.

- Ho sempre creduto che la mia vita non dovesse essere all'insegna della filosofia dello "scompartimento stagno", ovvero se faccio una cosa, questa stessa cosa non debba influire su altre cose della mia vita. Insomma, questi ringraziamenti varranno anche per quelle persone che a tutta prima non hanno a che fare con il lavoro di dottorato, ma che ugualmente mi hanno riempito il cuore, oppure mi hanno regalato un po' di stima per quello che sono.

- Credo che dare una pubblicità ai ringraziamenti in una forma così formale come quello della tesi, voglia significare assumersi la responsabilità di ammettere che l'altro è e sarà per me quanto lui è stato durante questo mio periodo di vita che è coinciso con il lavoro di dottorato.

Prima di iniziare il mio racconto, vorrei fare un'ultimissima premessa: l'ordine delle persone non sarà dettato da una questione di gerarchia affettiva, perché l'essere grato non ammette classifiche di alcuna sorta. L'ordine con cui appariranno sulla scena le persone, sarà, a volte, dettato da una questione stilistica di scrittura, altre volte perché, rispetto a

quella persona, sono in quel preciso momento in cui scrivo, più ispirato a capire il motivo della mia gratitudine.

Ringrazio Marco Ranzato, perché con me è stato il più delle volte buono e poco cattivo anche se adesso è sulla via della santità. Voglio ringraziarlo perché è stato un ottimo compagno di vita in questo mio periodo di ricerca dottorale soprattutto per quanto riguarda le molte discussioni che ci hanno visto protagonisti entrambi e che, credo, ci abbiano aiutato a chiarirci chi siamo rispetto a chi o a che cosa. Lo ringrazio perché ha avuto sempre il tempo e la volontà di sostenermi nei momenti per me più difficili, ma soprattutto perché ho sempre percepito la sua stima in quello che sono e che faccio. Insomma, da lui, ho sempre percepito una gran fede in me, al di là di un possibile dubbio!
Ringrazio Stefano Reolon, perché è presente in me e lo è sempre stato con tutta la sua sensibilità e acutezza di indagine. Lo ringrazio perché con lui e in lui ho sempre visto l'esempio di una persona tenace nel pensiero anche se delle volte oppressa da tante tribolazioni di vita. Ma in lui ho sempre apprezzato questa sua continua ricerca, fatta di costruire quel senso di vita che in qualche modo dovrebbe appartenere a tutti gli uomini di buona volontà. Io e lui siamo uomini di buona volontà, e io assieme a lui, ancora di più!
Ringrazio Federica Maino, perché anche questa volta è presente in questo mio momento importante di vita. Anche questa volta, infatti, Federica è una presenza che fino ad oggi si è rivelata una costante, una costante in senso fisico, ma più ancora per quanto riguarda quel sorriso dolce, attento e delle volte consolante di cui ho avuto bisogno.
Ringrazio Veronica Perozeni, la "numero uno", donna e mamma infaticabile. Donna tenace, da cui imparare come ci si risolleva sempre dai momenti più oscuri della vita, e mamma infaticabile e pronta a sostenere le sue amate figlie perché l'amore che porta verso di loro è quello stesso amore che ha saputo darsi in quanto persona degna di essere amata. La ringrazio perché in lei ho avuto sempre incoraggiamenti per quello che sono, mi ha sempre detto: " Ce la faremo, Corrado!". Be', Veroz, forse ce l'abbiamo fatta!
Ringrazio Anna Duce, perché mi ha sempre permesso di essere quello che sono anche nei momenti più bui della mia vita. E' riuscita con me a starmi vicino, assieme a me in quel pensiero che delle volte non ci permette di vedere alcun orizzonte di senso futuro. E' stata lì, complice anche una sua saggezza di pensiero maturata da una esperienza di vita che ha saputo anche trasmettermi in maniera opportuna.
Ringrazio Simonella Ruboli, in quanto "false friend" perché i suoi problemi sono diventati anche i miei, mio malgrado. Ma così è, è un modo come molti altri perché lei ti faccia capire che in te ha trovato qualcuno di fiducioso. Perciò, cara Simonella, grazie della condivisione, ma soprattutto della fiducia sottesa, sempre e comunque.
Ringrazio Mauricio Zambrano Bigiarini, perché è una persona che mi piace molto nella sua

attenzione spirituale dell'altro e, in particolare, nell'attenzione che ha avuto verso di me. Poche persone come lui sono così attente a piccole sfumature comportamentali ma gratificanti per l'altro, poche persone come lui hanno pensieri così valorosi da essere sostenuti con forza, ma comunque disponibile al compromesso se questo compromesso può salvaguardare un rapporto fatto di persone che si vogliono bene. L'ho sempre percepito come un fratello maggiore, sarà perché nelle discussioni che abbiamo avuto ha fatto sempre prevalere in me l'aspetto più razionale che, alle volte, coincide con l'aspetto più accomodante. E siccome a lui piace giocare con la probabilità, anche la più piccola, con me ha sempre puntato sull'aspetto più forte ma meno probabile!
Ringrazio Alfonso Vitti che è stato persona inseparabile di battaglie personali, vissute tra me e lui ma anche tra me e il mondo. Per queste utlime lui ha rappresentato un'ottima compagnia con cui condividere timori e riserve sul mio conto che delle volte mi facevano arretrare rispetto a una più profonda verità di cui lui era sempre testimone e pronto a ricordarmela.
Ringrazio Guido Zolezzi, perchè è una persona con cui ho condiviso il peggio ma anche il meglio di me. Una persona con cui ho condiviso quattro anni di vita lavorativa intensa, sia sotto il profilo scientifico, che di quello propiamente emotivo. Lo ringrazio per la fiducia che mi ha dato e la stima che ha saputo darmi.

Finiti i ringraziamenti, vorrei adesso iniziare la dedica di questa tesi. Dedica che, questa sì, è gerarchicamente sopra il resto, non perché si abbia il gusto nella vita di dare sempre delle liste in cui una cosa compare prima o dopo dell'altra, ma per dare alle cose un giusto valore. Ecco, se esiste un valore più nobile di tutti gli altri, allora vuol dire che tale valore comprende in piccola misura anche le cose che gli stanno sotto, ma sotto perché complementari ad esso. Se, dunque, non ci fosse l'amore nella vita, forse questa tesi non sarebbe stata, o meglio, non sarebbe stata così come è adesso. Perché l'amore tra due persone qualifica la vita, essendo l'amore un'unione di due persone: un te che è me e viceversa.
Dedico la tesi alla mia mamma Anna, al mio papà Roberto, alla mia sorella Margherita e ai miei due nipoti Enrico e Pietro.

Abstract

Fine-grained sediments represent a significant component of the total transport load in most fluvial systems around the world, not only including alluvial sand-bed rivers. A variety of natural or human actions, such as fire, logging, flow diversion, road construction, urban or agricultural development can increase the supply of sand to gravel- and cobble-bedded rivers. In rivers with regulated flow regime the coarsest part of the sediments mixture cannot be transported for most of the time, with only the fine fraction being frequently transported, often under conditions of supply-limitation.

The transport of fine sediments is a key and yet relatively unexplored process of many coarse-bed river systems with strong management and ecological relevance. It often affects ecosystem richness and riverine connectivity in the vertical and transverse directions. Sand accumulation over gravel beds can degrade the natural habitat of benthic organisms and therefore their ecological functions, as well as limit oxygen availability to spawning sites for several fish species through excessive pool filling. Moreover flushing flows are often prescribed downstream of dams with multiple objectives, and constitute one component of instream flow requirements for maintenance of aquatic and riparian habitat or for the maintenance of recreation functions. The ability to predict the temporal dynamics of sand surface under different flow scenarios is crucial to properly plan these operations in order for the desired management objectives to be achieved. Increased sand inputs over armored gravel-bed surfaces are also expected in the medium term following dam removals. Hydraulic computations for water level prediction requires quantification of the sand bedforms geometry that contribute to flow roughness thus affecting channel depth.

The present study addresses the dynamics of fine sediment transport in gravel-bed rivers, for which the modelling framework is still far from being complete. The general aim of the present work is to propose a morphodynamic modelling approach for the transport of the coarse fraction of fine sediments (sand) over a gravel bed that is assumed at rest. More specifically, the following research questions are addressed:

- Which are the key physical processes associated with near bed turbulence properties over rough beds, and how do they change when sand is present in variable proportion within the gravel bed? (Chapter 2)
- Which can be an appropriate form of a mathematical model for sand beform dynamics over immobile gravel? How do the continuity and momentum equations, as well as the closure relationships for friction and bedload transport change when the gravel bed is partially sand-covered? (Chapter 3)
- Which are the implications of such model when solved in the form of a stability

analysis that aims to predict the conditions for sand bedform stability and preferred wavelength selection over an immobile gravel bed? (Chapter 4)

A mathematical modelling approach is first developed to study the spatially-averaged morphodynamic evolution of a sand bed surface over an immobile gravel bed. The hydrodynamic and sediment transport properties of this mixed configuration differ from those of "homogeneous" bed configurations classically found in fluid mechanics. Here the hydrodynamic forces are directly determined by the interaction between the flow and a rough surface that is largely composed by the same sediment that can be transported.
The present modelling approach is based on (i) a two-fraction assumption for the bed composition (sand and gravel) and (ii) a spatially-averaged description of bed roughness geometry, near bed turbulence properties and closure relationships for bedload and suspended load.
The reach-averaged sand surface elevation and the relative size ratio between the sand and gravel diameter emerge as the key parameters that can be used to distinguish between different types of mixed bed configurations. A key distinction can be made between "gravel-clast framework" and "sand matrix" types of bed; these configurations are discriminated by a relatively sharp transition region in the sand surface elevation.
The analysis builds on a synthesis of a variety of empirical and theoretical work on rough-bed open channel flows and of experimental observations on the transport of fine sediments over gravel beds. A theoretical framework is presented to describe the typical vertical and horizontal scales of the mixed bed that can be relevant for spatial averaging. This allows to propose novel physically-based mathematical relations that link the variation of relevant flow and sediment transport properties with the sand surface elevation and the grain size ratio. Depending on these two parameters, the near-bed shear stress and bedload transport of sand depend on a varying dynamic balance between a "hiding" and a "bridge" effect, that are physically discussed and mathematically quantified.
The proposed relationships serve as closure formulaes to link the computation of the near-bed shear stress and of the sand bedload rates with the spatially-averaged flow field within a 2D (x, z) morphodynamic model that includes:

- the momentum conservation equations for the fluid phase in the x and z directions;
- the mass conservation equations for the fluid phase;
- a novel formulation of the mass conservation equations for the sand layer within an immobile gravel bed;

The flow model is formulated referring to physical balances formally valid only within the central flow layer, and indirectly accounting for the role of physical processes governing the hydrodynamics within near-bed (roughness) layer in the proposed closure relationships. Application to spatially-averaged uniform flow conditions shows satisfactory agreement with the few available experimental data and allows to make a preliminary quantifcation of the effect of the two key parameters describing different types of mixed bed configuration. The limits of validity of the model are also discussed.
The morphodynamic model is finally used to predict the sand bed morphodynamics under supply-limited conditions. The sand surface elevation is a measure of the sediment supply-limitation that crucially controls the sand bedform development. A limited volume of bedload sediment leads either to smaller dimensions, the sediment starved bedform or fewer isolated bedforms. The model is solved through a linear stability analysis that incorporates recent developments in the theoretical study of sand dune stability in homogeneous conditions. The theoretical outcomes allow to focus on the physical phenomena controlling the development of sand bedforms when sand is transported over an immobile gravel bed and to determine the hydraulic conditions under which sand dunes formation can be expected to develop within immobile gravel beds. Results also indicate a consistent effect of supply limitation to extend the instability region towards shorter bedforms, as observed by recent experimental investigations.

Contents

List of Figures

List of Tables

1 Introduction

1.1 Relevance of the problem

Fine sediment transport in gravel bed rivers is gaining increasing scientific and management interest because it is an important component in a wide range of geomorphic, engineering, and resource management applications. Fine sediment transport and/or storage in acquatic systems is environmentally significant, because fine sediment is both a vector for the transport of contaminants and in its own right a pollutant, particularly in the context of habitat quality (*Jobson and Carey* (1989)). This issue is not restricted to sandy alluvial rivers, where the bed and transported sediment belong to similar (fine) fraction; an increasing concern relates to gravel bed rivers.
Namely, in many gravel and cobble bed rivers, much of the sediment load may consist of sand or finer material that is transported primarily in suspension determining a proper morphology by depositing on bed and banks (*Grams* (2006)).
In regulated gravel-bed rivers subjected to a reduction of frequency and duration of channel-forming discharges, flow is competent to mobilize only the fine fraction for prolonged periods of time (*Schälchli* (1992)). Such alteration of sediment regime might result in progressive clogging of the gravel bed interstices (*Schälchli* (1992)) with consequent decrease of the hydraulic connectivity between the surface and the hyporeic flow, thus bearing severe effects for a variety of biogeochemical processes which ultimately affect the stream ecological integrity (*Weigelhofer and Waringer* (2003)). A huge body of research has long been indicating how infiltration of fine sediments in the interstices of gravel river beds can degrade the spawning habitat for fish species that lay the eggs on or within the gravel bed (*Koski* (1966); *Petticrew et al.* (2007)), while an excess of sand onto the gravel bed can cause excessive pool filling thus reducing the available fish habitats during the warm season (*Lisle and Hilton* (1991)).
For rivers that are managed for hydroelectric power generation for example, controlled flushing flow release are commonly required in order to restore or to improve habitat conditions for fish and macroinvertebrates (*Hesse and Sheets* (1993)). *Kondolf and Wilcock*

(1996) restate various ecological and management objectives in terms of physical changes for which flushing flow may be defined and which may be broadly divided into sediment maintenance and channel maintenance flow, depending on whether the flushing flows are designed to modify or maintain the channel sediment or the channel geometry. In some cases these objectives can be shown to conflict. Nevertheless, sustainable management of the fine sediment fraction in gravel beds rivers requires a better knowledge of the related physical processes that are still rather poorly understood.
The transport of fine sediments in gravel bed rivers is a complex phenomenon that results from reciprocal interaction between several physical processes. Existing model for fine sediment transport were developed for condition in which the bed is uniformly composed by the same material that is transported, i.e. the "homogeneous" case. The transport dynamics of fine particles over a gravel bed that is only partially covered by fine sediment are poorly understood and no modeling framework addresses this situation explicitly.

1.2 Overview of known physical processes

According to Wentworth classification (*Wentworth*, 1922) gravel size ranges from 2 mm to 16 mm, whereas sand size varies from 63 μm to 2 mm depending if sand is very fine or very coarse, respectively.

But what is known about this peculiar problem from physical point view? Both field and laboratory experiments have been performed during the past three decades, concerning the mechanisms of deposition/erosion and infiltration of fines in gravel matrices (see the introductory review of *Diplas and Parker* (1992)). In his pioneering laboratory experiments, *Einstein* (1968) studied the intrusion of silica flour (3.5-30 μm) into a gravel matrix. He pointed out that fines settled into the gravel, reaching the bottom of the flume and gradually filled the pores from the bottom upwards. The available studies on fine-grained sediments transported by free surface flows over a immobile gravel bed highlight the importance of the four main key research issues.

1. The bed surface composition depends on the proportion of sand in the gravel matrix. *Wilcock and Kenworthy* (2002) demonstrated that the bed load transport rate for both sand and gravel strongly depends on sand content, particularly with the transition from clast- to a matrix-supported bed and with the associate shift in entrainment mechanisms for the bed load transport rate for each fraction. Moreover, *Grams and Wilcock* (2007) proposed a new functional relation for prediction of the entrainment of the suspended fine sediments over immobile coarse bed, depending on the relative sand elevation in the gravel matrix.

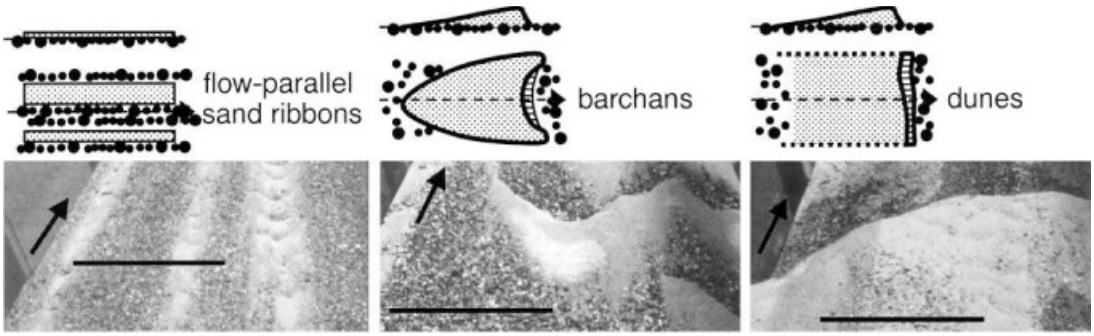

Figure 1.1: Bedform types observed in Kleinhans's experiments (*Kleinhans et al.*, 2002).Arrow indicate flow direction and scale bar are 0.5m.

2. The stability of the sand bed forms in gravel matrix is related to the degree of sediment supply limitation. *Kleinhans et al.* (2002) proposed a stability diagram for sand ribbons (stripes) and barchans dunes that occur in partially mobile conditions for mixed sand-gravel sediments when bed load transport is dominant and limited (see Figure 1.1 for key of bedform type). *Grams* (2006) proposed an analogous stability diagram for the case of dominant suspended transport.

3. The characteristics of near-bed turbulence in fully rough gravel bed actually control the near-bed transport dynamics of the fines. *Nikora et al.* (2001) have proposed the suitability of a double-averaged (in temporal and spatial domain) momentum equation for studying the hydraulics of irregular rough bed. *Mignot et al.* (2008), using the same double-averaging approach, found that flow heterogeneity induced by gravel bed topography play a dominant role in the mean hydrodynamics quantities such as velocity profile, turbulent shear, turbulent intensities, turbulent kinetic energy.

4. The process of sand infiltration takes place into the gravel matrix and might be coupled with surface processes. *Cui et al.* (2008) developed a theoretical model to describe the process of fine sediment infiltration into immobile coarse bed, which has been quantified experimentally by *Wooster et al.* (2008).

In order to focus the goal of the present research project, it is useful to review in more detail the present state of knowledge about these processes and their interactions.

1.2.1 Bed surface composition

The experiments of *Diplas and Parker* (1992) described the relationship between sand infiltration and the formation of a sand surface layer, which could give rise to bedforms

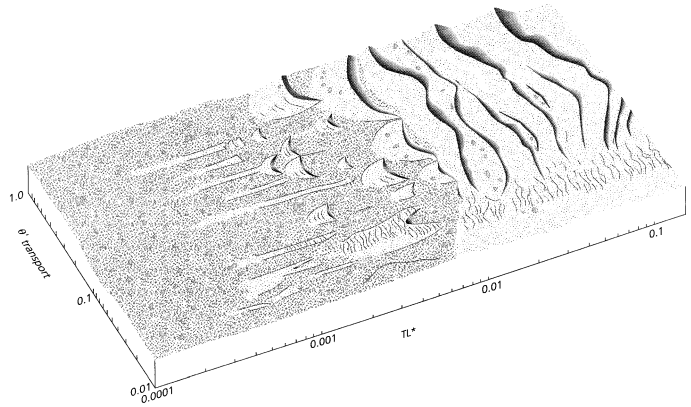

Figure 1.2: Conceptual explanatory model for the occurrence of bedforms in sediment supply-limitation. TL^* and θ' respectively represent the thickness of the transport layer divided by water depth and Shields stress related to the grains of transported sediment (from *Kleinhans et al.* (2002)).

in some cases. Flow-parallel transverse ribbons and flow transverse barchans have been observed in sand-gravel rivers and have been reproduced in flume experiments when the dominant mode of sand transport was bedload ((*Kleinhans et al.*, 2002)) or suspended load (*Grams* (2006)).
Kleinhans et al. (2002) found that sediment-supply limitation, i.e.a limitation of available transportable sediments, plays a key role in controlling the morphology of the bed forms; namely sand ribbons may occur both in the ripples and in the dunes regime and are strongly sediment-supply limited in the dune regime. When sediment availability increases, barchans emerge, and then grow together into barchanoid dunes up to fully delevoped dunes. Figure 1.2 ((*Kleinhans et al.*, 2002)) shows the bedform morphology with respect to the thickness of the transport layer scaled by water depth (i.e. TL^*) that is a measure of the volume of sediment in each bedform and the Shields stress of the transported grain sediment. The barchans have been plotted to the left of the dunes,the sand ribbons are even farther to the left, and the upper bound for TL^* is given by the maximum (equilibrium) height that a dune can attain in rivers, which is about 20% of water depth.

Similarly, the bed configuaration observed by *Grams* (2006) indicates a consistent progression from sand stripes to isolated barchans to full dunes.

The volume of mobile fine sediment, represented by the average thickness of the mobile sediment layer, and the near-bed hydraulic regime, quantified by grain stress and mobile sediment grain size, are the key factors that can distinguish among configurations with partial sand cover which determine different bedform types (see Figure 1.3).

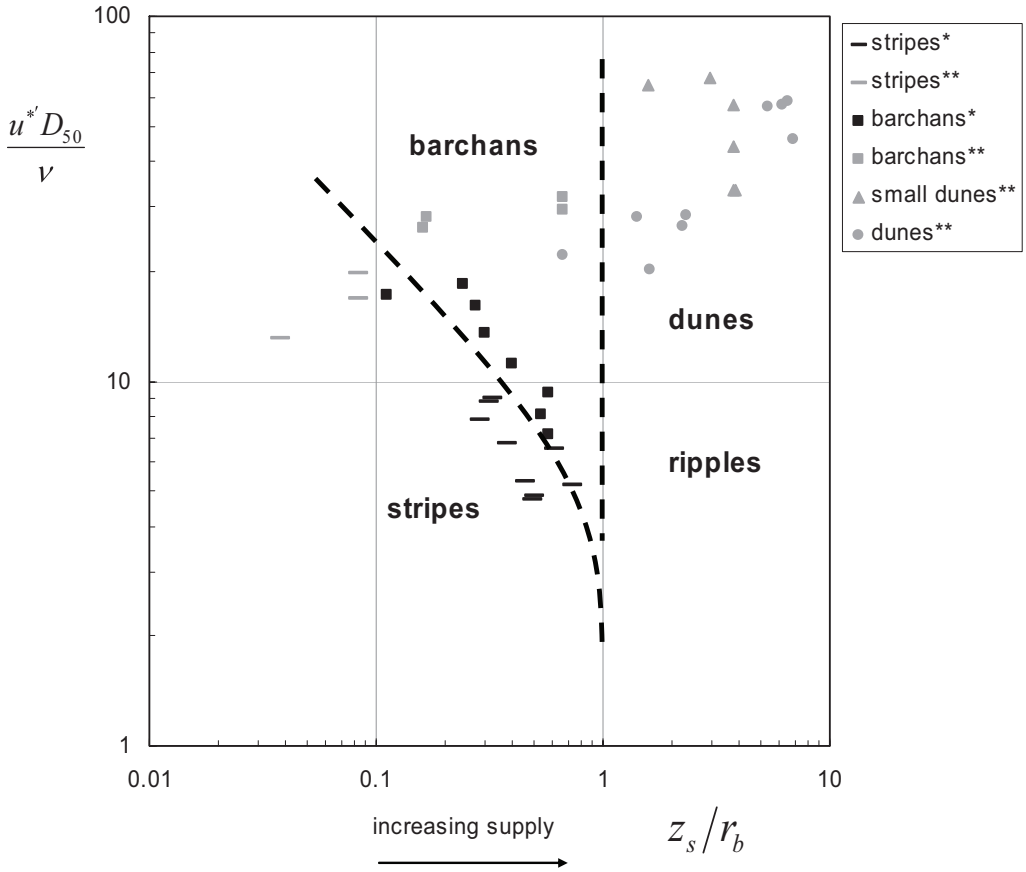

Figure 1.3: Bed-state stability diagram by proposed *Grams* (2006). Symbol marked with (*) in the legend indicate data collected by *Grams* (2006). Symbol marked with(**) are flume and field data collected and reported by *Kleinhans et al.* (2002). r_b denotes the bed roughness height.

1.2.2 Bedload and suspended load

Also the sand transport rate is affected by the relative proportion of sand within the gravel bed. The relative influence of the mechanisms controlling sand and gravel transport changes systematically with subsurface sand content f_s and the associate change of bed configuration from clast-supported to matrix-supported gravel bed. Clast-supported gravel beds consist of a framework of gravel clast where the sand tend to be well hidden among the gravel intersticies while in a matrix-supported gravel beds the proportion of gravel grains in direct contact is reduced and approaches zero as the content of sand f_s

exceeds 50% (*Wilcock* (1998); *Wilcock and Kenworthy* (2002)). *Wilcock and Kenworthy* (2002) developed a two-fraction model for sand and gravel bedload rate using a scaling parameter which is a proxy for the incipient motion of each fraction. This parameter is a "reference" Shields shear stress τ_{ri} where i stands for the gravel or for the sand fraction. Such "reference" τ_{ri} is defined as the value of τ_i at which the transport rate for each fraction is equal to a small reference value, tipically 0.002. Figure 1.4 shows the ratio of the reference shear stress for sand τ_{rs} and gravel τ_{rg} as a function of subsurface sand content f_s (*Wilcock and Kenworthy*, 2002). The trend shown in Figure 1.4 clearly indicates the non linear variation of τ_{ri} with f_s, particularly in the range $0.2 < f_s < 0.4$.

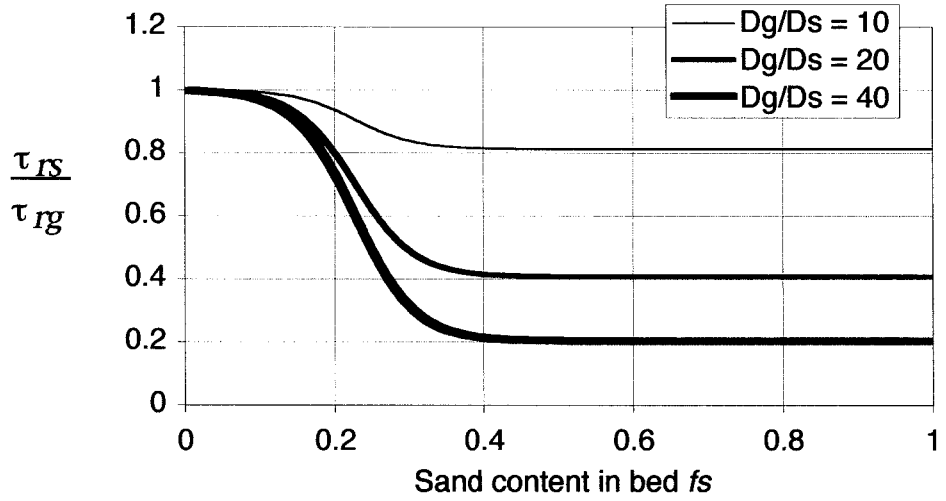

Figure 1.4: Ratio of the reference shear stress for sand τ_{rs} and gravel τ_{rg} as a function of subsurface sand content f_s, parameterised with ratio between the gravel (D_g) and sand (D_s) grain size (from *Wilcock and Kenworthy* (2002)).τ_{rs} and τ_{rg} are predicted using subsurface grain size.

As f_s tends to vanish the small amount of sand is largely hidden among the pores of gravel matrix and entrainment of sand requires entrainment of gravel. As f_s approaches unity, τ_{rg} decreases to a small value because the influence of surrounding grains on the motion of a gravel clast becomes small relative to the influence of the weight of the grains and to the drag force acting on it. For the sand, τ_{rs} at $f_s = 1$ is equal to the standard value for incipient motion of an homogenous bed (*Wilcock*, 1998). This has implication for the volumetric bed transport rate per unit of width for each size fraction i.
Considering the surface sand content F_s, the dimensionless reference Shields stress for the two fraction is reported in Fig.1.5 where the Shields stress for the sand fraction depends on the diameter ratio D_g/D_s between the gravel and sand component as well as on the

surface sand content.

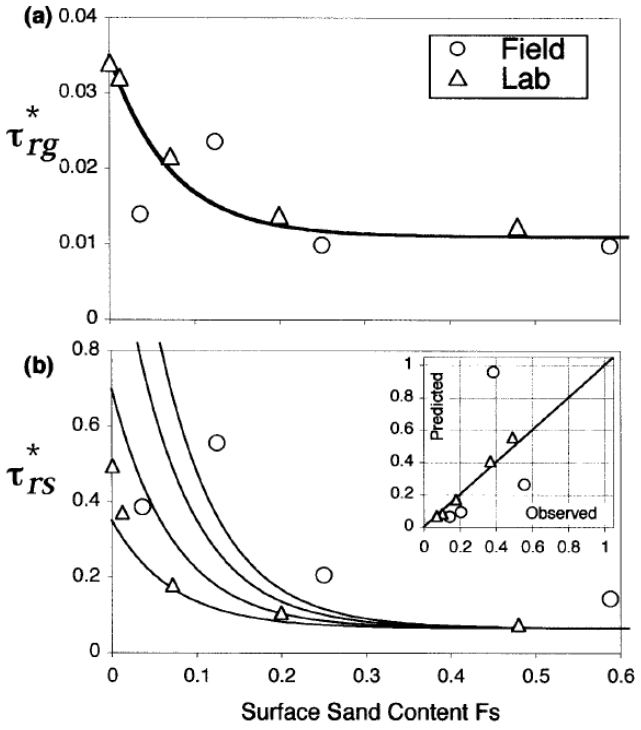

Figure 1.5: Dimensionless reference Shields stress τ^*_{ri} as a function of surface sand content F_s.The different curve are parameterized by different diameter ratio D_g/D_s=10,20,35 and 50 (*Wilcock and Kenworthy* (2002)

In the case of dominant suspended fine sediment transport over a coarse immobile bed, *Grams and Wilcock* (2007) suggest a new equilibrium entrainment formula for the fines. For the homogeneous case a general functional relation for sediment entrainment was presented by *Parker and Anderson* (1977) and expanded by *Garcia and Parker* (1991) so that the dimensionless sediment entrainment rate is a function of the hydrodynamic characteristics of the flow, i.e. the shear velocity near the bed, of the geometric characteristics of the flow, i.e. flow depth and of the geometric characteristics of the particles, i.e. the grain Reynolds number. For the case of sand transported in suspension over an

immobile coarse bed, *Grams and Wilcock* (2007) propose a relationship which accounts for the dependence on a new parameter of the entrainment rate of fines. Such parameter is somewhat analogous to the fraction of sand f_s, and more precisely is the ratio of sand cover thickness z_s to a characteristic roughness height of the coarse grains on the bed r_b. Specifically, *Grams and Wilcock* (2007) empirically derive a sand elevation correction function (SEC) that scales the entrainment rate for a bed partially covered by sand to the entrainment rate that would be predicted for the homogeneous case of sand -covered bed. This new sand elevation correction ε is a function of the ratio z_s to r_b and is represented in Figure 1.6 as a solid line that was chosen to fit the experimental observations.

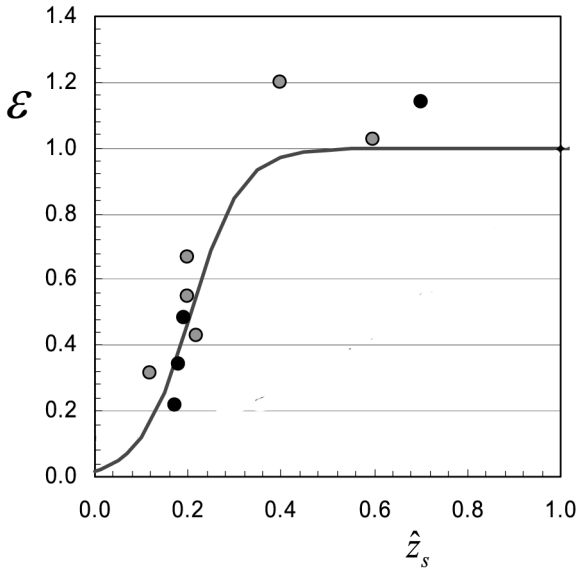

Figure 1.6: Sand elevation correction ε as a function of the ratio $\widehat{z_s}$ between z_s and r_b

1.2.3 Turbulence characteristics near gravel beds

Concerning the flow over fully rough bed, *Nikora et al.* (2001) proposed that the double-averaged (in time and in space domain) momentum equations should be used for studying the hydraulics over rough bed. The spatial averaging procedure permits to divide the flow domain into specific subregions depending on the possible new spatially averaged terms. These are different form-induced terms, which play a different role in the momentum equations for each subregion. Figure 1.7 sketches the key flow layers. Because of the

spatial averaging procedure, in the interfacial sublayer new turbulent stresses, form drag and viscous drag, appear in the momentum equations as a result of their dependence on roughness geometry and density of roughness elements, i.e., on the parameter $\mathcal{A}(z)$. This parameter is important if the roughness elements change their density with vertical coordinate, it disappears if they do not. The function $\mathcal{A}(z)$ is reported in the same Figure 1.7 and is called "roughness geometry function" at each elevation z. It represents the ratio of the horizontal area A_f occupied by the fluid to the total area A_0 of the region chosen for the spatial averaging procedure. In the form-induced and interfacial

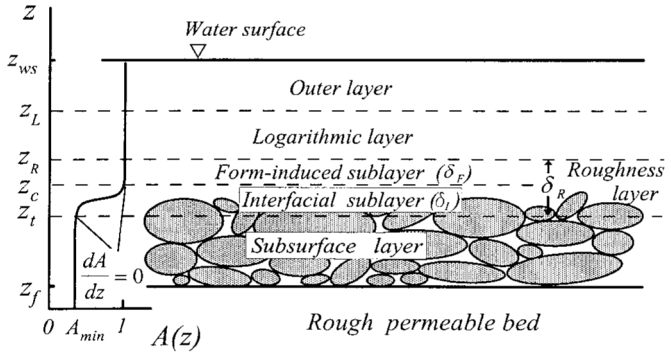

Figure 1.7: Flow subdivision into specific region for permeable bed (*Nikora et al.* (2001))

sublayer the flow is influenced by individual roughness element and the form-induced terms can play an important role in the momentum equations, specifically in the interfacial sublayer where the $\mathcal{A}(z)$ varies from 1 to a minimum value corresponding to the average porosity of the gravel matrix. These two sublayers can be identified together as roughness layer which indicate the entire layer dinamically influenced by length scale associated with roughness elements. Figure 1.8 shows examples of $\mathcal{A}(z)$ for water-worked (natural rivers) and unworked (manually created) gravel beds (*Nikora et al.* (2001)): the two curves behave similarly and are fairly close to a cumulative probability function for the normal distribution. *Nikora et al.* (2001) also show that in the specific case of regular spherical segment-type roughness, the double-averaged turbulence stresses and the form drag play a dominant role in the transfer of momentum in the near-bed region.

Bed load and suspended load are closely related with the shear stress pattern exerted by the flow on the bed. These stresses, in turn, are influenced by the rough bed elements of a gravel bed. In the roughness layer, which results from the interaction between the main flow and the bed roughness, two sublayers can be considered (*Nikora et al.* (2001)). In the form-induced sublayer (see Figure 1.7) a portion of the kinetic energy of the mean flow is

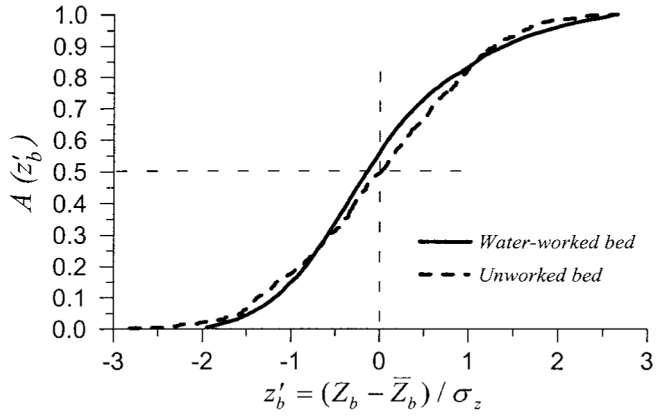

Figure 1.8: Roughness geometry function $\mathcal{A}(z)$ for water-worked and unworked gravel beds. Z_b is bed elevation,$\overline{Z_b}$ is average bed elevation and σ_z is standard deviation of bed elevations (from *Nikora et al.* (2001))

transformed into turbulent energy, intensifying the mixing or transfer of momentum and resulting in a continuous adjustment in the velocity profile. *Mignot et al.* (2008), applying the double averaging procedure to the turbulent kinetic energy equation, found that maximum turbulent kinetic energy production occurs at near-gravel crest levels z_c,when the bed is composed by macro-roughness elements. In the case of smooth and rough bed such peak energy production instead occurs much closer to the bed. Figure 1.9 shows that above the level $2z_c$ the production of turbulent kinetic energy P nearly balances the dissipation ε in the same manner as in the smooth boundary layer where the log-law occurs. In the form-induced layer the turbulent transport term T_t actively diffuses the turbulent kinetic energy flux F_k in both directions, particularly $F_k < 0$, $z < z_c$ in contrast with the smooth boundary layer where the turbulent energy fluxes are not directed towards the bed and where the production term P reaches its maximum value at reference level $z = 0$.

Because the sand content controls the transition of gravel bed configuration from "gravel-like" to "sand-like", the level above which the log-low occurs may depend on the sand elevation itself.

1.2.4 Sand infiltration into gravel beds

Fine-grained sediment can also infiltrate between the coarse immobile particles of the gravel bed. Laboratory flume studies generally agree on the importance of suspended sediments concentration in controlling infiltration rates (*Einstein* (1968); *Carling and Breakspear* (2006); *Carling* (1984); *Beschta and Jackson* (1979)), but they differ on the influence

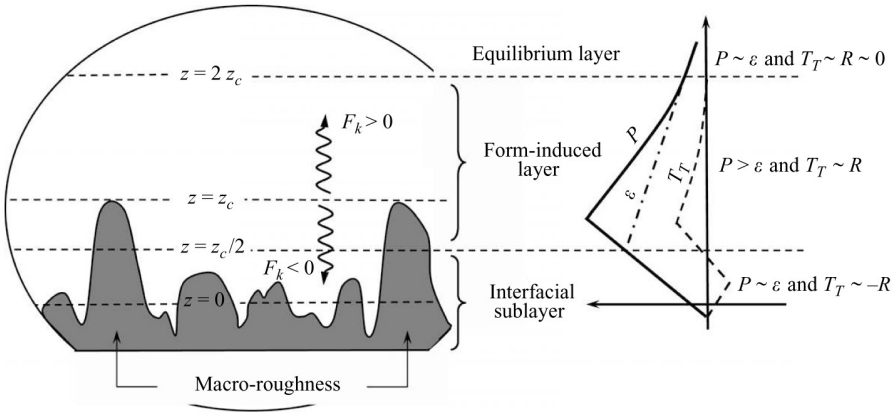

Figure 1.9: Schematic close-up of the bed/flow interface and turbulent kinetic energy (from *Mignot et al.* (2008))

of flow hydraulic parameters, such as velocity, shear stress and Froude number. Recently, *Wooster et al.* (2008) investigated the dynamics of fine sediment infiltration into immobile gravel deposit and particularly examined the effect of grain-size distribution of the coarse bed material and the infiltrating fine sediment, and the influence of feed rate and duration of fine sediment feed during the infiltration processes. Besides, *Cui et al.* (2008) contradicted the observations done by *Einstein* (1968) and developed a theoretical model able to describe the process of fine infiltration into a immobile coarse sediment deposits. *Cui et al.* (2008) used a constant fine sediment trapping coefficient, defined as a fraction of fine sediment load trapped in the coarse deposit for travelling unit distance. They demonstrated that the vertical profile of the fraction of fine sediment content decreases exponentially with depth into the deposit, starting from the bottom of the surface layer assumed to be twice the bed material geometric mean size.

1.3 Research goals and methodology

A summary of the above state-of-art review indicates the following considerations.

- Few morphodynamic modeling approaches have been proposed so far to predict the dynamics of sand bed evolution in gravel beds, taking into account the modifications of the turbulence properties due to varying sand surface levels;

- The basic ingredients of a suitable morphodynamic model for sand bedform dynamics over immobile gravel still need further investigation. A key gap is related to the closure relationship that should be used to evaluate the near-bed friction and turbu-

lence properties and the structure of the bedload and suspended load functions for the sand fraction. These closures are needed, and should be quite general, in order to complement the momentum and continuity equations for flow and sediments.

- Several experimental studies provide answers to some parts of the whole problem although no specifically designed experiment or modelling study on suitable model closures has been published so far.

- Although highly valuable, the main modelling approaches proposed so far cannot be used as morphodynamic models for sand transport over immobile gravel beds. either because of their restriction to sand being transported only in suspension with very simple flow models (Grams, 2006) or because they refer to spatial scales that are larger than the sand bedforms whose dynamics should be predicted by the model itself.

- the ratio between the sand bed elevation in the gravel beds and a characteristic spatial scale of roughness bed elements r_b is a crucial parameter which may control the stability of sand patterns, the entrainment of sand in the flow and the near-bed turbulence characteristics. Also the relative grain size ratio between the sand and the gravel fraction is likely to play a crucial role.

On the basis of these considerations, the general aim of the present work is to propose a morphodynamic approach for the transport of the coarse fraction of fine sediments (sand) over a gravel bed that is assumed at rest. More specifically, the research activity presented in the following chapters addresses the following research questions.

- Which are the key physical processes associated with near bed turbulence properties over rough beds, and how do they change when sand is present in variable proportion within the gravel bed? (Chapter 2)

- Which can be an appropriate form of a mathematical model for sand beform dynamics over immobile gravel? How do the continuity and momentum equations, as well as the closure relationships for friction and bedload transport change when the gravel bed is partially sand-covered? (Chapter 3)

- Which are the implications of such model when solved in the form of a stability analysis that aims to predict the conditions for sand bedform stability and preferred wavelength selection over an immobile gravel bed? (Chapter 4)

The research methodology used to address the above questions includes:

- a comprehensive and integrated analysis of already published work often with different specific goal compared to the present one. This has a strong potential for establishing the key steps needed to build a morphodynamic model for the sand bed surface over immobile gravel beds.
- A quantitative reinterpretation of published experimental data in the light of the proposed theoretical approach to model the key near-bed physical processes;
- The development of a linear stability analysis to solve the proposed morphodynamic model to predict the conditions of occurrence of sand bedforms over immobile gravel beds.

The relevance of the present work is mainly in offering a mechanistic tool that can be used to better understand which physical phenomena control the development of sand bedforms when sand is transported over an immobile gravel bed.
Indeed such a tool is based on developing a conceptual morphodynamic model accounting for the key processes of sand transport over a gravel matrix that uses the existing relationships for bed load transport and fines entrainment over gravel beds and accounts for near-bed conditions locally adapted to the evolving sand surface patterns relative to the turbulent near-bed characteristics and to the transport characteristics of fines.

2 Turbulence and sediment transport characterization for flow over immobile gravel beds: mixed case

In relationship with the overall goal of the present work illustrated in the Introduction, the analysis presented in this Chapter aims at developing a theoretical approach to the most relevant processes that determine the properties of near-bed turbulent flow and of sand transport when a rough gravel bed is partially covered with sand. This will eventually lead to propose physically-based closure relationships for friction and bedload transport at the end of the Chapter. These are key ingredients (but still largely to be improved with respect to the published literature) for a morphodynamic model of sand bedform evolution over immobile gravel beds.

The analysis presented in this Chapter is developed at three levels. After reviewing the spatial averaging approach, which underlies all the present work, the geometrical properties of a rough gravel bed are reviewed and the implications associated with the presence of a sand cover with variable height are discussed. Second, the near-bed hydrodynamic properties relevant for sediment transport over rough beds in general are reviewed and a novel theoretical approach is proposed to account for the effect of a variable sand cover on the near-bed shear stress and related spatially averaged turbulence properties. Third, the implications of varying sand surface level for threshold condition for sand bedload motion as well as for the rate of bedload transport are discussed and existing relationships derived on an empirical basis are integrated within the proposed theoretical approach.

Moving from flow to sediment transport, a fundamental hypothesis has been made in previous works to separate between "gravel" and "sand". The mobile sediment fraction often has a well distinct grain size curve with respect to that of the immobile gravel deposit (*Wilcock and Kenworthy* (2002)), which suggests the suitability of a two-fraction

approach ((*Wilcock and Kenworthy* (2002)) to predict the sediment transport dynamics and the temporal evolution of the mobile river bed. The bed and sediment load distribution can be conveniently represented through a bimodal distribution of one gravel and one sand fraction. Such apparent simplification of entire grains size distributions while retaining much of the practicality of a single grain size estimate.
The physical system is schematized as follows.We will refer to a "mixed" riverbed configuration when a certain amount of sand is present within the gravel particles. The correspondent hydrodynamic properties can be thought as those of a rough-bed open channel flow that progressively tend to reduce to those of a smoother bed flow when the sand content increases. Building a morphodynamic model to predict the evolving sand bed elevation in relation with the sand transport processes occurring over such "mixed" bed configuration therefore requires to specify how relevant hydrodynamic properties vary with the local sand surface elevation, and beforehand to quantify what "local" means, in relationship with the characteristic spatial scales of the bed with sand level-dependent roughness.This fundamental issue will be dealt with referring to the spatial-averaging approach (e.g. *Nikora et al.* (2001)) that constitutes a second basic assumption of the present work and allows to conceptually define the relevant spatial scales for the analysis and the dynamic balances holding at different scales and in different flow regions.
Such spatial scale are considered in the spatial averaging procedure(e.g. *Whitaker* (1999)), specifically referring to Double-Averaging Methodology(DAM) to investigate spatially heterogeneous rough bed flow (*Nikora et al.* (1998)). Within the DAM-approach, the Reynolds equations for flow field are area averaged over a specific spatial scale, depending on the characteristic of the gravel bed composition. Therefore, time averaged variables are decomposed into spatially averaged and spatial fluctuation parts according to $\widehat{\vartheta} = \langle\overline{\vartheta}\rangle + \widetilde{\vartheta}$, where the angle brackets denote spatial averaging, the overbar denotes temporal averaging, and the tilde denotes spatial fluctuation. In the same way the Eq.(2.4) becomes:

$$\begin{aligned} \widehat{\tau} &= \underbrace{\langle\overline{\tau_0}\rangle - \langle\overline{\tau'}\rangle - \langle\overline{\tau''}\rangle - \langle\overline{\tau'''}\rangle - ...\langle\overline{\tau^n}\rangle}_{} + \\ &= Spatial\,Average\,Component\,(SAC) \\ &+ \underbrace{\widetilde{\tau_0} - \widetilde{\tau'} - \widetilde{\tau''} - \widetilde{\tau'''} - ...\widetilde{\tau^n}}_{} \\ &= Spatial\,Average\,Fluctuation\,(SAF) \end{aligned} \tag{2.1}$$

Specifically, the operator $\langle . \rangle$ is defined as:

$$\langle \overline{\vartheta}(x,y,z,t) \rangle = \frac{1}{A_f} \int_{A_f} \int \overline{\vartheta}(x',y',z') dx' dy' \tag{2.2}$$

or

$$\langle \overline{\vartheta}(x,y,z,t) \rangle_s = \frac{1}{A_0} \int_{A_0} \int \overline{\vartheta}(x',y',z') dx' dy' \tag{2.3}$$

where (x, y, z) refers to three-dimensional Cartesian coordinates,A_f= area occupied by fluid within a fixed region on the $(x-y)$ plane, depending on the z-coordinate, and within the total area A_0. The eqs.(2.2,2.3) are known as *intrinsic spatial average* and *superficial spatial average*, respectively. They are related each other by a function named *roughness geometry function*(i.e.$\mathcal{A}$ (z)) (*Nikora et al.*, 1998) according to $\langle \overline{\vartheta} \rangle_s = \mathcal{A}(z) \langle \overline{\vartheta} \rangle$,with $0 \leq \mathcal{A}(z) \leq 1$ representing the ratio between the area occupied by fluid (i.e. A_f)in a fixed region with total area A_0.

It is worth of noticing that below roughness crests the averaging region is multiply connected, since it is intersected by roughness elements as a porous medium and the averaged operator in the eq.(2.2)is equivalent to the volume averaged operator when the averaging volume (i.e. V_0)is an extensive, infinitesimally thin horizontal slab (i.e. $V_0 = A_0 h_0, h_0 \mapsto 0$)(*Nikora et al.*, 1998).

Following *Whitaker* (1999),in the Eq.(2.2) we have assumed that the porous medium is uniformly distributed about the centroid of A_0 ,and the characteristic length scale L_0, W_0 of the averaging area A_0 are large compared to the characteristic length scale of the roughness elements composing the porous medium. Moreover, *Whitaker* (1999) suggested a definition of a disordered porous medium by which we assume that with respect to an averaging area A_0 the spatial moments of the porous medium up to zero order can be neglected and the spatial decomposition Eq.(2.1) may be interpreted as a decomposition of spatial scales, because the (SAC) component in the Eq. (2.1) changes only over the spatial scales L_0, W_0.

Referring to near-bed turbulence in fully rough gravel-bed open channel flow, *Mignot et al.* (2008) applied spatial averaging procedure (e.g. *Whitaker* (1999)) to the flow quantities with the presence of macro-roughness elements characterizing the rough bed composition,with length scale of 10 cm and with the maximum bed elevation above the average measured bed elevation of 2.8 cm. As a result of the flow heterogeneity induced by the bed topography, the turbulent kinetic energy balance in the roughness layer (sensu stricto *Nikora et al.* (1998)) shows that the turbulent diffusion actively diffuses the average turbulent kinetic energy flux in both directions in contrast with the smooth boundary layer where the average turbulent energy fluxes has only one direction (e.g. not directed to-

ward the bed). *Coleman and Nikora* (2008) have developed a new framework derived from the fundamental equations for fluid motions and particle stability. The framework describes the hydrodynamics entrainment of sediments covering a wide range of spatial and hydrodynamics scales, from that of the individual particle to spatial averaged entrainment at the scale of stream reach. Specifically, *Coleman and Nikora* (2008) have used spatial averaging concept (e.g. *Whitaker* (1999)) to review the Shields entrainment function and to propose an alternative view of the variation of the Shields function with river-bed system. In general, the Shields function responsible for entrainment of particles depends hydrodynamically on the across-particle difference in pressure and vertical fluxes (in the bed normal direction) and geometrically on the sediments bed characteristic. To that regard, international research have demonstrated that the grain-mobilizing Shields stress for a specific grain size is a function of particle protrusion (sensu stricto *Kirchner et al.* (1990)))into the flow, and intergranular friction angle (sensu stricto *Kirchner et al.* (1990)) ; the latter two depend on sediment sorting and the sediment length scale relative to its neighbors (*Kirchner et al.*, 1990; *Buffington et al.*, 1992; *Johnston et al.*, 1996).
The bed surface is a mixture of the protruding gravel particles and a patchy sand surface created by the fine sediments deposited within the immobile gravel. Such arrangement creates a peculiar roughness geometry that varies with the level of the sand surface relative to the protruding gravel.
Thus, the development of physically based model for bed-load morphodynamic modelling requires the adequate characterization of effects of the irregular surface on the turbulent boundary layer, which are governed by spatially heterogeneity of the bed surface(*Aberle et al.* (2008)).Moreover, the proper assessment of near bed hydrodynamics requires the consideration of the flow field over a certain spatial scale.
Moreover, the evolving elevation of the sand surface and the changes in the near-bed shear stresses τ , varies according to the proportion of sand that is locally stored within the surface immobile gravel particles. τ is that portion of the total boundary stress that is applied to the bed and responsible for sediment transport. It is defined as the total boundary shear stress (τ_0) acting on the bed at reference level and corrected for momentum losses caused by hydraulic roughness other than grain skin friction (*Buffington and Montgomery* (1999))

$$\tau = \tau_0 - \tau' - \tau'' - \tau''' - ...\tau^n \tag{2.4}$$
$$bed = total - banks - bedforms - ...other$$

A key issue is therefore to relate the distributions of double-averaged turbulence stresses

to roughness characteristics such as grain-size distribution or statistical roughness parameters over the spatial scales L_0, W_0 .
Referring to the DAM-approach,*Nikora et al.* (2007a) suggests that it may help in better understanding the spatially averaged Reynolds stress with regard to the different scale ranges defined by different physical mechanisms underlying the Reynolds stress production.As an example, the parameterizations for the spatially averaged Reynolds stress should include a sum of two parameterizations, one for large-scale shear turbulence, the other for small-scale wake turbulence, but all of two are function of different mixing length. Specifically, the first is linked to the distance from a reference bed, the second is linked to a roughness spatial scale.
The next section is devoted to the analysis of the geometrical properties of rough beds, with the aim to discuss the relevant geometrical properties for the computation of the near-bed shear stress. *Yager et al.* (2007) implicity assumed a characteristic planimetric spatial scale λ (the space between immobile grains)and a vertical spatial scale p (portion of the immobile grain diameter that is above the mobile sediment deposit) for the partitioning the total boundary shear stress in the Eq. (2.4) between the stress on the large, immobile, grains and the stress on the finer fraction. They derived an heuristic stress partitioning formula in which the two component of the shear stress are weighted with respect to two areas that are proportional to planimetric spatial scale λ that represents the spatial arrangement of the bed geometry.

2.1 Geometrical properties of rough beds: spatial scales

The first conceptual step in the determination of suitable spatially-averaged relationships for friction, near-bed shear stresses and sediment transport for flows over rough beds partially covered with sand requires to examine the geometrical properties of rough gravel beds in relation to the length scales that become relevant in the spatial averaging procedure. Relevant spatial scales for the problem tackled in the present thesis likely result from a combination of geometrical and hydrodynamic elements. The present section focuses on the geometrical scales that characterize rough beds.These quantities have direct implications for the spatial averaging approach that is commonly used in characterizing flow fields over rough beds (e.g. *Nikora et al.* (2001)).*Nikora et al.* (2004) explored hight-order statistics for studying the structure of water-worked gravel beds surface. The generalized

1-D form of high-order structure function can be expressed by (*Nikora et al.*, 2004):

$$D_{Gs}(l_x) = \frac{1}{(N-n)} \sum_{i=1}^{N-n} \{|Z(x_i + l_x) - Z(x_i)|\}^s \tag{2.5}$$

Where $n = \frac{l_x}{\delta_x}$ and δ_x is the sampling interval.
The shape of the two-dimensional structure functions of gravel beds can be related to their scaling behavior. One of the key outcomes of *Nikora et al.* (2004)analysis is that the boundary between the scaling range of the structure functions and their transition range is of order of d_{50} while the boundary between the transition range and the saturation range is of order of d_{90}.

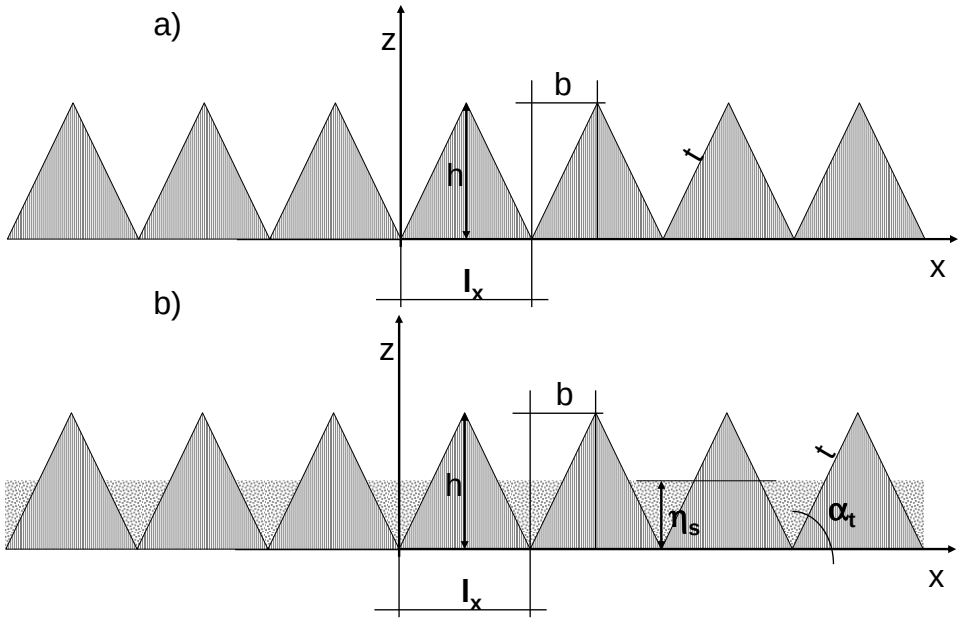

Figure 2.1: Roughness bed represented by triangles (panel a)) and triangles and sand (panel b))

In the present section a simplified geometrical arrangement of a rough bed is used for the sole purpose of highlighting (i) how the properties of high-order structure functions can be put in relationship with typical length scales of the rough bed and (ii) to suggest

on a conceptual basis how these scales may be affected by the presence of a sand layer with varying elevation within the fixed gravel particles. Figure 2 in *Nikora et al.* (2004) illustrates the distinction between the transition and the saturation regions for second-order structure functions computed referring to a gravel patch of the Sotover River in NZ. In order to define the boundary between the transition and the saturation regions the derivative $\frac{d}{dl_x}D_{Gs}(l_x)$ must be computed. The "saturation region" can be interpreted as the l_x - range where the "spatial memory" of the bed elevation vanishes, i.e. bed elevation values taken at these distance one another are reasonably non-correlated. It is worth noting that computing higher order structure functions results in clearer detection of the boundary between the different regions.

The focus of the analysis here is to make a simple conceptual attempt at quantifying a these lengths associated with vanishing spatial memory of the rough bed, which represent optimal candidates to quantify the length scale on which the spatial averaging procedure can be conveniently applied. In order to do this, a simplified 1D rough bed configuration made of an indefinite sequence of nearby triangles is used, which allow to derive a simple analytical expression for such geometrical length scale. Although such assumption might result in a quite crude approximation, it must be beard in mind that the present application has a mainly illustrative and conceptual purpose. Referring to the Figure 2.1 (panel a)), the rough bed has been represented by infinite triangles and the n-order structure function in the Eq.(2.5) is computed as follows:

$$d|Z_i(l_x)| = \frac{h}{b}l_x \tag{2.6}$$

$$D_{Gs}(l_x) = \frac{1}{n_t}\sum_{i=1}^{n_t}\{\frac{h}{b}l_x\}^s \tag{2.7}$$

with the geometrical constrains:

$$h^2 + b^2 = t^2 \text{ and } 0 \leq l_x \leq \widetilde{l_x} = b \tag{2.8}$$

Where n_t represents the number of triangles, assuming that the ratio h/b is equal for all triangles n_t then the Eq.(2.7) follows as:

$$D_{Gs}(l_x) = \{\frac{h}{b}l_x\}^s \tag{2.9}$$

The derivative of Eq.(2.9) with respect to l_x reads as:

$$\frac{d}{dl_x}D_{Gs}(l_x) = \frac{h}{b}s\{\frac{h}{b}l_x\}^{s-1} = \frac{h}{b}\{s^{\frac{1}{s-1}}\frac{h}{b}l_x\}^{s-1} \tag{2.10}$$

For each s-order of the function $D_{Gs}(l_x)$ the geometrical constraints stated by (2.8) have to be satisfied; particularly for each s-order $l_x^* = \frac{l_x}{s^{\frac{1}{s-1}}}$ then the (2.10)becomes:

$$\frac{d}{dl_x} D_{Gs}(l_x) = \frac{h}{b} s \{\frac{h}{b} l_x\}^{s-1} = \frac{h}{b} \{\frac{h}{b} l_x^*\}^{s-1} \tag{2.11}$$

For different order s of the structure functions:

$$s = \{1^+, 2, 3, 4, 5, 6\}$$

In the case of a rough bed composed by a sequence of identical triangles (Figure 2.1) the function associated with the normalized length scale l_x^* takes a simple analytical expression:

$$f(s) = s^{\frac{1}{s-1}} = \{e, 2, 3^{\frac{1}{2}}, 4^{\frac{1}{3}}, 5^{\frac{1}{4}}, 6^{\frac{1}{5}}\}$$

The geometrical constraints stated by (2.8)therefore implies that:

$$\begin{aligned} l_{x1+} &= b_1 = \frac{b}{e} \\ l_{x2} &= b_2 = \frac{b}{2} \\ l_{x3} &= b_3 = \frac{b}{3^{\frac{1}{2}}} \\ l_{x4} &= b_4 = \frac{b}{4^{\frac{1}{3}}} \\ l_{x5} &= b_5 = \frac{b}{5^{\frac{1}{4}}} \\ l_{x6} &= b_6 = \frac{b}{6^{\frac{1}{5}}} \\ ... &= ... \\ l_{x\infty} &= b_\infty \mapsto \frac{b}{1} \end{aligned} \tag{2.12}$$

Figure 2.2 reports the first derivative of the sth-order structure function of the simplified rough bed configuration made of triangular protruding elements in relationship with a normalized length scale $\frac{l_x}{(1-\eta_s^*)b}$ in a log diagram. Setting $\eta_s^* = 0$ corresponds to a rough bed completely empty with sand. The boundary between the transition and saturation regions can be clearly detected in correspondence of the abrupt slope variation of each represented curve. Such transition happens for l_x of the same order of the horizontal bed scale b. Such horizontal scale can be interpreted as a measure of the average horizontal distance between the protruding particles in real rough beds.

The effect of the presence of sand in the gravel bed forming a sand cover with elevation η_s can be incorporated in the above analysis in order to hypothesize how the characteristic scales can change with respect to the "clean" gravel bed.
Referring to the Figure 2.1 panel b), η_s represents the sand level in the gravel matrix composed by triangles, it follows that the horizontal scale $\widetilde{l_x}$ is modified and reduced, because the protruding elements' spacing increases due to the sand layer:

$$\beta_s = (1 - \frac{\eta_s}{h})b = (1 - \eta_s^*)b \tag{2.13}$$

$$\eta_s^* = \frac{\eta_s}{h} \tag{2.14}$$

Eq.(2.11)therefore becomes:

$$\frac{d}{dl_x} D_{Gs}(l_x) = \frac{h}{\{(1 - \eta_s^*)b\}} \left\{ \frac{h}{(1 - \eta_s^*)b} l_x^* \right\}^{s-1} \tag{2.15}$$

Figure 2.2 represents the function in Eq.(2.1) for the simple case in which the bed roughness has been represented by triangles and η_s^* represents the sand level as indicated by Eq.(2.14). It is noteworthy that as the exponent s in Eq.(2.1) approaches to ∞ then the characteristic length scale l_x approaches to the geometrical base b of the triangle in Figure 2.1 panel a) and panel b).
Thus Eq.(2.1) provides a simple conceptual explanation of how the high-order structure function of bed elevations can be modified by the presence of a sand layer, through the dimensionless parameter η_s^*. Two important spatial scales are present, related to the height of the protruding particles (vertical geometric scale) and to the horizontal spacing between roughness elements (horizontal geometric scale). The shape of the roughness geometry function (e.g. *Nikora et al.* (2001)) provides a quantification of the vertical variability of such characteristic spacing between protruding elements. The roughness geometry function $\mathcal{A}(\eta_s)$ (*sensu Nikora et al.* (2001))can be defined as the ratio between the horizontal (bed parallel) area occupied by fluid (i.e. A_f) within a defined horizontal region with total area A_0, which for 1-D rough bed reads:

$$A_0 = l_{x\infty} \tag{2.16}$$

Assuming that the sand fraction fills the space available between the rough elements as in Figure 2.1 (panel b)), the area A_f occupied by sand is proportional to the sand elevation

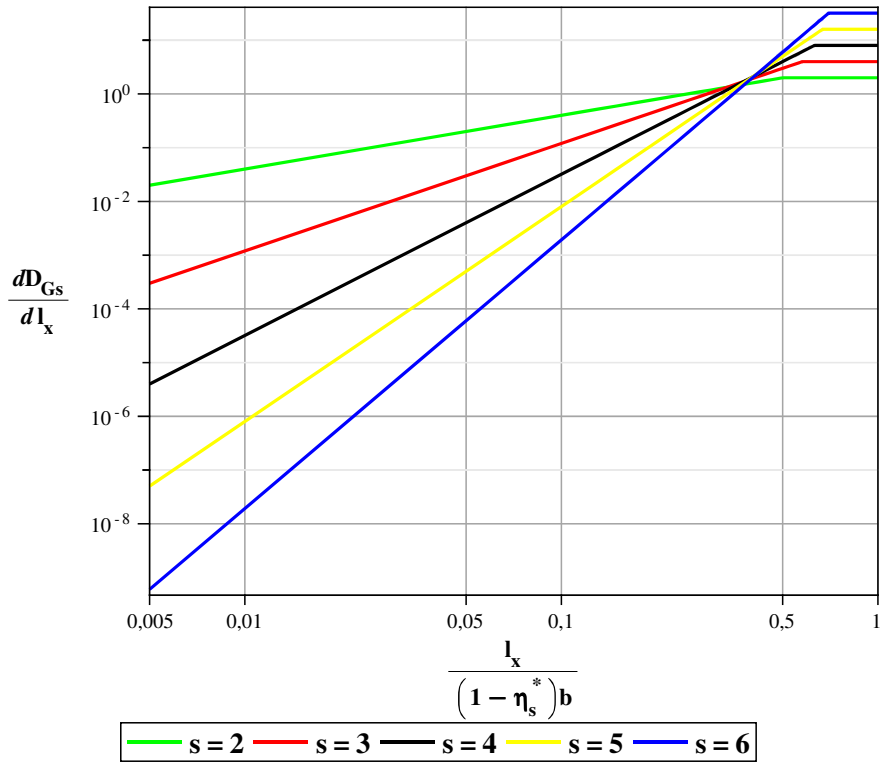

Figure 2.2: S-order derivative of the structure functions for a rough bed composed by triangles

η_s^* itself as follows:

$$\begin{aligned} A_f &= \eta_s^* l_{x\infty} \\ \mathcal{A}(\eta_s^*) &= \frac{A_f}{A_0} = \eta_s^* \\ \eta_s^* &= \frac{\eta_s}{l_{x\infty}\tan\alpha_t} \end{aligned} \tag{2.17}$$

The roughness geometry function and the dimensionless quantity η_s^* in Eq.(2.17) depends on the geometrical length scale $l_{x\infty}$ that is the spatial length scale characteristic of the rough bed composition with a specified η_s sand level.
This basic concept has been presented referring to a oversimplified bed geometry having

in mind a mainly illustrative purpose. A key issue is related to the quantification of the geometrical scales for irregular rough bed surfaces as typical of real streams. The concluding part of this Section is devoted to envisage a suitable approach to quantify the relevant geometrical scales in the framework of a spatial averaging procedure. The patches of a rough, water-worked gravel beds show properties typical of "disordered porous media" as stated by *Whitaker* (1999). A schematic vertical view of a 2D gravel bed patch with indication of the averaging area A_0 is reported in Figure 2.3. The averaging area is composed by two phase, specifically the rough phase (indicate in Figure 2.3 as r-phase) and the fluid phase indicated in the same figure as fluid phase. The details of this averaging area are presented in the same Figure 2.3 where vector $\mathbf{R_c}$ locates the centroid of the averaging area, the position vector $\mathbf{r_f}$ locates any points in the fluid phase with respect to the orthogonal coordinate system $(x' - y')$ that has its origin in the centroid of the averaging area. Differently, the orthogonal coordinate system $(x - y)$ defined any centroid of a specified averaging area A_0=$W_0 L_0$ where W_0 and L_0 are characteristic geometrical length scale that define the averaging area.The position vector $\mathbf{R_c}$ may lie in either the r-phase or f-phase. In the framework of a spatially-averaged approach, the exponent s in Eq.(2.5) has an important meaning in terms of the spatial scale characteristic of porous medium , particularly in relationship with the probability density function of the length scale l_x. Considering the spatial average operator in Eq.(2.2), the spatial averaged fluctuation of a *generic* quantity $\widetilde{\vartheta}$ reads as:

$$\widehat{\vartheta} - \langle \overline{\vartheta} \rangle_{O(\Gamma_0^2)} = \widetilde{\vartheta} \tag{2.18}$$

or equivantely, in dimensionless form:

$$\begin{aligned} \frac{\widehat{\vartheta}}{\langle \overline{\vartheta} \rangle_{O(\Gamma_0^2)}} - 1 &= \frac{\widetilde{\vartheta}}{\langle \overline{\vartheta} \rangle_{O(\Gamma_0^2)}} \\ &\Downarrow \\ \widehat{\vartheta}^* - 1 &= \widetilde{\vartheta}^* \end{aligned}$$

where the spatial operator $\langle . \rangle$ is computed over an averaging area that can be represented through the characteristic spatial scale Γ_0^2 of Eq.(2.20).Such spatial scale measures the lowest possible resolution at which the spatially averaged quantities can be described. This implies that smaller-scale phenomena would be neglected within a spatially averaged approach.The characteristic spatial scales for the spatial averaged fluctuation $\widetilde{\vartheta}$ can be quantified following *Whitaker* (1999), who suggested that the fluctuations relative to the spatial average can be interpreted as higher-order terms of a Taylor series expansion of

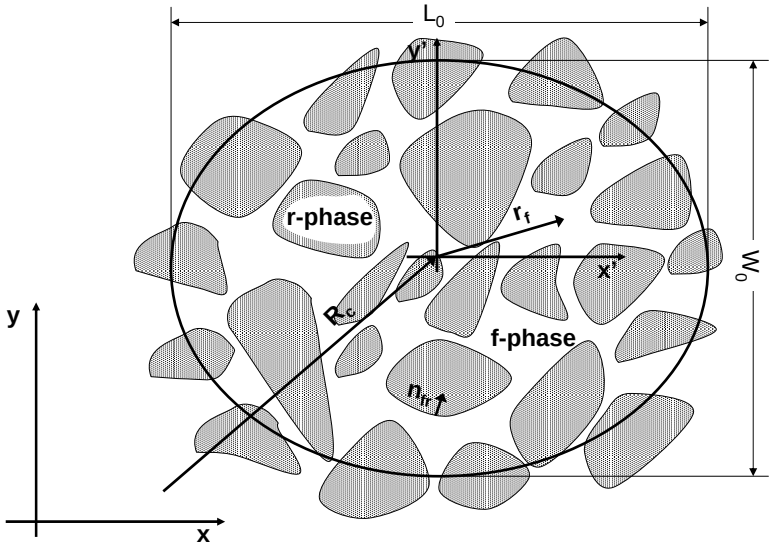

Figure 2.3: Averaging area A_0 for fluid and rough phase (i.e. f- and r-phase, respectively) referring to the centroid located with the vector $\mathbf{R_c}$ in the orthogonal coordinate system $(x-y)$.W_0 and L_0 are two characteristic geometrical length scales that define the averaging area in the same orthogonal coordinate system. The relative position vector $\mathbf{r_f}$ locates any points in the fluid phase (i.e. f-phase).Moreover, $\mathbf{n_{fr}}$ represents the unit normal vector pointing from f-phase to r-phase

the local variable $\widetilde{\vartheta}$ about the centroid R_c (see Figure2.3). Therefore $\widetilde{\vartheta}$ in Eq. (2.19) can be represented as a function of the spatial moments as follows:

$$\begin{aligned}
\frac{1}{A_0}\int_{A_f}\int \mathbf{n}_{fr}dx'dy' &= -\nabla\langle 1\rangle \qquad (2.19)\\
\frac{1}{A_0}\int_{A_f}\int \mathbf{n}_{fr}\mathbf{r}_f dx'dy' &= -\nabla\langle \mathbf{r}_f\rangle\\
\frac{1}{A_0}\int_{A_f}\int \mathbf{n}_{fr}\mathbf{r}_f\mathbf{r}_f dx'dy' &= -\nabla\langle \mathbf{r}_f\,\mathbf{r}_f\rangle\\
..... &= .....\\
\frac{1}{A_0}\int_{A_f}\int \mathbf{n}_{fr}\mathbf{r}_f^s dx'dy' &= -\nabla\langle \mathbf{r}_f^s\rangle
\end{aligned}$$

where

$$\mathbf{r}_f = \sqrt{x'^2 + y'^2}\,\hat{\mathbf{r}}_f \tag{2.20}$$

$$r_{f_{min}} \leq \sqrt{x'^2 + y'^2} = r_f \leq \sqrt{L_0^2 + W_0^2} = \Gamma_0 \tag{2.21}$$

or

$$r^*_{f_{min}} \leq \frac{\sqrt{x'^2+y'^2}}{\sqrt{L_0^2+W_0^2}} = r^*_f \leq 1$$

$\mathbf{r}_f$ is the position vector relative to the centroid of the averaging area A_0 as illustrated in Figure 2.3, $\mathbf{n}_{fr}$ represents the unit normal vector and is directed from the f-phase to r-phase. The operator ∇ represents the traditional three-space gradient operator and the operator $\mathbf{r}_f^s$ refers to the dyadic product of the vector $\mathbf{r}_f$ with the exponent s indicates the order of the dyadic tensor.

Considering Eq.(2.19), $\widetilde{\vartheta}^*$ can be expanded as a Taylor series about the centroid of the averaging area.In terms of orders of magnitude this leads to the following expression for the scales of dimensionless fluctuations $\widetilde{\vartheta}^*$:

$$O(\widetilde{\vartheta}^*) = O(1)\left\{ O\left(\frac{l_1}{\Gamma_0}\right) + O\left(\frac{l_2}{\Gamma_0}\right)^2 + O\left(\frac{l_3}{\Gamma_0}\right)^3 + ... \right\} \tag{2.22}$$

$$\Gamma_0 > l_1 > l_2 > l_3 > ... \tag{2.23}$$

Where $l_1, l_2, l_3....$ represents a characteristic length scale by which the spatial moments in the Eqs.(2.19) are defined and the operator ∇ represents the traditional three-space gradient operator. The geometrical condition in Eq.(2.23) is satisfied having considered the "disorder porous medium" property for which $\nabla\langle\mathbf{r}_f\rangle << \mathbf{I}$ where $\mathbf{I}$ is the identity tensor. Therefore, each of the length scale $l_1, l_2, l_3, ...$ are higher order infinitesimal with respect to the length scale Γ_0 characteristic of the averaging area A_0. It is noteworthy that the "disorder porous medium" property is well-suited for the method of volume averaging because of the consistency of the expansion in Eq.(2.22), but the condition $\nabla\langle\mathbf{r}_f\rangle << \mathbf{I}$ can be found also in other studies of disorder systems (*Whitaker* (1999)).

In general, the approximation of a function by the Taylor expansion depends on the the nth order of derivative of the function itself. Considering the superficial spatial moments, as in Eqs.(2.19), the nth order of derivative in the Taylor expansion, corresponds to the nth superficial spatial moments.

In the line of the above reasoning, the difference in bed elevations between two points in the gravel bed, spaced l_x (see Eq. 2.5) $Z(x_i + l_x) - Z(x_i)$ can be written as follows, in the

case of 1-D gravel beds:

$$Z(x_0 + l_{x0}) = Z(x_0) + \frac{d}{dl_{x0}} Z(x_0, l_{x0}) dl_{x0} + \frac{1}{2!} \frac{d^2}{dl_{x0}^2} Z(x_0, l_{x0}) dl_{x0}^2 + ... \quad (2.24)$$

$$x_0 \in A_0 = L_0 W_0 \quad l_{x0} = (x - x_0) \quad (2.25)$$

In Eq.(2.24) l_{x0} represents a characteristic length scale referring to the averaging area whose centroid is located at (x_0, y_0). Moreover,in Eq.(2.24) it has been assumed that $Z(x_0+l_{x0})$ is a continuous and nth derivable function of the variable x_i, where the subscript 0 refers to the centroid of the area A_0. Therefore, the difference $Z(x_0+l_{x0})-Z(x_0)$ referring to the centroid (x_0, y_0) of the averaging area A_0 reads as:

$$Z(x_0 + l_{x0}) - Z(x_0) = \frac{d}{dl_{x0}} Z(x_0, l_{x0}) dl_{x0} + \frac{1}{2!} \frac{d^2}{dl_{x0}^2} Z(x_0, l_{x0}) dl_{x0}^2 + ... \quad (2.26)$$

$$\Downarrow$$

$$|Z(x_0 + l_{x0}) - Z(x_0)|^s = \left| \sum_{n=1}^{\infty} \frac{1}{n!} \frac{d^n}{dl_{x0}^n} Z(x_0, l_{x0}) dl_{x0}^n \right|^s \quad (2.27)$$

where n is the order of the derivative and s is the order of the structure function in Eq.(2.5).When only a finite number n of the derivatives are taken into account, then Eq.(2.27) reads as:

$$|Z(x_0 + l_{x0}) - Z(x_0)|^s = \left| \sum_{n=1}^{m} \frac{1}{n!} \frac{d^n}{dl_{x0}^n} Z(x_0, l_{x0}) dl_{x0}^{n-m} \right|^s |dl_{x0}|^{ms} \quad (2.28)$$

$$= \left| \sum_{n=1}^{m} \frac{1}{n!} \frac{d^n}{dl_{x0}^n} Z(x_0, l_{x0}) dl_{x0}^{n-m} \right|^s |dl_{x0}|^{\widetilde{s}}, \quad m = \frac{\widetilde{s}}{s} \quad (2.29)$$

The function $Z(x_0 + l_{x0})$ refers to a local value of Z respect to the centroid x_0 of an averaging area A_0. the spatial averaging procedure is now applied to the expansion 2.29.This requires to define the averaging area A_0 in terms of the length scale l_x. In order to evaluate the length scale l_x , we introduce the spatial averaging operator for the function Z and analyze how the length scale l_x can be influenced by the properties of the function $|Z(x_0 + l_{x0}) - Z(x_0)|^s$. Let us assume the spatial averaging operator (*Whitaker* (1999)):

$$\langle Z \rangle_{x_0 + l_{x0}} = \frac{1}{A_0} \int_{A_f(x_0 + l_{x0})} Z(x_0 + l_{x0}) dl_{x0} \quad (2.30)$$

The spatial average of Eq.(2.29) therefore gives:

$$|\langle Z\rangle_{x_0+l_{x0}} - \langle Z\rangle_{x_0}|^s = \left|\sum_{n=1}^{m} \frac{1}{n!} \left\langle \frac{d^n}{dl_{x0}^n} Z(x_0, l_{x0}) \right\rangle_{x_0} \langle dl_{x0}^{n-m}\rangle_{x_0+l_{x0}}\right|^s \langle |dl_{x0}|^{\widetilde{s}}\rangle_{x_0+l_{x0}} \tag{2.31}$$

where $\langle Z\rangle_{x_0}$ is the spatial averaging operator referring to the centroid of the area A_0 which is invariant with respect to time and space. *Whitaker* (1999) assumed that "the process of spatial smoothing begins by associating with *every* point in space an averaging volume which is invariant with respect to time and space". Therefore, the operator $\langle Z\rangle_{x_0}$ refers to the spatial averaged value of Z calculated on the invariant area A_0 (see Figure 2.3).
In Eq.(2.31) the geometrical functions $\langle |dl_{x0}|^{\widetilde{s}}\rangle_{x_0+l_{x0}}$, $\widetilde{s} = (1, ..., n_s)$, represent the first, second and higher, superficial spatial moments as indicated by Eqs. (2.19) and $\widetilde{s}$ represents the $\widetilde{s} - th$ order of these spatial moments. Moreover, each superficial spatial moment corresponds to the different terms in the expansion (2.22) with the geometrical constraints of Eq.(2.23).
The main outcome of the above analytical treatment is that the spatial length scales resulting from the analysis of the s-th order structure function of bed elevation are in close relationship with those arising from the spatial average of the bed elevation function performed as a Taylor expansion up to the s-th derivative order. In other words, the s-order function in Eq.(2.5) represents, in terms of spatial averaging procedure the different spatial length scales by which the function Z takes into account its spatial variability in the invariant area A_0.
If the sand fraction is present in the gravel framework, then the different spatial scales $l_1, l_2, l_3, ...$ change with the sand level into the gravel framework as indicated by the simple case represented in Figure 2.2 where the parameter $l_x/((1-\eta_s^*)b)$ changes between $(l_x/b \div \infty)$ depending on the sand level η_s^*. Consequently, the length scales $l_1, l_2, l_3, ...$ change because of the sand level that has a direct influence on the spatial arrangements of the rough bed. When the spatial average refers to turbulent flow variables over the rough bed, the approximation based on 2.22 depends on near-bed turbulence scales. Introducing hydrodynamics into the geometrical considerations exposed above is the focus of the next Section.

2.2 Hydrodynamics characterizations:turbulence properties near immobile gravel beds

The present section reviews existing literature on near-bed turbulence properties for rough-bed open channel flows, and theoretically analyzes the spatially-averaged momentum equations in the nearby of a rough bed with the aim to set the basis to derive suitable closure relationship for spatially - averaged near-bed shear stress and sediment transport when a gravel bed is partially covered with sand.
The closure relationships will be derived on the basis of a theoretical analysis of the governing spatially-averaged turbulent flow equations and with reference to existing experimental data. A vertically varying, longitudinally uniform flow will be considered; the derived closure relationships can then be used following of a "slowly varying" approach, as is commonly done in morphodynamic modelling. This "slowly varying" approximation can be acceptable when the spatially-averaged variations of bed and channel geometry in space are "slow enough". This therefore allows to use the closure relationship for shear stress and sediment transport, derived under uniform flow conditions, with local values of the spatially-averaged flow properties.
In a first instance, near-bed turbulence properties will be examined in the absence of sand cover; afterwards the analysis will focus on how these properties can be modified by the presence of a sand layer of variable height.
Figure 2.4 reports the main notations that will be used to characterize the physical system: a turbulent free-surface flow over an immobile gravel bed.

Referring to Figure 2.4, *Nikora et al.* (2001, 2007b) suggested the subdivision of the different flow into specific layer, depending on flow submergece, i.e. $\langle D_0/l_z \rangle_s$. ($\langle D_0 \rangle_s$ denotes the spatially-averaged water depth in the reference area A_0 and $\langle l_z \rangle_s$ is a spatially-averaged length scale referring to the gravel bed elements composition in the same reference area).According to Nikora et al. (2001), momentum conservation is controlled by different physical effects in each flow layer represented in Figure (2.4), which results in different spatially-averaged vertical velocity profiles. The following layers are sketched in Figure 2.4:

1. Outer layer: in this region the viscous effects and form-induced fluxes are negligible and the spatially averaged equations are identical to the time-averaged equations.

2. Logarithmic layer: in this flow region the viscous effects and form-induced fluxes are negligible and the spatially averaged equations are identical to the time-averaged equations, as for the outer layer. However, the characteristic scales for the logarith-

mic layer are different from those for the outer layer.

3. Form-induced sublayer: the flow in this region is influenced by individual roughness elements. The form-induced sublayer occupies the region just above the roughness crests. The name "form-induced" reflects the appearance of the form-induced stresses which are due to flow separation from the roughness elements and are not present in the logarithmic layer.

4. Interfacial sublayer: this sublayer is also influenced by individual roughness elements and occupies the flow region between roughness crests and troughs, i.e., where the roughness geometry function $\mathcal{A}(z)$ changes from 1 to 0 for impermeable beds, or from 1 to $\mathcal{A}_{min}$ for permeable beds. An important feature in this sublayer is that associated with form drag.

The form-induced and interfacial sublayers together may be identified as the roughness layer. The main characteristic scales of the roughness layer are the shear velocity u_* and characteristic lengths of the bed topography discussed in the previous Section.

Specifically, the present analysis refers to a "Flow type I" (*sensu Nikora et al.* (2001, 2007b)) characterized by high relative submergence, where the logarithmic layer is fully developed because the submergence is large enough to form an overlap region, i.e. the "outer layer" (see Fig.(2.4)). "Flow type I" occurs when $< D_0 >$ is at least one order of magnitude larger than $< l_z >$, although also larger values have been reported. *Jiménez* (2004) justified the logarithmic layer for deep flow when $\langle D_0/l_z \rangle_s > 80$, but data available in other flow conditions show that the distribution of double-averaged velocity above the roughness layer is logarithmic for the ratio $\langle D_0/l_z \rangle_s$ much smaller than 80 (*Mignot et al.* (2008); *Franca et al.* (2008)).

The physical quantities that are mainly transported by hydrodynamics forces in the interfacial sublayer and in the form-induced sublayer are different. Specifically, and referring to uniform two-dimensional open channel flow, the double-averaged (in time first and in space second) momentum equation (*Nikora et al.* (2001, 2007b); *Mignot et al.* (2008)) reads:

$$\frac{\partial}{\partial z}\left(\overbrace{\mu\frac{\partial\langle\overline{U}\rangle_s}{\partial z}\underbrace{-\rho\langle\overline{u'w'}\rangle_s-\rho\langle\widetilde{u}\widetilde{w}\rangle_s}_{\tau_t}}^{\tau}\right)+f_p(z)+f_\nu(z)=-\rho g i_f\mathcal{A}(z) \tag{2.32}$$

where $\langle\dot{\cdot}\rangle_s=\mathcal{A}(z)\langle\dot{\cdot}\rangle$ and the roughness geometry function $\mathcal{A}(z)$ has been defined in the set $[0,1]$ because this analysis doesn't take into account permeable beds so that when

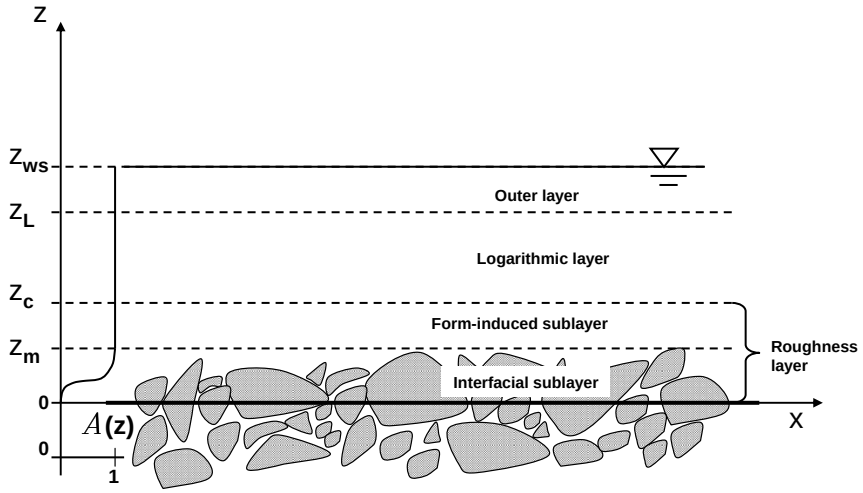

Figure 2.4: Flow subdivision into specific regions in gravel-bed flows for impermeable beds

$z = 0$ then $\mathcal{A}(0) = \mathcal{A}_{min} = 0$ (*Nikora et al.* (2001)). Moreover, i_f is the bed slope, $f_p(z)$ and $f_\nu(z)$ are the drag forces induced respectively by pressure distribution along gravel particles and by the viscous forces integrated on the contour of the roughness elements in the specific area A_0.

The total shear stress τ results from the sum of viscous shear stress and the bed-form shear stress (or dispersive stresses). In the roughness layer the form-induced stresses can not be negligible in the momentum balance, because they can reach a contribution up to 6-30% of the total shear stress τ (*Nikora et al.* (2001); *Aberle et al.* (2008); *Mignot et al.* (2008)). Experimental results (*Aberle et al.* (2008)) suggest that the local distributions of form-induced shear stresses are almost constant with varying discharge, i.e. they are almost constant regardless of the value of Reynolds number defined as $R_e = \frac{\langle \overline{U} D_0 \rangle_s}{\nu}$ with a specific rough bed configuration. However so far and to Author's knowledge there are no

studies that relate the distributions of form induced stresses to roughness characteristics of bed composition in terms of rough bed particle size distribution or statistical roughness parameters (*Buffin-Bélanger et al.* (2006); *Aberle et al.* (2008)).
A similar concept applies for the Turbulent Kinetic Energy (TKE) balance, where terms related to the form-induced stresses play a significant role in the roughness layer. The double-averaged (in time first and in space second) TKE budget equation for longitudinally uniform two-dimensional open channel flow can be written as (*Mignot et al.* (2008)):

$$\begin{aligned} & \overbrace{-\langle\overline{u'w'}\rangle_s\frac{\partial\langle\overline{U}\rangle}{\partial z}}^{P}\underbrace{-\langle\overline{u_i'u_j'}\rangle_s\left\langle\frac{\partial\widetilde{u_i}}{\partial x_j}\right\rangle-\left\langle\widetilde{u_i'u_j'}\frac{\partial\widetilde{u_i}}{\partial x_j}\right\rangle_s}_{P_t} \\ = \;& \langle\epsilon\rangle_s \\ + \;& \frac{\partial}{\partial z}\left[\underbrace{\langle\overline{k'w'}\rangle_s+\langle\widetilde{k}\widetilde{w}\rangle_s}_{F_t}\right] \\ + \;& \frac{\partial}{\partial z}\left[\underbrace{\left\langle\frac{\overline{p'w'}}{\rho}\right\rangle_s-\nu\frac{\partial}{\partial z}\langle k\rangle_s}_{F_e}\right] \quad \text{for } i,j=1,2 \end{aligned} \tag{2.33}$$

where $\langle\epsilon\rangle_s$ represents the dissipation rate , $k' = (u'^2+v'^2+w'^2)/2$, $k = \overline{k'}$ and the water density ρ and the kinematic viscosity ν have been assumed constant in the flow domain. No experimental observations exist at present to quantify the variation of the properties of the characteristic flow layers with the height of a sand coverage over the gravel bed. However, examining Eq. (2.33) in the light of existing experimental observations for gravel-bed rivers, allows to formulate reasonable working assumptions for the development of suitable closure relationships to be used in the framework of double-averaged morphodynamic models.

Referring to a specific bed composition, *Mignot et al.* (2008a) suggest that the term P_t in Eq.2.33 can not be neglected in the interfacial sublayer (i.e. $z < z_m$ in Figure 2.4), specifically for the contribution of the first term in the P_t component. In fact, it reaches the same order of magnitude of the first term of the total production term P, and it represents the work of the double-averaged velocity against the double-averaged shear stress. *Mignot et al.* (2008) indicate that, for rough beds, the turbulent kinetic energy flux F_t is directed upwards and toward the bed differently from the smooth bed case where it is directed only upwards. Moreover, it reaches its maximum value in the interfacial sublayer

(slightly below z_m in Figure 2.4) and it vanishes above the form-induced sublayer , i.e. $z > z_c$ in Figure 2.4(*Mignot et al.* (2008), *Mignot et al.* (2008a)).
Referring to (2.32) the linear behavior of the total shear stresses τ is, in principle, recovered for $z \geq z_c$ because the drag forces and the influences of form-induced shear stresses vanish (*Nikora et al.* (2001)). Physically, this means that the presence of the turbulent kinetic energy flux F_t throughout the roughness layer shifts the region where the vertical shear stress profile is linear to the level z_c, where the logarithmic streamwise velocity profile is recovered.
Mignot et al. (2008) present a simplified treatment of the near bed turbulence proprieties, by assuming that the turbulence macro scales for the logarithmic layer and for the interfacial sublayer are of the same order of the water depth D_0. Besides, for $z \leq z_m$ the turbulence small scales have been assumed of size equal to $L_s = \langle z_m \rangle_s$, and the double-averaged shear stress profile have been assumed to be linear. In other words, and assuming that the velocity shear generate a hierarchy of eddies throughout all the water depth with characteristic scales proportional to the distance from the rough wall, the energy production flux P in Eq.(2.33) across the hierarchy of eddies depends on the scale under consideration. In turn this scale depends on how the energy is distributed or dissipated throughout all the water depth, as stated by right hand side of (2.33). Above a given distance from the rough bed, i.e. $z \geq z_c$, the energy production term P balances the energy dissipation ϵ and a turbulence eddy characteristic scale L varies in the range $a_i \langle D_0 \rangle_s \leq L \leq b_i z_c$, with a_i,b_i scaling coefficients depending on the flow fields velocity components. In the range $z < z_c$ smaller eddies exists and a eddy characteristic scale L varies in the range $a_i \lambda \leq L \leq b_i z_c$ (known as the inertial subrange, *sensu Nikora* (2008)) where λ denotes an appropriate roughness height. It is remarkable that it has been assumed z_c as a reference level to divide the two zones because above that level all the fluxes in the right hand side of (2.33) vanishes except for the dissipation rate ϵ.
Consequently, the production term P in (2.33) reads as (*Mignot et al.* (2008)):

$$P = -\langle \overline{u'w'} \rangle_s \frac{\partial \langle \overline{U} \rangle}{\partial z} = -\langle \overline{u'w'} \rangle \frac{\partial \langle \overline{U} \rangle}{\partial z} = \frac{\langle u_*^3 \rangle_s}{kz} \left(1 - \frac{z - z_m}{\langle D_0 \rangle_s - z_m} \right) \tag{2.34}$$

where $\langle u_* \rangle_s$ represents the double-averaged friction velocity and k the Von Kármán constant. The Eq.(2.34) has been assumed valid for specified rough bed composition and in the range $0.88 \leq z/z_m \leq 1.47$. Specifically, we refer to Case 1 of bed configuration in *Mignot et al.* (2008), represented by a Gaussian distribution with mean bed elevation μ_b=3.1 cm and standard deviation σ_b=9.7·10^{-1} cm, see Figure 2.11. Moreover, Eq.(2.34) has been phenomenologically justified for completely developed logarithmic layer above z_m. Differ-

entiating Eq.(2.34) with respect to z_m and computing the derivative in a specified gravel bed bed configuration $(z_m)_0$, it follows that:

$$\frac{\partial P}{\partial z_m} = \frac{\langle u_*^3 \rangle_s}{k \langle D_0 \rangle_s} \frac{1}{(z_m)_0 (1-\Delta)} \tag{2.35}$$

or

$$\frac{\partial P^*}{\partial z_m^*} = \frac{1}{k(1-\Delta)} \tag{2.36}$$

where $\Delta = (z_m)_0 / \langle D_0 \rangle_s < 1$ represents a measure of flow submergence, $P^* = P \langle D_0 \rangle_s / \langle u_*^3 \rangle_s$ and $z_m^* = z_m / (z_m)_0$. Eq.(2.36) means that the variation with geometrical height z_m of the TKE production term P scaled with appropriate hydrodynamic external scales is only function of the flow submergence Δ. The expression (2.36) is formally valid provided the spatially averaged water depth $< D_0 >_s$ is significantly larger than the typical vertical scale associated with the rough bed surface. It can be thought as a representation of the turbulent fluxes in the near-bed region, which controls the thickness of the flow sublayers and therefore of the "small" turbulence scales of the near-bed flow properties

Referring to Eq.(2.36) and considering the general case where the turbulence scales in the form-induced sublayer are influenced by the bed composition, the production term P in the Eq. (2.33), when $0 \leq z \leq z_c$, reads as:

$$P \sim O\left(\left\langle \frac{u_*^3}{L_c} \right\rangle_s \right) = O\left(\frac{\langle u_*^3 \rangle_s}{z_c} \right) \tag{2.37}$$

where L_c is used to denote the measure of a generic "small" turbulence scale close to the bed region as explained before. Eq.(2.37) is consistent with the experimental data in *Mignot et al.* (2008) and *Mignot et al.* (2008a) where it os shown that the fluxes F_t diffuse turbulent kinetic energy throughout the roughness layer also changing the flux direction.

The analysis described above supports the fact that the first hydrodynamic ingredient to be introduced for the quantification of the near-bed turbulence scale is the water depth, namely through its ratio to the typical vertical scale of the rough bed geometry, discussed in the previous section.

Following the conventional dimensional analysis we can express the double-averaged turbulence small scale $\langle L_c \rangle_s$ for the roughness layer as:

$$\langle L_c^* \rangle_s = f\left(\left\langle \frac{l_z}{D_0} \right\rangle_s, \langle \gamma_i \rangle_s \right) \tag{2.38}$$

where $\langle l_z \rangle_s$ represents a typical length scale for bed elements. A typical measure of $< l_z >_s$

is the standard deviation of the bed elevation distribution σ_z in the case the roughness geometry function has been defined as the cumulative probability function of bed elevation *Nikora et al.* (2001)).
Equation (2.38) also includes the links with the horizontal bed geometry scale l_x that emerges from the geometrical analysis of the previous section. Indeed the term $\langle \gamma_i \rangle_s$ represents a dimensionless measure of the horizontal arrangement of bed configuration (e.g. density of roughness elements, intergranular friction angle (*sensu Kirchner et al.* (1990)).

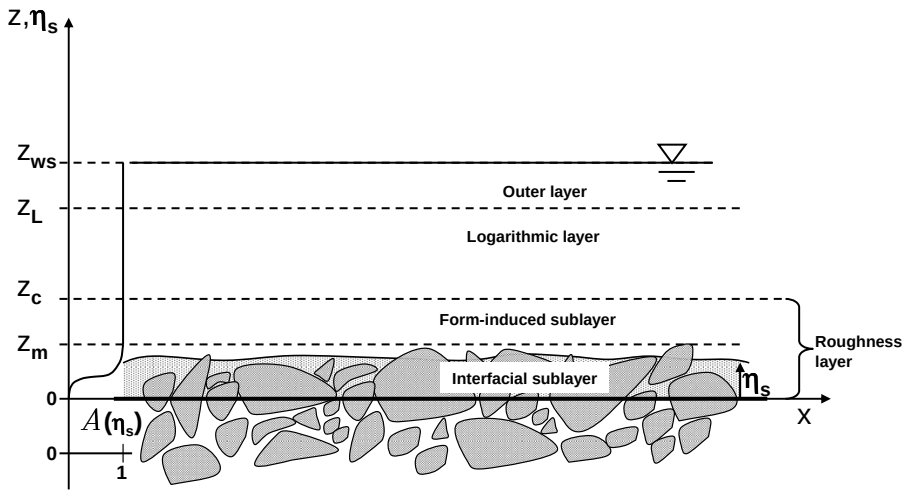

Figure 2.5: Flow subdivision into specific regions in gravel-bed flows for impermeable beds and presence of sand fraction

The presence of a sand cover in the gravel bed is likely to affect the small turbulence scales. To quantify how these scales change because of a variable sand level partially covering the immobile gravel bed is crucial for the scope of the present work. These

characteristic lengths are indeed those that define the properties of the spatially-averaged turbulent flow (vertical velocity profile, near bed shear stress, eddy viscosity) that are needed for the purpose of morphodynamic modelling.
However, apart from the recent contribution of *Wren et al.* (2011), nearly no experimental investigation is at present available concerning the effect of sand addition in gravel beds on the spatially-averaged turbulent flow properties. The present Chapter is a first attempt towards defining such dependency on the basis of a newly proposed theoretical analysis related to published experimental data.
To examine such dependence we refer to Figure 2.5 where the sand fraction has been added in the composition of the rough beds. In this case we consider $\mathcal{A}(0) = \mathcal{A}_{min} = 0$, corresponding to an impermeable bed, which physically means that the present work doesn't take into account the downwards sand infiltration phenomenon (*Cui et al.* (2008)). The function $\mathcal{A}(z)$ represents the spatially-averaged horizontal portion of the sand surface available to be transported by the flow.
The dependency expressed by Eq.(2.38), when the sand fraction is present in the gravel bed composition , becomes:

$$\langle L_c^* \rangle_s = f\left(\left\langle \frac{l_z}{D_0} \right\rangle_s, \langle \gamma_i \rangle_s, \frac{\langle \eta_s \rangle_s}{l_g}, \frac{d_s}{l_g} \right) \tag{2.39}$$

where $l_g$represents a measure of maximum gravel elements length scale (i.e. $l_g = O(d_g)$, and d_g represents the maximum gravel diameter),measured from a reference level, so that the ratio $\eta_s^* = \frac{\langle \eta_s \rangle_s}{l_g}$ has been defined between 0 and 1. When the sand level $\eta_s^* = 0$ means that no sand is available to be transported by the flow, similarly when the sand level $\eta_s^* = 1$ then the sand completely buries the gravel bed elements and the "homogeneous" case is recovered .The diameter d_s represents the sand diameter of the sand fraction, and $\left\langle \frac{l_z}{D_0} \right\rangle_s$ represents a measure of the flow submergence Δ, with $\langle l_z \rangle_s$ a characteristic gravel bed elements length scale in the area A_0.
Equation (2.39) indicates that near-bed turbulence scales depend on a measure of the relative bed roughness (protrusion) and on the arrangement of the bed particles, which are both likely to depend on the sand surface level. Moreover a dependence of these scales is reasonably expected from the sand-to-gravel grain size ratio. No explicit data exist at present on the variation of near-bed turbulence scales with the relative sand surface elevation η_s/l_g and with the grain size ratio d_s/l_g. Therefore in the following published literature data are used and original analysis are performed in order to propose functional forms that these dependencies might take, and focus on their physical meaning.

2.3 Turbulence closure and spatially-averaged velocity profiles for clean gravel beds

Assuming that $z_c \simeq z_m$ so that above z_m the production term P is equal to the dissipation rate $\langle\epsilon\rangle_s$ and the logarithmic profile is recovered, then Eq.(2.36) reads as:

$$\frac{\partial P^*}{\partial z_m^*} = \frac{\partial}{\partial z_m^*}\left(-\langle\overline{u'w'}\rangle_s^* \frac{\partial\langle\overline{U}\rangle^*}{\partial z_m^*}\right) \tag{2.40}$$

$$= -\frac{\partial\langle\overline{u'w'}\rangle_s^*}{\partial z_m^*}\left(\frac{\partial\langle\overline{U}\rangle^*}{\partial z_m^*}\right) - \langle\overline{u'w'}\rangle_s^*\left(\frac{\partial^2\langle\overline{U}\rangle^*}{\partial z_m^{*2}}\right) \tag{2.41}$$

$$= \frac{1}{k(1-\Delta)} \tag{2.42}$$

From (2.40) it follows that the logarithmic profile of the spatially-averaged longitudinal velocity $\langle\overline{U}\rangle^*$ is also a function of $\Delta = (z_m)_0/\langle D_0\rangle_s < 1$. Referring to Eq.(2.39), the velocity profile reads as:

$$\langle\overline{U}\rangle^* = \frac{1}{k} ln\left(\frac{z-d}{\lambda_0}\right) \quad \text{for } z \geq z_m,\ 0 \leq \frac{d}{z_m} < 1 \tag{2.43}$$

where d represents the zero-plane displacement and λ_0 is the roughness length (*Jackson* (1981); *Nikora et al.* (2002); *Poggi et al.* (2004)).
Nikora et al. (2002) found that the displacement height d is linearly (or quasi linearly) related to the thickness of the roughness layer z_c; referring to Figure 2.4 the reference level for the z-coordinate has been assumed where the roughness geometry function $\mathcal{A}(z)$ vanishes. On the basis of existing experimental observations, it is possible to assume that $d \approx 0.43 z_c$ (*Nikora et al.* (2002)); moreover *Nezu and Nakagawa* (1993) found $d \approx (0.3-0.6) r_s$ with r_s the radius of the spheres composing the rough bed and assuming that $z_c \equiv z_m = r_s$.
Mignot et al. (2008) found that for a specific bed configuration (Case 1) the ratio $z_c/z_m \simeq 1.47$, and $z_m = 5.9cm$. Moreover, *Mignot et al.* (2008) for the same bed configuration (Case 1) calculated, by fitting process, a zero-plane displacement $d = 3.1cm$ with respect to the reference z-level as in Figure 2.4. The value of the friction velocity has been determined from a Clauser-type analysis on the double averaged velocity. This outcome independently supports the linear correlation between d and z_c revealed by *Nikora et al.* (2002). Indeed the experimental data of *Mignot et al.* (2008) yield:

$$z_c = \frac{z_c}{z_m} z_m = (1.47 \times 5.9)\, cm = 8.7cm;$$

therefore following *Nikora et al.* (2002) one finds the following value of the displacement height d:

$$d = 0.43 z_c = (0.43 \times 8.7)\, cm = 3.74 cm,$$

with a 17% difference with respect to the value of 3.1 obtained through direct fitting the velocity data by *Mignot et al.* (2008). For the reason illustrated above, it is reasonable to rewrite (2.43) as follows:

$$\langle \overline{U} \rangle^* = \frac{1}{k} ln \left(\frac{z - 0.43 z_c}{\lambda_0} \right) \quad \text{for } z \geq z_c \tag{2.44}$$

Since $z_c = O(z_m)$ then Eq.(2.43) still hold also for the level z_c.Combining (2.43) and (2.39) it can be assumed the following general dependency of the spatially averaged vertical profile of the longitudinal velocity:

$$\langle \overline{U} \rangle^* = f_U \left(\left\langle \frac{l_z}{D_0} \right\rangle_s, \langle \gamma_i \rangle_s, \frac{\langle \eta_s \rangle_s}{l_g}, \frac{d_s}{l_g} \right) \tag{2.45}$$

This is based on recognizing that the relevant hydrodynamic turbulent scales (λ_0, d or z_c) are dependent on the same dimensionless parameters. According to (2.39) one can indeed write:

$$\begin{aligned} z_c &= f_z \left(\left\langle \frac{l_z}{D_0} \right\rangle_s, \langle \gamma_i \rangle_s, \frac{\langle \eta_s \rangle_s}{l_g}, \frac{d_s}{l_g} \right) \\ \lambda_0 &= f_\lambda \left(\left\langle \frac{l_z}{D_0} \right\rangle_s, \langle \gamma_i \rangle_s, \frac{\langle \eta_s \rangle_s}{l_g}, \frac{d_s}{l_g} \right) \end{aligned} \tag{2.46}$$

Equation (2.43) already expresses the dependance of the spatially averaged velocity on the first of the four parameters that appear in (2.45). The dependence from the second of these parameters, i.e. the arrangement of bed particles in the gravel bed, is discussed in the following paragraphs.
The first step in doing this is to review the existing literature data to determine the values of z_c and λ_0 with different geometric packing.

Considering Figure 2.6, we defined the areal close-packing of the roughness elements trough the parameter γ_i defined as:

$$\gamma_i = \frac{2 r_s^2 \sqrt{3}}{A_0(l_x, l_y)}, \quad 2 r_s \leq l_x < \infty, \quad 2\sqrt{3} r_s \leq l_y < \infty \tag{2.47}$$

where A_0 represents the area of the rectangle with sides (l_x, l_y) computed with respect to a cartesian coordinate system as in Figure 2.6. It measures the packing of a given bed

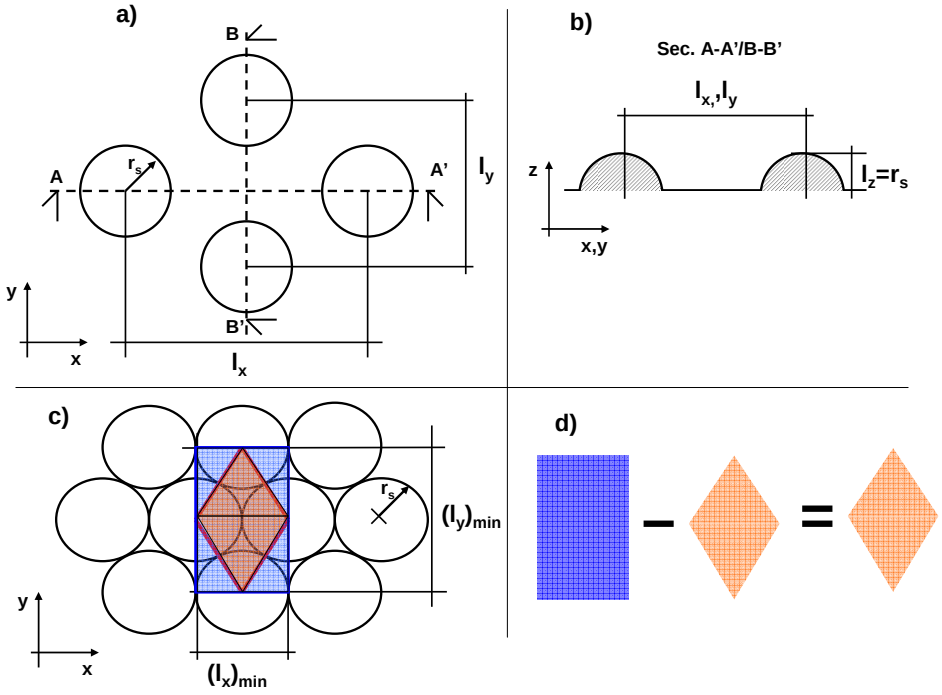

Figure 2.6: Panel a) and b) vertical and side view of the relative position of roughness elements represented by spheres of area πr_s^2. The panels c) and d) refers to the maximum close-packing of a rough bed configuration by sphere (i.e. the minimum value of the parameter γ_i in Eq.(2.47)), particularly the blue area in the panel c) is twice the area of red triangles.

configuration. The numerator of the ratio γ_i in Eq.(2.47) represents the area of the red lozenge in Figure 2.6, and has been arbitrarily chosen as a reference measure of the closest packing arrangement of the bed particles, being sole function of a representative grain size. The value of γ_i in the Eq. (2.47) is defined in the range:

$$0 < \gamma_i \leq \frac{1}{2} = \gamma_{max} \tag{2.48}$$

Comparison from different existing data is showed in the Tab.2.1, where heterogeneous case (*Het.*) stands for a composition of angular gravel elements (stones) with $d_{50} = 2$ cm which are deposited randomly on the bottom of the experimental flume (see *Mignot et al.* (2008) for more details). Tab.2.1 shows that changing the packing arrangements of the bed rough elements is associated with variations of the hydrodynamics quantity λ_0. Moreover,

	Hom^1	Hom^2	$Het.^3$
Roughness elements	*Sphere* r_s	*Sphere* r_s	*R.A.B.*
Elements arrangements	$\gamma_i = \frac{1}{2}$	$\gamma_i = 0.41$	$\gamma_i < \frac{1}{2}$
z_c^*	r_s^*	$0.66 r_s^*$	$1.47 z_m^*$
z_m^*	r_s^*	$0.66 r_s^*$	0.31
λ_0^*	$1.74 \cdot 10^{-2} r_s^*$	$2.04 \cdot 10^{-2} r_s^*$	$1.8 \cdot 10^{-1}$

Table 2.1: Comparison of geometrical and hydrodynamics characteristic for homogeneous (*Hom.*) and heterogeneous (*Het.*) case. The star * refers to a dimensionless quantity, obtained by normalizing the reference quantity trough the spatially-averaged water depth $\langle D_0 \rangle_s$. Data are taken from: [1]*Nezu and Nakagawa* (1993); [2]*Nikora et al.* (2001); [3]*Mignot et al.* (2008) (Case 1) where R.A.B. stands for Randomly Arrangements Bed. The parameter λ_0^* was calculated considering that the displacement height d equals to $0.43 z_c$ (*Nikora et al.* (2002)).

in the heterogeneous condition (*Mignot et al.* (2008)) the two levels z_c and z_m are different because of the strong spatial heterogeneity of the bed elements, with a bed mean level z_{mean} =3.1 cm and the maximum rough elements elevation of 2.8 cm above it. The spatial rough bed elements distribution influences the energy quantities throughout the roughness layer (*Mignot et al.* (2008);*Mignot et al.* (2008a)). Assuming a fixed value of Von Kármán constant, the variability of the two quantities z_c, λ_0 is considered as a measure of turbulent transport phenomena over a rough bed. A different choice (*Nikora* (2008)) is to assume a possible variation of Von Kármán parameter as a function of relative flow submergence, admitting that this kind of variability has to be yet properly tested.
The main outcomes of the analysis illustrated above can be summarized by stating that the spatially-averaged near-bed flow properties over a rough gravel bed essentially depend on the ratio between a characteristic measure of bed particle size (vertical geometric scale) to the flow depth and on the packing arrangement of the gravel particles within the gravel bed. When sand is present in the gravel bed the above properties change because they can both depend on the sand surface elevation and also on the relative ratio between the representative sand and gravel grain size.This issue is the subject of the next Section.

2.4 Effect of a sand layer within the gravel bed

The present Section aims to examine the expected physics controlling the dependence of z_c and λ_0 on the presence of sand layer of varying heigth and to propose suitable functional relationship that can be used to represent it. The proposed functional forms are also

	Triangles	Spheres	W.W.B.
$\mathcal{A}(z)$	$\frac{z}{h}$	$\frac{z^2}{r_s^2}$	$\frac{1}{2}\text{erfc}\left[-\left(\frac{ln(z)-\mu_b}{\sqrt{2\sigma_b^2}}\right)\right]$
l_x	b	$2r_s$	$O(d_{90})$
l_z	h	r_s	$4\sigma_d \approx 1.5d_{50}^1$

Table 2.2: Geometric characterization for different bed configuration related to different forms of the roughness geometry function $\mathcal{A}(z)$ (see Figure 2.8). The function $\mathcal{A}(z)$ for Water Worked Bed (W.W.B.) has been represented by a CDF of a log-normal distribution of rough bed elevations with μ_b and σ_b the mean and variance of the log-transformed bed elevation z.The symbol σ_d refers to the standard deviation of bed elevations and d_{50} is the 50th percentile of particle size distribution of the rough elements in the interfacial sub-layer. The function erfc is the complementary error function. [1] *Nikora et al.* (2001)

discussed in the light of the few available experimental observations. For this purpose the analysis can be referred to the three different bed configurations reported in Figure 2.7. Two idealized configurations with triangular (Panel (a), Figure 2.7) and semi-cilindrical bed elements (Panel (b), Figure 2.7) are analysed, as schematic representations of the general case (Panel (c), Figure 2.7). With the aim to investigate the effect of a sand cover that fills the voids within the gravel bed, a first key property to be examined in detail, is the roughness geometry function $\mathcal{A}(z)$ of a given gravel surface (*Nikora et al.* (2001)). The three different configurations correspond to different vertical distributions $\mathcal{A}(z)$. It can be expected these varying behaviors relative to different rough bed compositions affect also the behavior of the spatially-averaged shear stresses and its derivative with respect to vertical coordinate, particularly in the interfacial sub-layer.
The problem faced in the present study refers to a fully 2D (x, z) flow and rough bed. Coherently panels *a*) and *b*) in Figure 2.8 represent the vertical section of two types of bed elements configuration so that for each value of y-coordinate (i.e.: the orthogonal coordinate to the $x - z$ plane) the vertical section remains identically the same. These bed arrangements also match the choice that the roughness geometry function $\mathcal{A}(z)$ has its minimum value equal to zero (impermeable bed).

Figure 2.7 qualitatively represents different roughness geometry function $\mathcal{A}(z)$ for the three different bed configuration shown in Figure 2.8. Panel *a*) is relative to a linear behavior, panel *b*) is relative to a parabolic behavior and panel *c*) refers to a cumulative distribution function (CDF), associated with a probabilistic bed elevation distribution whereby the roughness geometry function $\mathcal{A}(z)$ can be interpreted as the probability for a bed elevation to be smaller a given elevation z (*Nikora et al.* (2001)).

Tab. 2.2 reports the geometric length scales and to roughness geometry function char-

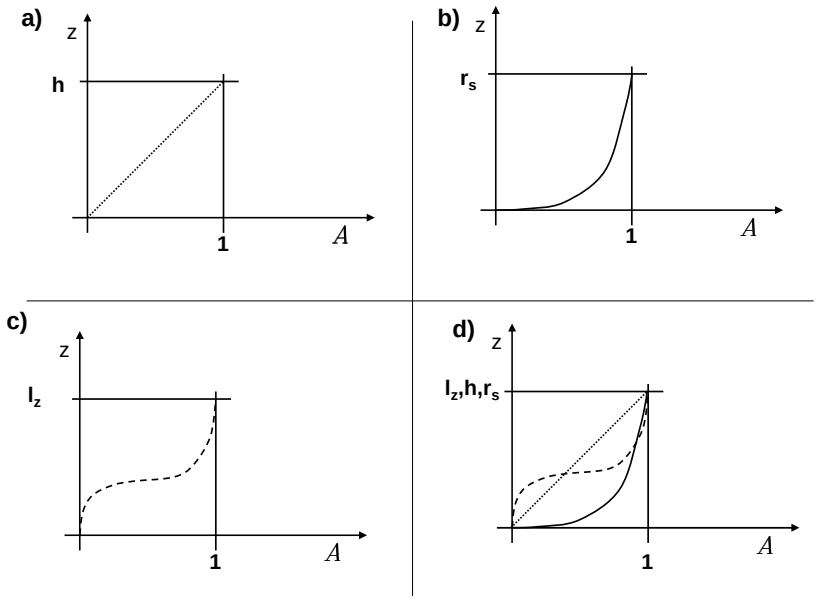

Figure 2.7: Roughness geometry function $\mathcal{A}(z)$ for different bed elements configuration

acterization $\mathcal{A}(z)$ for different rough bed elements composition as in Figure 2.8. The CDF in the same table has been assumed as log-normal distribution for the bed elevation in the interfacial sub-layer, because its domain (i.e. the rough bed elements elevations) consists in the set of real numbers $[0, \infty)$ and the shape of the related PDF is not symmetrical with respect to the expected value. For a gravel beds subject to armoring processes, *Aberle and Nikora* (2006) found that the PDF of the water-worked armor layer is positively skewed and therefore for that kind of gravel beds the Gaussian distribution could not be accepted. A second key characteristic of gravel bed composition that can be accounted for to investigate the effect of a sand cover within the gravel voids is the distribution of the bed grain size. This is conceptually different from the distribution of bed elevations quantified by means of a roughness geometry function.

Grain-size distributions for natural gravel beds population are rarely normally distributed and are frequently bimodal (*Carling and Reader* (1982); *Wilcock* (1998)). Moreover, *Carling and Reader* (1982) assumed that the grain-size distribution of gravel beds may be represented by a two grain-classes grainsize population: a framework of self-supporting

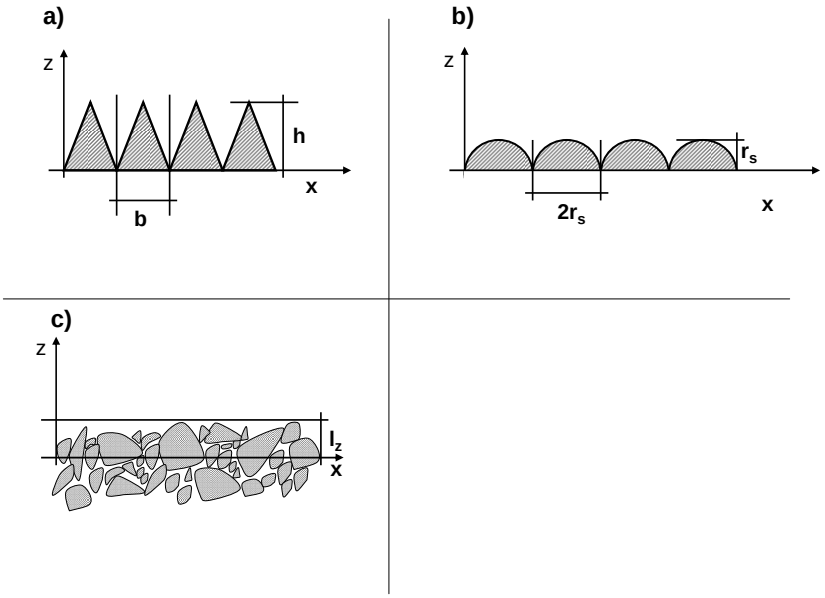

Figure 2.8: Different spatial rough bed elements configuration

interlocking large clasts, and a "matrix" population consisting of fines material (sand fraction) in size less than 2mm that infills the void space in fabric.
When a sand fraction is present in a mixed size sediments rough bed composition, modeling the transport phenomena of the sand particles when the gravel fraction is at rest requires to take into account the nonlinear effects of sand fraction on transport rate (*Wilcock and Kenworthy* (2002)). The roughness geometry function $\mathcal{A}(z)$ in Tab.2.2 represents the horizontal area occupied by sand fraction that is available to be transported by the flow, when the z-coordinate is evaluated at the spatially-averaged sand surface level η_s in the gravel matrix. Under these conditions, Tab.2.2 can be rewritten in the form of Tab.2.3.

2.5 Turbulence closures and spatially-averaged velocity profiles: mixed case

We first consider the simple case in which the rough bed elements consist of a triangles or spheres arrangement. The function $\mathcal{A}(\eta_s)$ can be interpreted as a measure of the rough

	Triangles	Spheres	W.W.B.
$\mathcal{A}(\eta_s)$	$\frac{\eta_s}{h}$	$\frac{\eta_s^2}{r_s^2}$	$\frac{1}{2}\text{erfc}\left[-\left(\frac{ln(\eta_s)-\mu_b}{\sqrt{2\sigma_b^2}}\right)\right]$
l_x	b	$2r_s$	$O(d_{90})$
l_z	h	r_s	$4\sigma_d \approx 1.5d_{50}^1$

Table 2.3: Same as Tab.2.2 but with $z = \eta_s$. The level η_s represents the sand elevation computed with respect to a reference level, i.e.$\mathcal{A}(z) = 0$

bed elements protrusion ζ above the sand level η_s that takes in this case a very simple dimensionless expression:

$$\begin{aligned} \zeta^* &= \frac{\zeta}{l_z} = 1 - \eta_s^* \\ \mathcal{A}(\eta_s^*) &= 1 - \zeta^*, \quad \text{for triangles} \\ \mathcal{A}(\eta_s^*) &= (1 - \zeta^*)^2, \quad \text{for spheres} \end{aligned} \tag{2.49}$$

It follows that the dimensionless protrusion ζ^*, for a generic, irregular gravel bed with partial sand cover, reads as:

$$\zeta^* = 1 - f[\mathcal{A}(\eta_s)] \tag{2.50}$$

Nikora et al. (2001) assumed that the function $\mathcal{A}(\eta_s)$ can be defined as the CDF of the rough bed elements elevations for irregular impermeable rough beds; therefore in Eq. (2.50) the function $f[\mathcal{A}(\eta_s)]$ can be interpreted as the probability for a bed elevation z to be less than a given elevation z_0. For simplified geometries $f[\mathcal{A}(\eta_s)] \equiv \mathcal{A}(\eta_s)$, hence in these cases:

$$\zeta^* = 1 - P(z < z_0) = 1 - \mathcal{A}(\eta_{s0}) = P(z > z_0) \tag{2.51}$$

where $P(z > z_0)$ is the CDF of a rough bed elements protrusion over a given elevation $z_0 = \eta_{s0}$. These considerations give the opportunity to quantify the variability of the spatially-averaged protrusion of the immobile gravel bed elements with the sand surface elevation η_s.

This therefore represents a first important step in building the functional relationship qualitatively expressed by Eq.(2.39) and Eqs.(2.46). Namely it allows to quantify how the first parameter $< l_z/D_0 >_s$ can change with varying sand elevations in the gravel bed. The effect of sand level, however, is not limited to a modification of this "protrusion-related" effect, but it is also felt in the whole bed composition, because when the sand level progressively increases it can be expected that that the equivalent of the bed particle arrangement (expressed with $< \gamma_i >$ in the clean gravel bed case) will be significantly

related to the presence of a variable sand surface height.
To this purpose, a detail analysis of sediment-transport related literature suggests a possible approach to account for such physical effects, which will appear of great relevance in modeling the dynamics of gravel beds with partial sand cover.
Wilcock and Kenworthy (2002) proposed a two-fraction model for the transport of sand-gravel mixtures. One of the key outcomes of their analysis is the empirical quantification of the nonlinear effect of sand content into the gravel bed on the sediment transport rate. Such effect mainly displays itself through a nonlinear effect on the critical shear stress for the motion of both fractions (sand and gravel) and on the effective near-bed shear stress for the entrainment of both sediment fractions. In the present analysis the findings of *Wilcock and Kenworthy* (2002) are revisited and reinterpreted. Focusing on the flow forces acting on the sand particles when the gravel is assumed at rest allows to propose physically-based relationships that link the characteristic near-bed turbulent scales z_c and λ_0 with the variation of the sand level in the gravel bed. These relationships are derived by focussing on *how* the fluid shear stress varies with the sand level η_s in the gravel framework by referring to available experimental observations.

It is convenient to normalize the sand bed elevation η_s with a measure of the elevation range occupied by most of the gravel particles in the bed. For this reason the quantity $\eta_s/6\sigma_d$ will be used in the following. The variability of the shear stress throughout the interfacial sublayer links two limits cases: when $\eta_s/(6\sigma_d)$=1 the bed is composed by homogeneous sand spheres with radius equal to r_s, when $\eta_s/(6\sigma_d)$=0 the bed is composed by homogeneous gravel particles whose elevations with respect to a reference level is represented by the roughness geometry function $\mathcal{A}[(\eta_s/(6\sigma_d)]$. Figure 2.9 represents the superficial spatially-double averaged shear stress measured by *Mignot et al.* (2008) at differen heights within the roughness layer over a gravel bed identified by the roughness geometry function $\mathcal{A}$ plotted with a solid red line. Other geometrical characteristics of this gravel bed are reported in the caption of Figure 2.11.

The shape of the vertical distribution of the spatially-averaged measured shear stress in Figure 2.10 rather closely matches that of the roughness geometry function describing the properties of the experimental gravel bed in *Mignot et al.* (2008). This suggests a relatively simple functional relationship to quantify the vertical variability of spatially-averaged shear stress in rough gravel beds. Such relationship can be put in dimensionless form, where the shear stress can be conveniently normalized with the commonly used factor ρu_*^2. It reads:

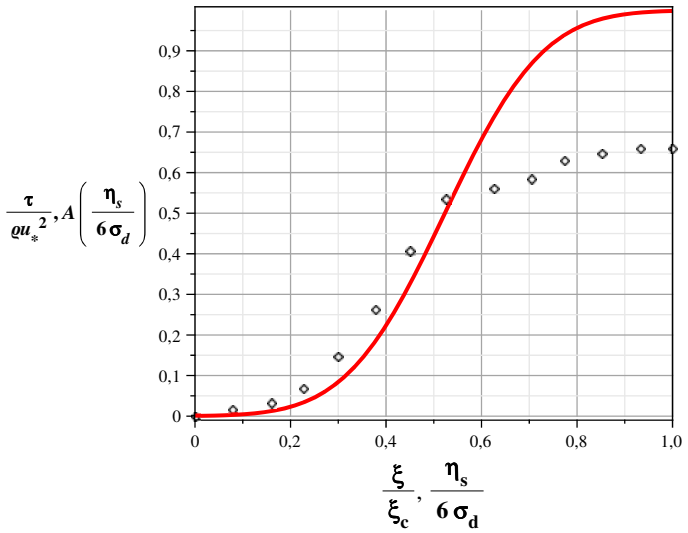

Figure 2.9: The black points refer to the superficial double averaged shear stress τ in *Mignot et al.* (2008). The red line refers to the roughness geometry function $\mathcal{A}(\eta_s/(6\sigma_d))$ in *Mignot et al.* (2008) and represented also in Fig.(2.11).

$$\begin{aligned} \tau_s^* &= \frac{\tau_s}{\rho u_*^2} = 0.6607(1-\zeta^*) && (2.52)\\ &= 0.6607 \cdot CDF[N(\mu_b, \sigma_d)] && (2.53)\\ (\mu_b, \sigma_d) &= (3.1cm, 9.7 \cdot 10^{-1} cm) \end{aligned}$$

where $CDF[N]$ is the cumulative distribution function referring to a Gaussian distribution of the rough bed elevations with mean μ_b and standard deviation σ_d.
Eq. (2.52) refers to the limit configuration of a clean gravel bed. Of course the value 0.66 is actually depending on the mean (uniform) flow conditions and channel geometry. For the mixed case, when sand is present into the gravel bed (i.e. $\eta_s > 0$), the experimental observations on sand bedload transport by Wilcock and Kentworthy provide useful indications on how to express the functional relationships (2.45, 2.46)

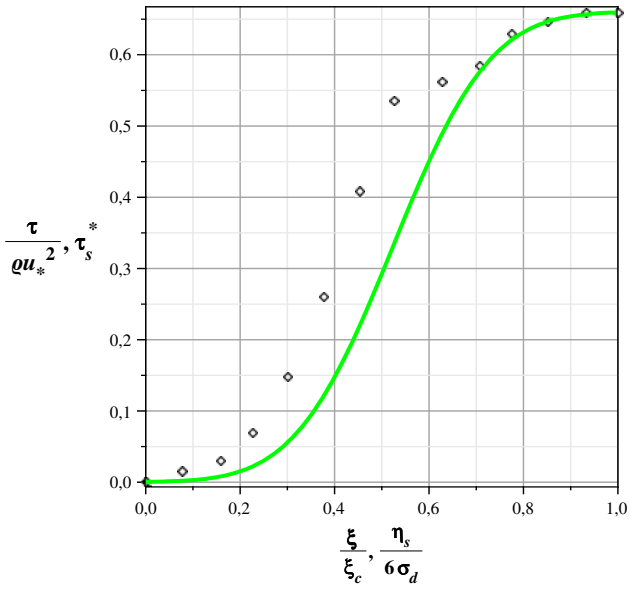

Figure 2.10: The black points refer to the superficial double averaged shear stress τ in *Mignot et al.* (2008). The green line represents the superficial double averaged shear stress τ_g^* as a function of $\mathcal{A}(\eta_s/(6\sigma_d))$ represented also in Figure 2.11.

Wilcock and Kenworthy (2002) predicted the Shields stress for incipient motion (i.e. τ_{ri}) relative to the sand and gravel fraction. Specifically for the sand fraction they propose:

$$\theta_{rs}^* = \frac{\theta_{rs}}{(\theta_{rs})_1} = (1 + \Theta \exp^{-14.\mathcal{A}(\eta_s)}) = (1 + \Theta F(\eta_s)) \tag{2.54}$$

where $(\theta_{rs})_1$ is a reference value for the Shields stress for incipient motion of sand fraction in the case of well-sorted, homogeneous sand bed and Θ represents the Shields stress required for the entrainment of the gravel fraction when the sand is largely hidden among the pores of the gravel grains, i.e. when $\eta_s \simeq 0$.

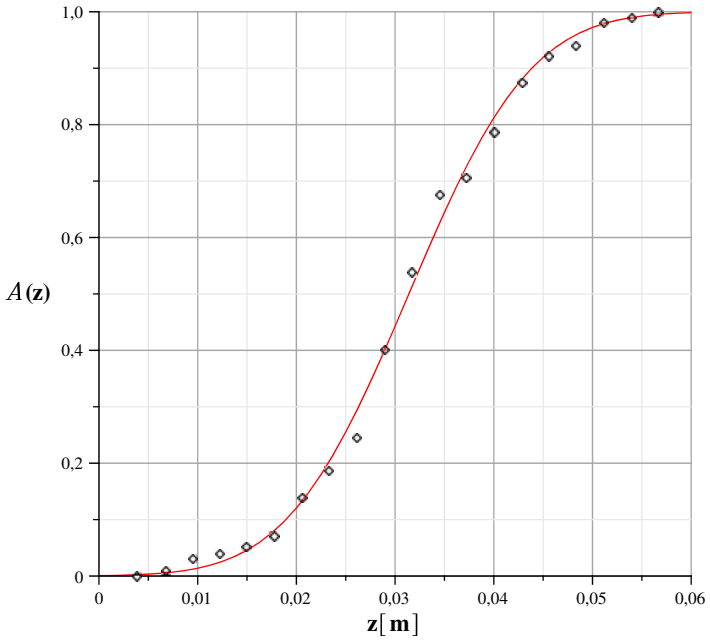

Figure 2.11: Roughness geometry function $\mathcal{A}(z)$ for Case 1 in *Mignot et al.* (2008), the red line represents a Gaussian CDF, with mean bed elevation μ_b=3.1 cm and standard deviation σ_d=9.7·10^{-1} cm, the black dots represent the measured bed elevation respect to a reference level

Following the general dependencies (2.45, 2.46), it can be written :

$$\Theta = f\left(\frac{l_g}{d_s}, \frac{d_g}{\langle D_0 \rangle_s}\right) = f\left(\alpha \frac{d_g}{d_s}, \Delta\right) \tag{2.55}$$

$$F(\eta_s) = f\left(\frac{\sigma_d}{d_g}, \langle \gamma_i \rangle_s, \eta_s\right) \tag{2.56}$$

where the length scale l_g has been defined previously in the Eq.(2.39), Δ is the relative flow submergence for incipient entrainment of gravel particles and the parameter α is an appropriate constant that *Wilcock and Kenworthy* (2002) assumed to be of order one for the specific case in which the characteristic diameter d_g and d_s refer to surface rough bed elements composition. Specifically d_g and d_s can be represented by the d_{50} or d_{90} of the surface grain size distribution of the two sediment fractions .

Typical values for the function Θ in (2.55) for incipient sand entrainment are reported in *Wilcock and Kenworthy* (2002). The function Θ can be written as:

$$\Theta = \frac{(\theta_{rs})_0 - (\theta_{rs})_1}{(\theta_{rs})_1}, \quad (\theta_{rs})_0 = \alpha(\theta_{rg})_0 \frac{d_g}{d_s} \tag{2.57}$$

where θ_{rs} refers to the Shields stress for incipient sand and the subscript refers to the sand level. Namely the subscript "0" indicates a nearly vanishing sand content into the gravel bed ($\eta_s^* = 0$) while the subscript "1" indicates a full sand cover ($\eta_s^* = 1$).
It is noteworthy that the Shields stress for incipient movement of gravel fraction θ_{rg} is proportional to the ratio between the two diameters that have been chosen as representative for each fraction. This is basically a consequence of the definition of the Shields stress and may also put in relationship with the fact that the drag forces in the interfacial sublayer are proportional to the particle surface.
The function $F(\eta_s)$ in (2.56) expresses an empirically detected global variation of the effective shear stress for sand movement within a variably sand-covered gravel layer. Besides its empirical derivation, we aim here at disclosing the possible physical effects that contribute to such variation with the relative sand content into the gravel bed and with other possibly relevant parameters. As a first approximation it is reasonable to assume that, in general, the function F may depend also on the typical geometrical scales characterizing the gravel bed structure, both in the average bed-parallel and bed-orthogonal directions. These can be therefore expressed through the parameters σ_d and $< \gamma_i >_s$, where σ_d is the standard deviation of the bed elevations and $\langle \gamma_i \rangle_s$ is an appropriate parameter for the measure of the areal close-packing of the roughness elements in the plane coordinates x, y, referring to a characteristic area A_0. Assuming in Eq.(2.50) a log-normal CDF for the function $P(z > z_0)$ with the statistical and geometrical characteristics reported in Tab.2.4 (*Aberle and Nikora* (2006)), the characteristic vertical dimension that affects the near-bed turbulent shear stress can be assumed to coincide with the bed particle protrusion function ζ already examined in its dimensionless form ζ^* in Eq.(2.51) for simple geometrical bed configurations.
Such dimensionless protrusion function ζ^* is plotted with red lines in Figure 2.12, where the function F is also reported with blue lines. The subscript 1 (solid line) or 2 (dot line) refers to the two bed configurations described in Tab.2.4. The horizontal axis refers to a dimensionless measure of the sand surface elevation, which has been conveniently normalized with a representative vertical scale of the gravel-bed surface. This vertical scale has been taken to coincide with six times the standard deviation of the gravel bed elevation distribution. Therefore the dimensionless coordinate $\eta_s/6\sigma_d$ ranges from 0 (absence of

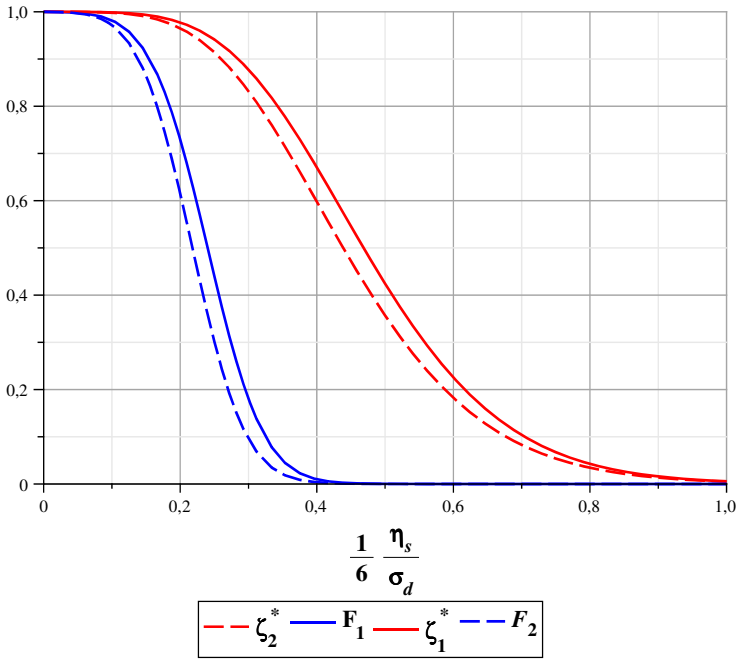

Figure 2.12: Protrusion function ζ^* as stated by Eq.(2.51) in red color and F function as stated by Eq.(2.56) in blue color. The subscripts 1 (solid line) and 2 (dot line) refer to the two bed configuration in Tab.2.4. The horizontal coordinate represents the ratio between the sand level in the interfacial sublayer η_s and the standard deviation σ_d of the bed elevations in the same sublayer.

exposed sand) to 1 (fully sand-covered bed).

It appears that the two protrusion-red curves are shifted with respect to the two pairs of F-functions.The sharp decrease of the blue curves in Figure 2.12 occurs when the sand level is in the range 0.1-0.4.

Wilcock and Kenworthy (2002) suggest that such relatively sharp, nonlinear variation of the sand-related Shields stress with the sand surface content in the gravel bed can be due to a combination of two key physical effects. The first is the role of gravel clasts that "protrude" out of the sand surface and determine a hiding effect on the sand particles lying on the portion of the sand surface that falls beneath the wakes created by the interaction between turbulent flow and the protruding gravel particles. The second, less obvious, physical effect is the tendency of the sand to "bridge" between gravel clasts and prevent

deeper percolation. This "bridge" effect allows the sand to congregate into patches on the bed surface and thus increases its relative ease to transport (*Wilcock and Kenworthy* (2002)). This therefore suggests that the sand content, i.e. η_s, controls the amount of sand available to be transported by the flow, and also influences the inherent mobility of the two different fractions (*Wilcock and Kenworthy* (2002)). It is interesting to point out that the above transition range corresponds to the transition from a framework gravel clasts to a sandy matrix bed, *sensuCarling and Reader* (1982).Following Wilcock and co-workers, f_s can be defined as the relative sand content in the bed, with $0 < f_s < 1$. This implies that the transition range occurs for $0.1 < f_s < 0.4$ (specifically $0.2< f_s <0.40$ for *Wilcock* (1998) and $0.1< f_s <0.30$ for *Wilcock and Kenworthy* (2002).
Figure 2.13 represents the sand volume function defined as:

$$f_s = \frac{V_s}{(V_s)_{tot}} = \int_0^{\eta_s^*} \mathcal{A}(\widehat{\eta_s^*}) d\,\widehat{\eta_s^*}, \quad \widehat{\eta_s^*} = \frac{\eta_s}{(4-6)\sigma_d} \tag{2.58}$$

where V_s is the volume of sand referring to that sand level η_s^* and $(V_s)_{tot}$ represents the total volume available to the sand deposition inside the gravel framework .
It is noteworthy that the derivative of the function f_s is *always* positive, differently for the derivative of the function $\mathcal{A}(z)$ that can be also equal to 0. Consequently, the last one has the geometrical characteristics to represent the transition behavior from the gravel framework to the sand matrix. As pointed out before, the sand level η_s^* controls not only the sand exposure to the flow entrainment, but also the volume of sand available to be transported by the flow. Therefore, these two effects mutually control the morphodynamics of sand bedforms in the mixed case because the sand level can be viewed as a measure of the sand supply-limitation in term of sand volume but also in term of sand exposure (*Kleinhans et al.* (2002); *Tuijnder et al.* (2009); *Tuijnder* (2010)).
Figure 2.12 represents just only one of the ingredients affecting the near-bed shields stress acting on the sand, since it accounts only for the protrusion ζ^* of the gravel fraction above the sand level. The other ingredient,i.e. the "bridge" effect and the patching phenomenon, can be quantified by conveniently relating the two pairs of curves shown in Figure 2.12. A reasonable option is to assume that the protrusion and the bridge effect can act somewhat independently, which leads to quantify the variation of the bridge effect with the sand surface elevation through the ratio between the functions F and ζ^*. The result are the functions κ_i where $(i = 1, 2)$ reported in Figure 2.14. Figure 2.14 represents the ratio κ

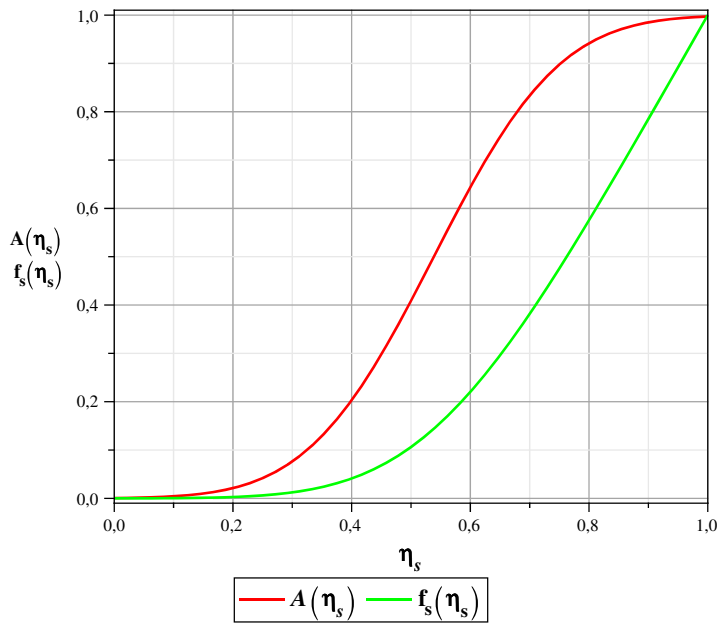

Figure 2.13: Sand volume function f_s as a function of sand level η_s computed with the roughness geometry function $\mathcal{A}(z)$ represented by solid red line with geometric characteristics as in *Mignot et al.* (2008)

between the function F and the protrusion ζ^* computed as follows:

$$\begin{aligned}
\kappa_1 &= \frac{F_1}{\zeta_1^*} = 1 - P[f_1(\zeta^*)] \\
&= 1 - \frac{1}{2} erfc\left[- \left(\frac{ln\left(\frac{\eta_s}{6(\sigma_d)_1}\right) + 1.4}{0.27\sqrt{2}} \right) \right] \\
\kappa_2 &= \frac{F_2}{\zeta_2^*} = 1 - P[f_2(\zeta^*)] \\
&= 1 - \frac{1}{2} erfc\left[- \left(\frac{ln\left(\frac{\eta_s}{6(\sigma_d)_2}\right) + 1.5}{0.28\sqrt{2}} \right) \right]
\end{aligned} \tag{2.59}$$

where $(\sigma_d)_1$ and $(\sigma_d)_2$ represent the standard deviations of rough bed elevation as reported in Tab.2.4 for case 1 and 2, respectively from Eqs. 2.59. It follows that the median value μ_{κ_i} of the function κ_i can be interpreted as an average measure of the sand surface level

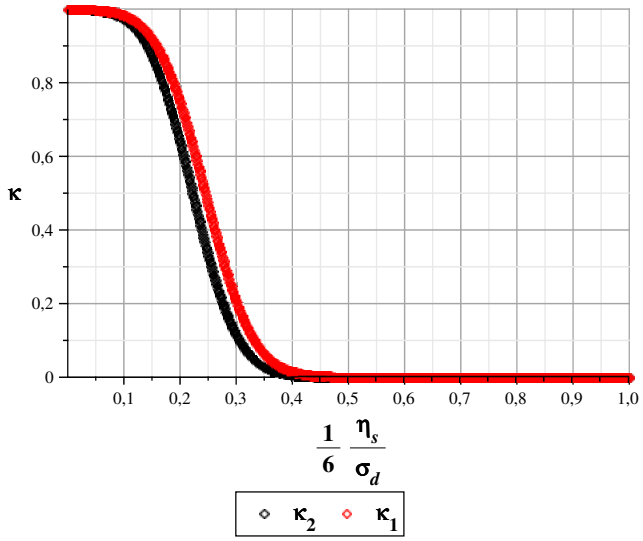

Figure 2.14: Ratio κ_1 and κ_2 relative to the two bed configuration in Tab.2.4. The horizontal coordinate represents the ratio between the sand level in the interfacial sublayer η_s and six times the the standard deviation σ_d of the bed elevations in the same sublayer.

below which the bridge effect quickly vanishes. The expected value μ_κ and the variance σ_κ of the variable η_s read as:

$$\begin{aligned} \mu_{\kappa 1} &= 1.5(\sigma_d)_1, \ \sigma_{\kappa 1} = 2.9 \cdot 10^{-2}(\sigma_d)_1 \\ \mu_{\kappa 2} &= 1.38(\sigma_d)_2, \ \sigma_{\kappa 2} = 2.59 \cdot 10^{-2}(\sigma_d)_2 \end{aligned} \tag{2.60}$$

Recalling *Wilcock and Kenworthy* (2002); *Wilcock* (1998) and *Wilcock* (1998) it appears (see also the bottom paragraph at page 43) that this level also nearly coincides with the mean bed elevation at which the transition from gravel framework clasts to sandy matrix occurs in the rough bed configurations with data reported in Tab.2.4. According to Eq.(2.60), this value is in the range 1.38-1.5 times the standard deviation of gravel bed elevations. The differences between the two mean values is likely due to the different ratio

Curve	d_{g50}, mm	d_{g84}, mm	d_{g50}/d_{s50}	d_{g84}/d_{s84}	σ_d, mm	S_k	K_u	Θ_{50}	Θ_{84}
1	13.6	28.7	9.0	15.5	6.3	0.6	3.3	3.84	7.34
2	25.0	48.8	16.6	26.3	12.6	0.7	3.4	7.9	13.16

Table 2.4: Statistical and geometrical characteristic for a gravel bed made of with a two coarse sediment mixtures with 2 mm $< d_g <$ 64 mm and sand fraction 0.5 mm $< d_s <$ 2 mm.The data for the gravel fraction have been taken from *Aberle and Nikora* (2006), where S_k,K_u and σ_d are the skewness, the kurtosis and the standard deviation of bed elevation, respectively. The incipient values for the gravel and sand fraction are reported by *Wilcock and Kenworthy* (2002),assuming that the reference dimensionless transport rate is equal to 0.002

between the gravel diameter and sand diameter as suggested by *Wilcock and Kenworthy* (2002), because the diameters ratio can be view as a measure of the sand diameter capability to bridge the space between two gravel particle close to each other with reference diameter, preventing any other sand percolation.
It is now useful to summarize the main outcome of analysis of the physical effects that can control the variation in the sand-related Shields stress with the sand surface elevation η_s. From Eq.(2.56), it follows that:

$$F(\eta_s) = \underbrace{\underbrace{\zeta^*(\eta_s)}_{\text{"Hiding" effect}} \cdot \overbrace{\kappa(\eta_s)}^{\text{"Bridge" effect}}}_{\text{Geometrical effect}} \tag{2.61}$$

Eq. 2.61 is a key relationship stating that variation with the sand surface level of the energy expenditure required by the flow to move the sand particles is basically related to the two physical effects of "hiding" and of "bridging", which can be quantified through (2.50) and (2.59) respectively. This has been derived on the basis of experimental estimates of the reference shear stress for sand transport, which variability is an indicator of the energy that is absorbed by gravel particles protruding out of a sand surface. The F function (2.61) together with (2.50) and (2.59) quantifies such variability and therefore provides an indirect estimate of how the spatially-averaged near bed shear stress changes with different values of the sand level η_s.
Since in the mixed case the "bridge" effect has consequences on the distributions of the shear stress in the interfacial sublayer as stated by (2.61), then (2.52) follows as:

$$\tau_s^* = \frac{\tau_s}{\rho u_*^2} = 0.6607 \cdot (1 - \zeta^* \cdot \kappa_N) \tag{2.62}$$

$$\tag{2.63}$$

where κ_N depends on the CDF of the probability distribution of rough bed elevations as follows:

$$\kappa_N = 1 - CDF(\mu_d, \sigma_d, \eta_s, \frac{d_g}{d_s}), \tag{2.64}$$

with μ_d is the mean rough bed elevation and σ_d the standard deviation of rough bed elevations.
In a general case, following (2.55,2.56), τ_s^* can be rewritten as follows:

$$\begin{aligned} \frac{\tau_s}{\rho u_*^2} &= \Theta\left(\frac{d_g}{d_s}, \frac{\langle D_0 \rangle_s}{(4-6)\sigma_d}\right) && (2.65) \\ &\cdot \left(1 - F\left(\frac{\mu_b}{(4-6)\sigma_d}, \frac{\eta_s}{(4-6)\sigma_d}\right)\right) && (2.66) \end{aligned}$$

Considering the function $\mathcal{A}$ as in the specific case of *Mignot et al.* (2008), then $\mathcal{A}$, κ and protrusion ζ^* take the following expression:

$$\begin{aligned} \mathcal{A}\left(\frac{\eta_s}{6\sigma_d}\right) &= CDF[N(0.51, 1.61 \cdot 10^{-1}, \eta_s, 31)] && (2.67) \\ \zeta^* &= 1 - \mathcal{A}\left(\frac{\eta_s}{6\sigma_d}\right) \\ \kappa\left(\frac{\eta_s}{6\sigma_d}\right) &= 1 - CDF[N(0.24, 1.6 \cdot 10^{-2}, \eta_s, 31)] \end{aligned}$$

Figure 2.15 represents the function F when the roughness geometry function has the geometric characteristics as in *Mignot et al.* (2008) (see Figure 2.11) and assuming $d_g/d_s = 31$.
On the basis of the above reasoning, it is now possible to derive a physically-based quantitative expression for the dependence on the sand surface properties of the spatially-averaged vertical velocity profile and of the near-bed turbulence related quantities z_c, λ_0 that was initially assumed through (2.45, 2.46). First of all a shifted vertical coordinate ξ is introduced, such that its origin coincides with the mean elevation of the sand surface.
The streamwise velocity profile in Eq.(2.44) in the new coordinate system (x, ξ) can be written as follows:

$$\langle \overline{U} \rangle^* = \frac{1}{k} ln\left(\frac{\xi - 0.43\xi_c}{\lambda_0}\right) \quad \text{for } \xi \geq \xi_c \tag{2.68}$$

where ξ_c represents physically the protrusion of gravel elements above the sand level η_s:

$$\xi_c = \zeta^* + \frac{d_s^*}{2}; \tag{2.69}$$

with d_s^* the dimensionless sand sphere diameter. The dimensionless roughness height λ_0^*

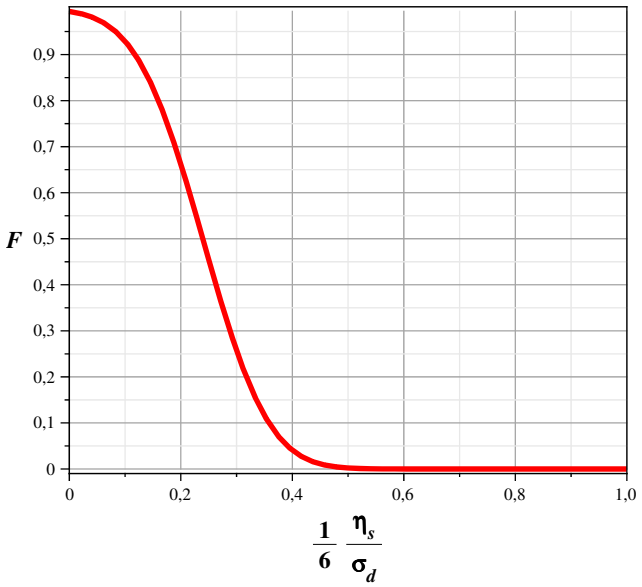

Figure 2.15: Function F with A as in Figure 2.11

takes into account the transition from gravel framework to sand matrix, i.e. λ_0^* is a function of F as follows:

$$\lambda_0^* = f\left[F\left(\frac{\mu_b}{(4-6)\sigma_d}, \frac{\eta_s}{(4-6)\sigma_d}, \frac{d_g}{d_s}\right)\right] \tag{2.70}$$

$$\eta_s^* = \frac{\eta_s}{6\sigma_d} \leq (0.4 \div 0.5) \Longrightarrow gravel\ framework \tag{2.71}$$

$$\eta_s^* = \frac{\eta_s}{6\sigma_d} > 0.5 \Rightarrow \lambda_0^* = f\left[\frac{d_s^*}{2}\right] \Rightarrow sand\ matrix \tag{2.72}$$

Considering the gravel framework as in the specific case of the experimental condition of *Mignot et al.* (2008) (see Figure 2.11), so that the flow submergence is $\langle D_0\rangle_s/(6\sigma_d) = 4.1 = \Delta$, and considering the data in Tab.2.2, we have:

$$\lambda_0^* = 1.8 \cdot 10^{-1}\Delta^{-1}F + 1.7 \cdot 10^{-2}\frac{d_s^*}{2}\Delta^{-1} \tag{2.73}$$

$$\xi_c^* = \zeta^* = \left\{1 - \mathcal{A}\left(\frac{\eta_s}{6\sigma_d}\right)\right\}\Delta^{-1} + \frac{d_s^*}{2}\Delta^{-1} \tag{2.74}$$

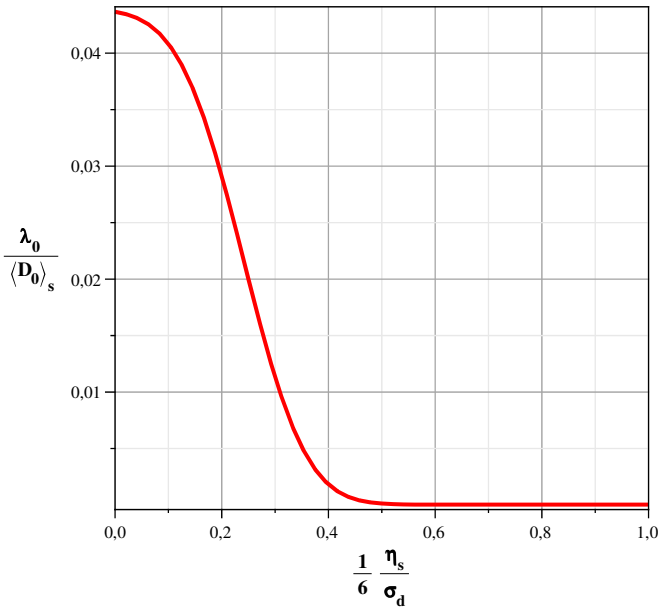

Figure 2.16: Roughness height λ_0^* as function of sand level as stated by Eq.(2.73)

Figure 2.16 and Figure 2.17 represent the roughness height λ_0^* and protrusion $\zeta^* = \xi_c^*$ as a function of $\eta_s/(6\sigma_d)$.

Equations (2.73, 2.74) are the final outcome of the procedure that is herein proposed to quantify the assumed dependencies (2.46). The sequence of operations described above illustrate how these dependencies can be quantified using relatively simple properties of the gravel bed (first and second moments of the bed elevation distribution function, together with a representative grain size) and of the sand layer (its height and a representative grain size). From the quantification of z_c, λ_0 in mixed sand-gravel beds (with immobile gravel) it is relatively straightforward to derive suitable relationships for the spatially-averaged velocity profiles and the friction coefficient that can be used as closures in hydrodynamic and morphodynamic models.

Figure 2.18 represents the streamwise velocity profile for different values of the sand level η_s in the "logarithmic" layer, above the level ξ_c, with the parameterizations (2.73) and (2.74), where $d_s^* = d_s/(6\sigma_d)$.For all profiles the value of the water depth and of

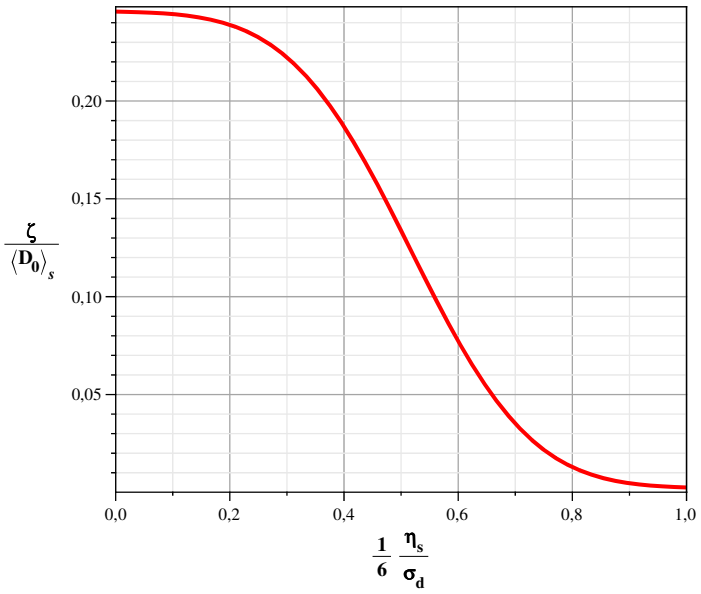

Figure 2.17: Protrusion ζ^* as a function of sand level as stated by Eq.(2.74)

the longitudinal channel slope have been kept constant. As it can be expected, reduced sand surface elevations are associated with higher near-bed friction and therefore reduced velocity. Because the longitudinal slope and depth are constant for all profiles, increasing sand elevation in the plot is associated with a reduction in the flowing discharge.
The dimensionless Chezy coefficient is defined through its conventional expression:

$$\begin{aligned} C^*(\eta_s^*) &= \frac{C}{\sqrt{g}} = \frac{\langle \overline{U} \rangle_s}{\langle u_* \rangle_s} = \frac{F_r}{\sqrt{i_f}}. \\ \langle \overline{U} \rangle_s &= \int_{\xi_c^*}^{1} \langle \overline{U(z^*)} \rangle_s dz^*, \quad z^* = \frac{z}{\langle D_0 \rangle_s}, \quad \langle D_0 \rangle_s = z_{ws} - \langle \eta_s \rangle_s; \\ \langle u_* \rangle_s &= \sqrt{g i_f \langle D_0 \rangle_s}. \end{aligned} \tag{2.75}$$

In (2.75) i_f represents the mean bed slope of the gravel framework and the mean stremwise velocity $\langle \overline{U} \rangle_s$ has been computed trough the integral between the level ξ_c and the water surface.Recalling (2.75), different values of η_s are associated with different values of

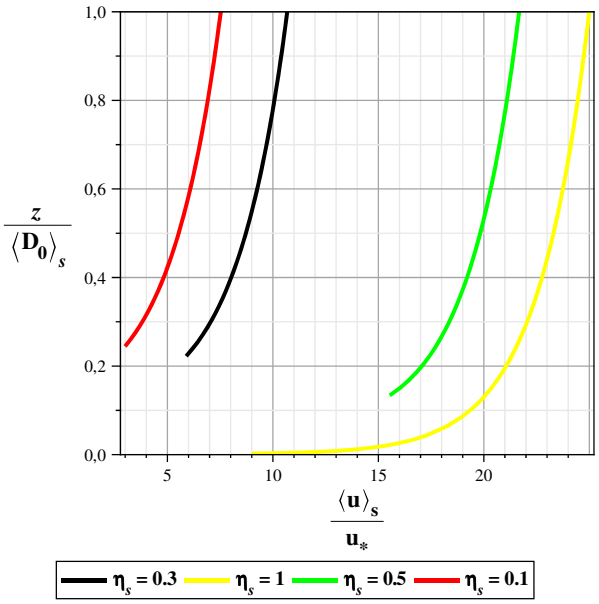

Figure 2.18: Spatially-averaged streamwise velocity profile above the level ξ_c, for different sand level values with parameter indicate in (2.73) and (2.74).

the dimensionless Chezy coefficient, which is indirectly represented in Figure 2.16 because $i_f = Fr^2/C^2$. When the sand surface occupies most of the bed surface the bed is much smoother than for lower values of η_s: therefore smaller slope values are required to produce the same hydraulic conditions represented by the same Froude number Fr. Figure 2.19 represents the mean bed slope i_f and Froude number F_r as a function of sand elevation in the gravel matrix η_s.

The vertical variability of the dimensionless Chezy number as with sand level inside the gravel framework is represented in Figure (2.20). It is noteworthy that the dimensionless Chezy reflects the transition region of the gravel framework when sand fraction is present, because most of its variation occurs for η_s^* between 0.3 and 0.6.

The only available experimental data to test the hydrodynamic closures proposed in the present Chapter are those of *Wren et al.* (2011). In the following a preliminary comparison with their data is attempted with the aim to make a first test of the present closure submodel against data that have been collected independently from those on which its

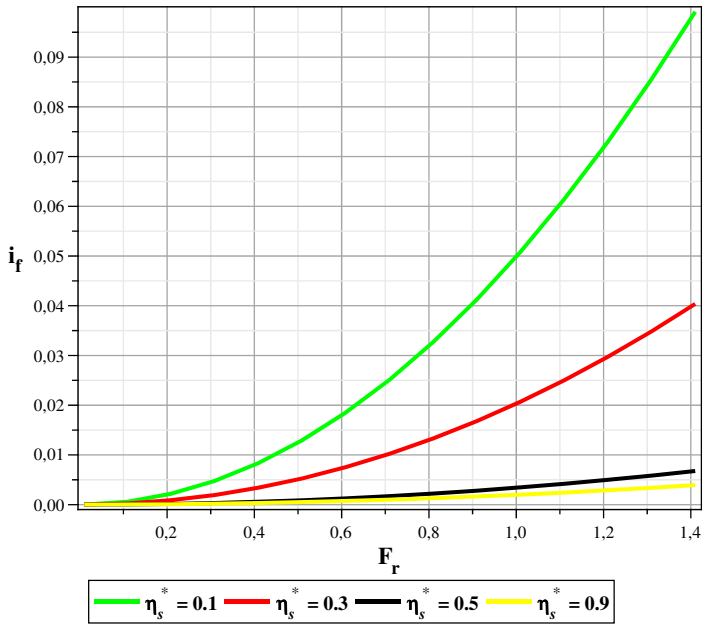

Figure 2.19: Relationship between the mean bed slope and the Froude for different values of the sand level η_s^* for flow submergence $\Delta = 4.1$ (data as in *Mignot et al.* (2008))

derivation is based.

Wren et al. (2011) measured the changes in flow and turbulence proprieties caused by sand ($d_{s50} = 0.3$mm) added to an immobile gravel bed with $d_{g50} = 35$ mm. Tab.2.5 reports the hydraulic data for the bed configuration Case 1 in *Mignot et al.* (2008) and for several runs in *Wren et al.* (2011), where the minimum sand level in gravel framework assumes the value $\eta_s/(6\sigma_d) = 0.5$ (i.e. $0.5 \leq \eta_s/(6\sigma_d) \leq 0.92$) and $6\sigma_d = 5.5cm$.

Wren et al. (2011) estimated the bed shear stress with three different methods: from spatially-averge velocity profiles, from Reynolds shear stress projection and with the relationship $\tau = \rho g i_f \langle D_0 \rangle_s$ also taking into account the wall corrections. In this way it has been possible to characterize the variability of the absolute bed shear stress value when the sand is present in the gravel framework. Specifically, *Wren et al.* (2011) found that for 65 and 50 l/s flow discharge there is a 2-3 Pa spread in bed shear stress estimated from the three methods, which represents a range of about 25%-50%, although all three methods generally follow similar trends. Moreover, the mean difference between the depth-slope

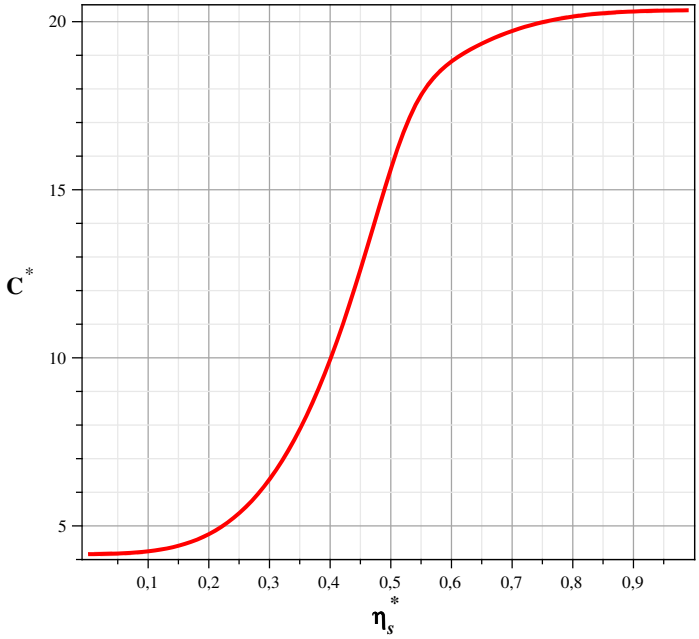

Figure 2.20: Dimensionless Chezy number as a function of η_s^* for flow submergence $\Delta = 4.1$ (*Mignot et al.* (2008)

shear stress estimator and that based on the Reynolds stress projection across all flow discharges was 20%.

Wren et al. (2011) considered sand level values well above the transition range between gravel framework and sand matrix (*Wilcock and Kenworthy* (2002); *Wilcock* (1998)), so that we assume, for consistency with the proposed relationship that the roughness height λ_0 is represented by the radius of the sand grain and the level ξ_c remains constant and equal to the value for homogeneous case reported in the Tab.2.1.
Therefore, assuming that the roughness height λ_0 is a function of the radius of the sand grain in the range $0.5 \leq \eta_s/(6\sigma_d) \leq 0.92$, then we can determine by the Eq.(2.75) a mean value of equivalent sand grain for taking into account the variability of the hydraulics conditions with sand level η_s^* as stated by the experimental data od *Wren et al.* (2011) and reported in Tab.2.5. Considering experimental data for 50-60 l/s then we can find a mean equivalent sand radius equal to 5.86 times the radius of an equivalent sand sphere, with a standard deviation of 1.19 times the radius of an equivalent sand sphere r_s.It has

Case	u_*^2 $[ms^{-1}]$	F_r	i_f [%]	$\frac{\eta_s}{(6\sigma_d)}$	$\frac{\langle D_0 \rangle_s}{d_{g50}}$	$\overline{Q}$ [l/s]	E.S.R. $[r_s^*]$	Mean E.S.R. $[r_s^*]$	σ_d E.S.R. $[r_s^*]$
	0.082	0.45	0.38	0.5	6.28	50	7.06		
	0.072	0.45	0.30	0.7	6.28	50	4.24		
	0.070	0.42	0.28	0.78	6.28	50	6.83		
	0.081	0.48	0.39	0.85	6.28	50	5.39		
	0.071	0.46	0.31	0.92	6.28	50	5.48	5.86	1.19
Wren[a]	0.082	0.55	0.59	0.5	6.28	60	7.52		
	0.072	0.59	0.47	0.7	6.28	60	7.53		
	0.070	0.57	0.48	0.78	6.28	60	4.65		
	0.081	0.59	0.49	0.85	6.28	60	5.01		
	0.071	0.62	0.53	0.92	6.28	60	4.85		
Mignot[b]	0.053	0.46	0.2	0	7.93	40			

Table 2.5: Comparison between two hydraulic configuration in two different study: [a] *Wren et al.* (2011); [b] *Mignot et al.* (2008); E.S.R. stands for Equivalent Sand Radius and $r_s^* = r_s/\langle D_0 \rangle_s$ and $r_s = r_{s50} = 0.15mm$ as in *Wren et al.* (2011).$\overline{Q}$ is the mean flow discharge

been assumed that r_s is equivalent to the $r_{s50} = 0.15mm$ of *Wren et al.* (2011).In Tab.2.5 are reported for each experiment the equivalent sand radius sphere for characterising the roughness height λ_0, having assumed that the level ξ_c remains constant and equal to the $r_{s50} = 0.15mm$ as stated by the homogeneous conditions in Tab.2.1.

Figure 2.21 refers to a comparison between the Eq.(2.75) for different sand level and the experimental data from *Wren et al.* (2011). It is noteworthy that the computed equivalent sand sphere radii have a variability of about 20 % with respect to the averaged value of equivalent sand sphere radius, representing the absolute mean variability between the depth-slope shear stress estimator and Reynolds stress projection across all flow discharge.

2.5.1 Bedload transport of sand over an immobile gravel bed

Prediction of bedload transport rate in response to different flow and bed conditions is a key step in building a morphodynamic model. The present work focuses on the transport of sand occurring over a gravel bed that keeps at rest, i.e. under hydrodynamic conditions which cannot entrain the gravel particles. Moreover conditions under which the sand is mainly transported as bedload are considered, although extension to the case of dominant suspended load would be relatively straightforward (see *Grams and Wilcock* (2007) for a possible options to correct classical approaches for homogeneous sand conditions).

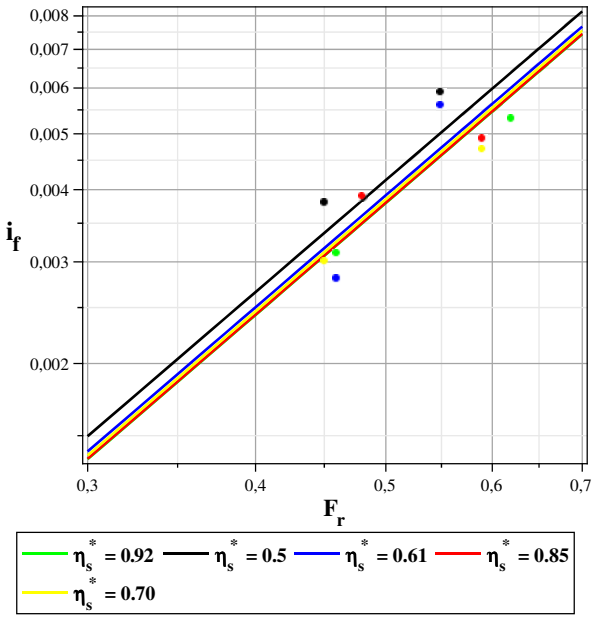

Figure 2.21: The different solid lines are function of the sand level η_s^* and refer to the Eq.(2.75), while the solid circles refer to the experimental data form *Wren et al.* (2011).

Typical predictors of bedload rates typically require the computation of the near-bed shear stress, i.e. that value of the shear stress that is effective for sediment entrainment and transport, and the specification of a threshold value below which sediment transport does not occur. The aim of the present Section is to propose a physically-based relationship for sand bedload transport over an immobile gravel bed by investigating how these two parameters (near-bed and critical shear stress) can be expected to change with the level of the sand surface beneath the gravel particles and with the sand-to-gravel diameter ratio. Before proceeding with the analysis an important specification is in order. To the Author's knowledge, only one sand bedload predictor over immobile gravel beds has been proposed so far by *Tuijnder* (2010). This predictor has been derived on the basis of a comprehensive set of laboratory experiments on the formation of sand bedforms over immobile gravel. Its key characteristic is the ability to account for the additional frictional effect induced by the presence of the sand bedforms on the near-bed shear stress and therefore on the bedload rate. The experimental outcomes allow to build empirically-based relationships

that quantify the variation of bedform geometry (height, wavelength) in dependence of the sand layer properties.
The analysis proposed herein is somewhat complementary to that performed by *Tuijnder* (2010). Coherently with the aim of the present Ph.D. research, the relationships that are proposed within this Section seek to quantify sand bedload rates at a "local" scale, smaller than that to which the analysis of *Tuijnder* (2010) is referred. Indeed the bedload predictor that will be proposed in the following is based on a spatially-averaged approach , where the horizontal scale for the spatial averaging procedure is defined through the loss of "spatial memory" by means of high-order structure functions of the bed elevation . Such scale is of the order of the d_{90} of the gravel bed grain size distribution. Also the sand bedload predictor proposed by *Tuijnder* (2010) is intrinsically spatially-averaged, but on a much larger averaging scale, which order of magnitude is basically the sand bedform wavelength. The properties of sand bedforms are therefore part of the input data needed for bedload rate computation and cannot be predicted with a morphodynamic model that implements the bedload relationship of *Tuijnder* (2010). Since one of the purposes of the present Ph.D work is to develop a mathematical model able to predict the morphodynamics of sand bedforms over immobile gravel beds at different scales, including that of sand dunes, a complementary approach to bedload prediction is therefore required.
The analysis illustrated in the previous Section has set the basis for the evaluation of the near-bed and for the critical shear stress for bedload movement. The fluid shear stress τ represents the maximum value of the fluid shear stress computed at $\xi = \xi_c$; above $\xi = \xi_c$ a linear behavior of the shear stress has been assumed and the streamwise velocity is represented by the log-law. Moreover the proposed relationship allow to quantify the variability of the shear stress throughout the interfacial sublayer as function of the rough bed elements protrusion and of the "bridge" phenomenon.
Wilcock and Kenworthy (2002) have developed a two-fraction (sand and gravel) transport model using a similarity collapse of the transport rate of the sand and the gravel fractions as stated by Eq.(2.81). Specifically,

$$W_{bs}^* = f\left(\left\langle \frac{\theta_s}{\theta_{rs}} \right\rangle_s\right) \tag{2.76}$$

$$= \begin{cases} 0.002\Theta_s^{7.5} & \Theta_s = \left\langle \frac{\theta_s}{\theta_{rs}} \right\rangle_s \quad \text{if } \Theta < \Theta'_s \\ \Gamma\left(1 - \frac{\chi}{\Theta_s^{0.25}}\right) & \Theta_s = \left\langle \frac{\theta_s}{\theta_{rs}} \right\rangle_s \quad \text{if } \Theta_s \geq \Theta'_s \end{cases} \tag{2.77}$$

where θ_s is the Shields stress acting on the sand fraction. The fitting parameters of the sand fraction sediment discharge function W_{bs}^*, are reported in Tab.2.6(*Wilcock and*

Table 2.6: Parameters for the sediment discharge function W_{bs}^*.

Type of data	Γ	χ	Θ_s'
Laboratory data	70	0.908	1.19
Field data	115	0.923	1.27

Kenworthy (2002)).

As pointed out before in the mixed case of two fraction bed composition (i.e. gravel and sand fractions) the maximum value of shear stress depends on the sand level η_s by the geometrical variability of the incipient sand Shields stress, having estimated the reference value for the incipient bed load transport rate with respect to the maximum value of the shear stress. This means that, the latter has to be greater than the threshold for sand particles motion as also indicated in the analysis of *Coleman and Nikora* (2008), precised for the mixed case where the sand particles move as a bed load in a gravel framework (*Carling and Reader* (1982)).

The closure relationship for the shear stresses in the mixed case,proposed in the previous section, is reviewed referring to Fig. 2.23 and 2.22, referring to the mixed configuration when sand fraction is present in the gravel framework.

The orthogonal reference system (x, ξ) is shifted above the spatially-averaged sand level η_s so that all the physical variables that depend on the vertical coordinate are function of the new variable ξ. The qualitative behavior of the shear stresses and of the stream-wise velocity in Figures 2.23 and 2.22 graphycally represents the physical idea that the shear stress has to take into account the drag forces that the turbulent flow exert on the gravel elements in the interfacial sublayer. Therefore, in the limit case of sandy beds, i.e. $\eta_s/(4\sigma_d) \simeq 1$, panels d) of Figures 2.23 and 2.22 the shear stress are less comparable than the case depicted in the other panels of the same figures.

In order to exemplify the application of the predictor (2.76) to different values of the sand bed elevation an application is presented below referring to the experimental conditions of *Mignot et al.* (2008), where an ideal sand addition is simulated under mean uniform flow conditions.

Assuming that the gravel framework has the same geometric characteristics as in *Mignot et al.* (2008) and the ratio $d_g/d_s = 31$, Figure 2.30 represents the dimensionless shear stress $\tau_s^* = \langle \tau_s \rangle_s / (\rho \langle u_*^2 \rangle_s)$ acting on the sand fraction as a function of sand level $\eta_s^* = \eta_s/(6\sigma_d)$. The variability of the shear stress τ with respect to η_s plotted in Figure 2.30 has been

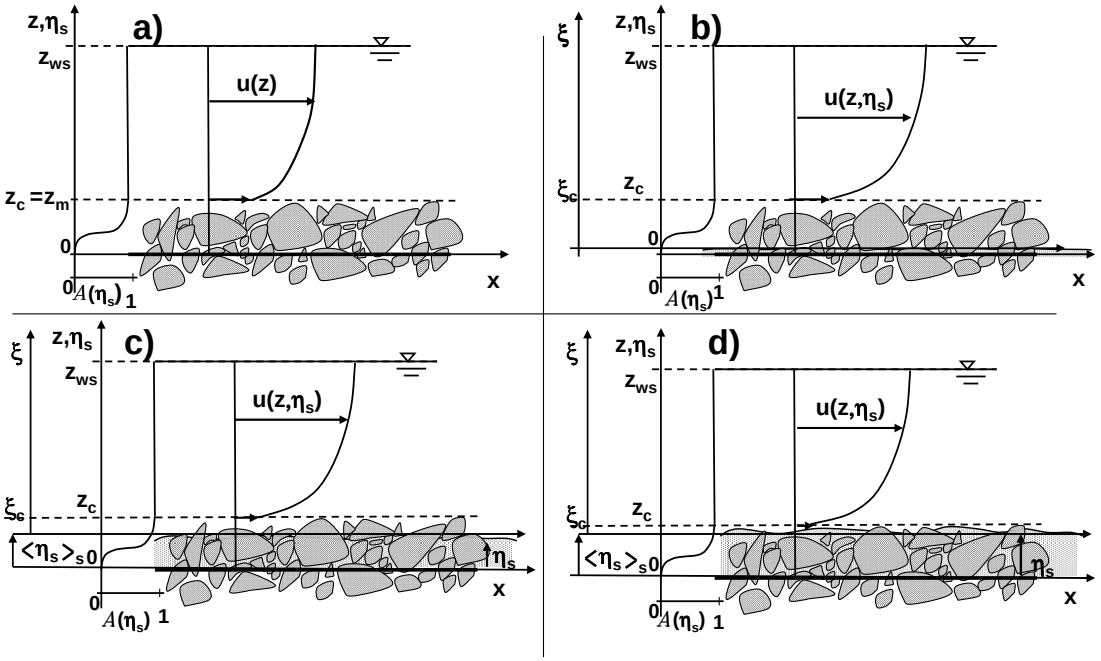

Figure 2.22: Sketch for independent variables notation for the logarithmic streamwise velocity above z_c. It has been assumed that the level z_m coincides with the level z_c. The orthogonal system (ξ, x) refers to a shifted orthogonal system above the spatial averaged sand level η_s.

computed through (2.65) and accounts for both the hiding and bridge effects detected above. It reflects the sharp transition between a gravel-framework and a matrix-supported sand bed, which occurs for relative sand surface elevation η_s^* between approximately 0.2 and 0.5.

Moreover, Figure 2.25 represents the ratio between the sand Shields stress $\langle\theta_s\rangle_s$ and the reference Shields stress for sand transport $\langle\theta_{rs}\rangle_s$ as a function of sand level η_s^*. Also from this ratio behavior it is possible to identify clearly the transition range between the gravel framework and the sand matrix from hydraulics point of view and with specific geometric gravel and sand characteristics.The reference Shields stress $< \theta_{rs} >_s$ has been computed through (2.54).
Since η_s varies between $\mathcal{A}(\eta_s) = 0$ and 1, then the moving sand is affected by a reference shear stress that depends on the distribution of the double-averaged shear stresses and on the drag forces as stated by Eq.(2.32), specifically in the above range of variability of

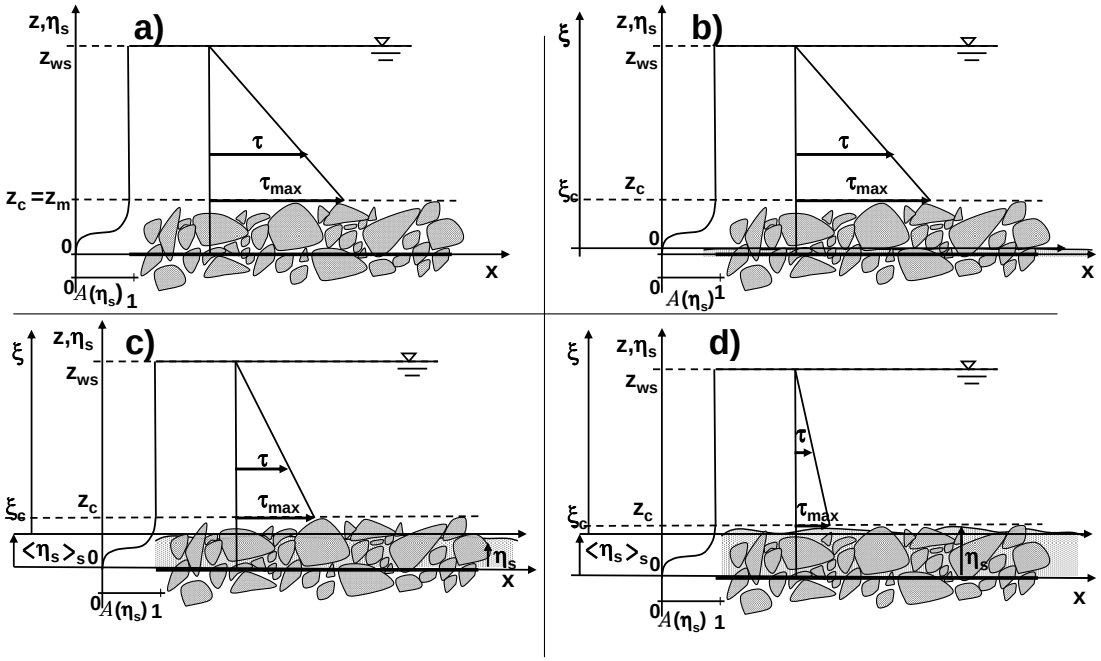

Figure 2.23: Sketch for independent variables notation for the shear stress in the logarithmic layer above z_c. It has been assumed that the level z_m coincides with the level z_c. The orthogonal system (ξ, x) refers to a shifted orthogonal system above the spatial averaged sand level η_s.

the function $\mathcal{A}(\eta_s)$, i.e. in the interfacial sublayer. Therefore, the reference shear stresses for moving sand has to take into account the energy loss due to the work done by the drag forces in the interfacial sublayer for the presence of the gravel particles. The energy loss due to the hydrodynamic fluctuating pressures and to the viscous surface drag forces (*Coleman and Nikora* (2008)) acting on the gravel particles surface, are comparable higher than the same forces acting on the sand particles surface, because the ratio between the two fraction diameters is much larger than unity. *Wilcock and Kenworthy* (2002) assumed for testing Eq.(2.54) values of d_g/d_s ratio corresponding to 10,20,35 and 50.
From Tab.2.4 and Eq.(2.54) , it follows that:

$$\theta_{rs} = O\left[\Theta_{n-th}(\theta_{rs})_1\right] \tag{2.78}$$

where Θ_{n-th} refers to the n-th percentile of the gravel grain size distribution in the in-

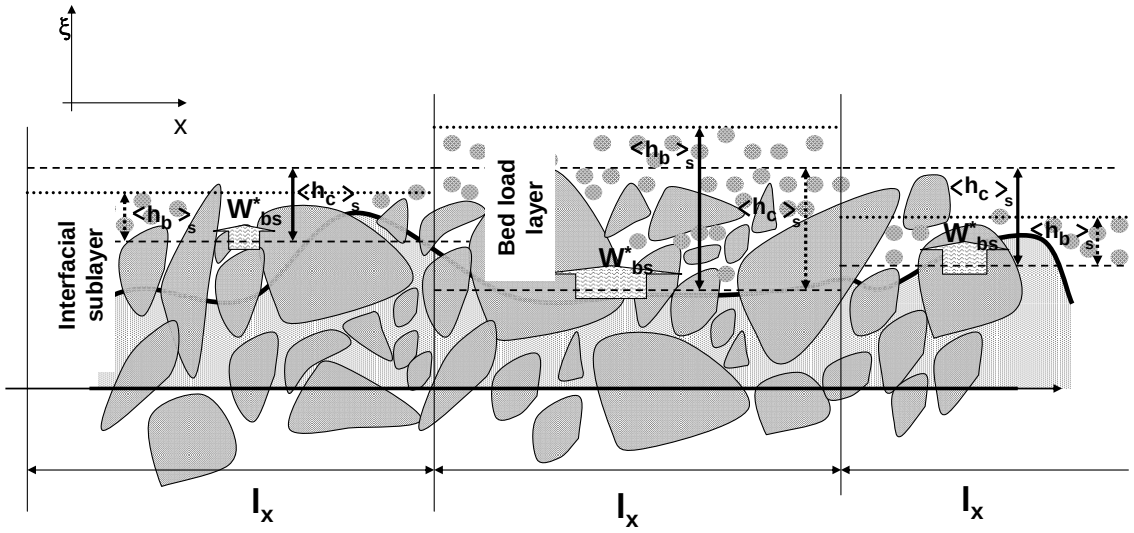

Figure 2.24: Sketch for bed load layer as a function of the thickness $\langle h_b \rangle_s$ that depends on the sand level η_s. The sand bed load transport rate W^*_{bs} refers to the Eq.(2.81) and l_x refers to a characteristic length scale in x-direction. In the figure is also reported the thickness $\langle h_c \rangle_s$ as a measure of interfacial sublayer functions of the sand level η_s.

terfacial sublayer. For the specific case show in the Tab.2.4, the reference shear stress for sand incipient motion spans in the range:

$$\theta_{rs} = 3 - 13(\theta_{rs})_1 \tag{2.79}$$

depending on the relative size of the sand diameter with respect to the gravel diameter and considering a reference bed load discharge (*Wilcock and Kenworthy* (2002)). It is noteworthy that *Wilcock and Kenworthy* (2002) implicity assumed that Eq.(2.79) refers to a spatial average for the reference sand Shields stress θ_{rs}, because its variability depends on the spatially-averaged sand area that is available to be transported by the flow, as Eq. (2.61) shows.More correctly, Eq.(2.79) can be written as:

$$\langle \theta_{rs} \rangle_s = 3 - 13\langle (\theta_{rs})_1 \rangle_s \tag{2.80}$$

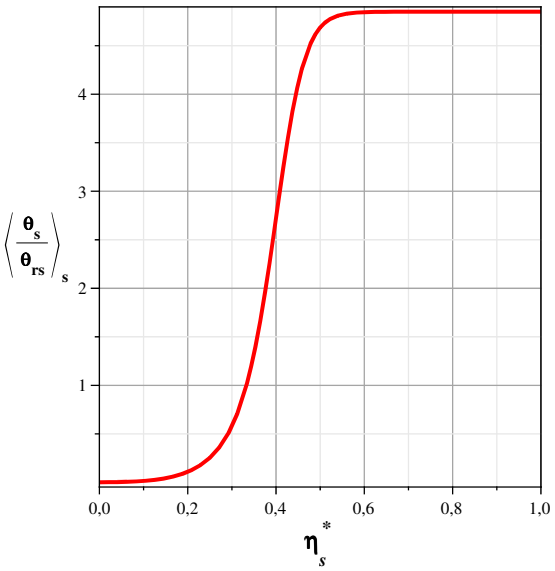

Figure 2.25: Ratio between the sand Shields stress and reference Shields stress (*Wilcock and Kenworthy* (2002)) $\left\langle \frac{\theta_s}{\theta_{rs}} \right\rangle_s$ for different sand level $\eta_s^* = \eta_s/(6\sigma_d)$.

Wilcock and Kenworthy (2002) found an empirical prediction for dimensionless bed load transport rate W_{bi}^* for the two fraction i, sand and gravel.The dimensionless bed load rate W_{bi}^* reads as:

$$W_{bs}^* = f\left(\left\langle \frac{\theta_i}{\theta_{ri}} \right\rangle_s\right) \tag{2.81}$$

where W_{bs}^* is the spatially-averaged volumetric sand transport rate per unit width of sand fraction . *Wilcock and Kenworthy* (2002) assumed that $\theta_s \geq \theta_{rs}$, i.e. $W_{bs}^* = 0.002$ as a reference sand bed load transport rate.
Eq.(2.81) can be explained in terms of orders of magnitude as follows:

$$O(W_{bs}^*) = O\left(\frac{\mathcal{A}\left(\frac{\eta_s}{4\sigma_d}\right)\langle u_*^3\rangle_s}{(r-1)g}\right) \tag{2.82}$$

where r is the ratio of sediment to water density, g is gravity acceleration, $\langle u_*\rangle_s = \langle(\tau/\rho_w)^{0.5}\rangle_s$ is the spatially-averaged shear velocity and τ is the shear stress at a reference level. It is noteworthy that *Wilcock and Kenworthy* (2002) assumed that the spatially-averaged shear stress acting on the sand fraction is simply proportional to the exposure area of the sand itself, so that the total shear stress τ is distributed among the two fractions by means of the roughness geometry function, as the numerator of Eq.(2.82) points out. *Wilcock and Kenworthy* (2002) estimated the total shear stress τ using the Einstein/Keulegan relation, where a specified value for the mean streamwise velocity, for the flume slope and for roughness height has been assumed constant and equal to $0.84d_{g90}$. Despite *Wilcock and Kenworthy* (2002) provided consistency with laboratory and field data, from the physical point of view the drag forces acting on the gravel elements as highlighted above do not seem to have been explicitly considered. In this regard, *Coleman and Nikora* (2008) pointed out that the Shields stress for particle entrainment is markedly influenced by the gradients in pressures in the interfacial sublayer. Specifically in the mixed case of sand and gravel at rest, the reference Shields stress for sand movement has to be increased because of the presence of gravel elements that potentially hide the sand fraction as stated by Eq.(2.61) and contribute to energy loss by the drag forces acting on the rough elements surfaces.
Neverthless, despite the two-fraction model of *Wilcock and Kenworthy* (2002) could be improved by an explicit incorporation of such effect, Eq.(2.61) still holds because it concerns the variability of the Shields stress with respect to the sand level and not the absolute Shields stress acting on one of the two fractions.

Figure 2.26 and Figure 2.27 represent the dimensionless sand transport rate W_{bs}^* as a

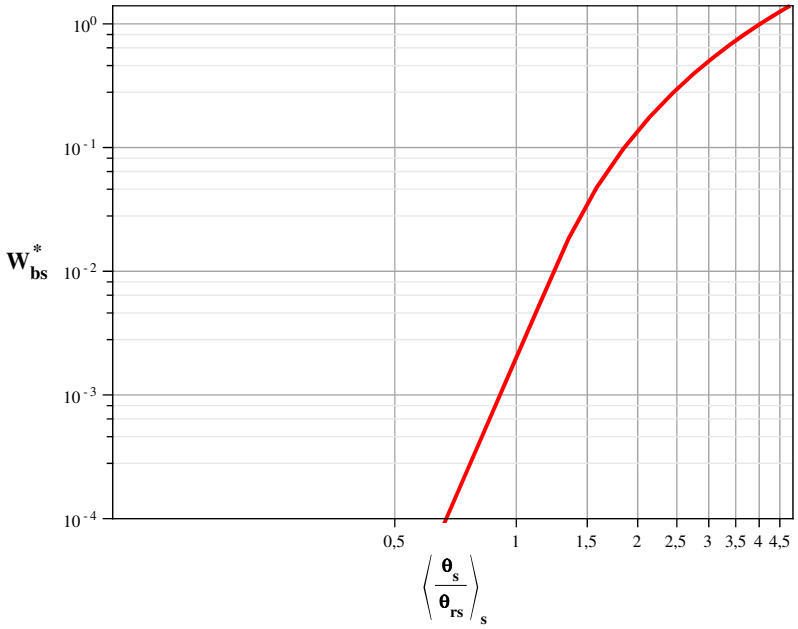

Figure 2.26: Dimensionless transport rate for sand fraction W^*_{bs} (*Wilcock and Kenworthy* (2002)) as a function of $\left\langle \frac{\theta_s}{\theta_{rs}} \right\rangle_s$.

function of $\langle \theta_{rs} \rangle_s$ and $\eta^*_s = \eta_s/(6\sigma_d)$, respectively.

It is noteworthy from Figure 2.27 that the reference transport rate W^*_{bs}=0.002 (*Wilcock and Kenworthy* (2002)) occurs in the transition range from gravel framework and sand matrix. More understanding is needed in order to clearly investigate from physically point of view the sand transport as bed load in a gravel framework and in sand matrix.
Figure 2.28 represents the variability of the dimensionless sand transport rate W^*_{bs} as function of $\eta^*_s = \eta_s/(6\sigma_d)$ and of the dimensionless Chezy coefficient $C^* = C/\sqrt{g}$ for a mean flow velocity, as defined by Eq.(2.75) $\langle \overline{U} \rangle_s$=0.66 m/s and d_s=0.15 mm.

Figure 2.29 indicates the critical hydraulic conditions for mobilizing the gravel fraction. Specifically Fig.(2.29) indicates that the gravel remains at rest when the dimensionless sand level ($\eta^*_s = \eta_s/(6\sigma_d)$) varies between 0 and 1 in the gravel framework, having assumed the geometric characteristics as in *Mignot et al.* (2008), where $d_{g50} = 3.1$ cm. The red solid line in Figure 2.29 reports the hydraulic conditions for which the gravel fraction starts to be transported as bed load with transport rate proportional to the parameter $(\theta_g - \theta_{rg})/\theta_{rg}$

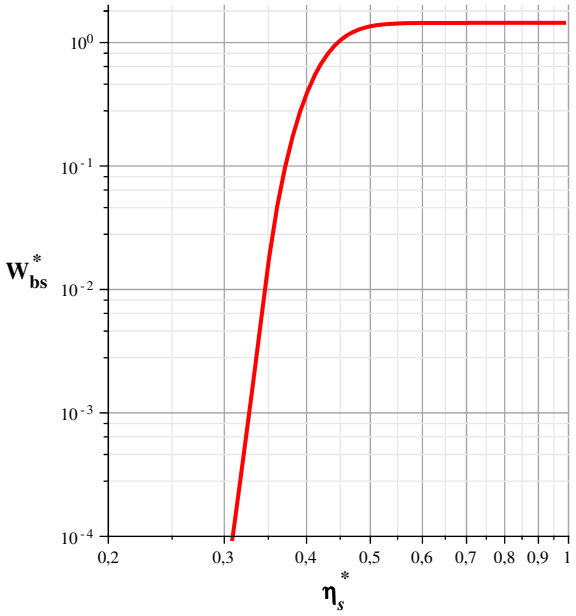

Figure 2.27: Dimensionless transport rate for sand fraction W^*_{bs} (*Wilcock and Kenworthy* (2002)) as a function of $\eta^*_s = \eta_s/(6\sigma_d)$.

as indicated in the horizontal axis.

This parameter represents physically the hydraulics capability of the flow to transport a given gravel diameter. The green solid line in Figure 2.29 represents the critical hydraulic conditions for the bed load transport of the sand fraction. It is noteworthy that the blue solid line refers to the hydraulic conditions when the sand fraction is well hiding (i.e.$\eta^*_s = 0.2$) among the pores of the gravel framework. Since the blue curve is above the red one, then the sand entrainment will require entrainment of the gravel framework, as indicated by *Wilcock and Kenworthy* (2002).

The physical idea underlaying the bed load transport phenomenon in the mixed case takes the physical idea of the Bagnoldean formulation, according to which the bed load layer (see Figure 2.24) is described as a finite layer whose thickness coincides with h_b. Above this bedload layer we have clear fluid in uniform motion and inside the bedload layer it has been assumed that a dynamic equilibrium may exists maintained by a balance between entrainment and deposition of the sand particles. If the rate of sand particles en-

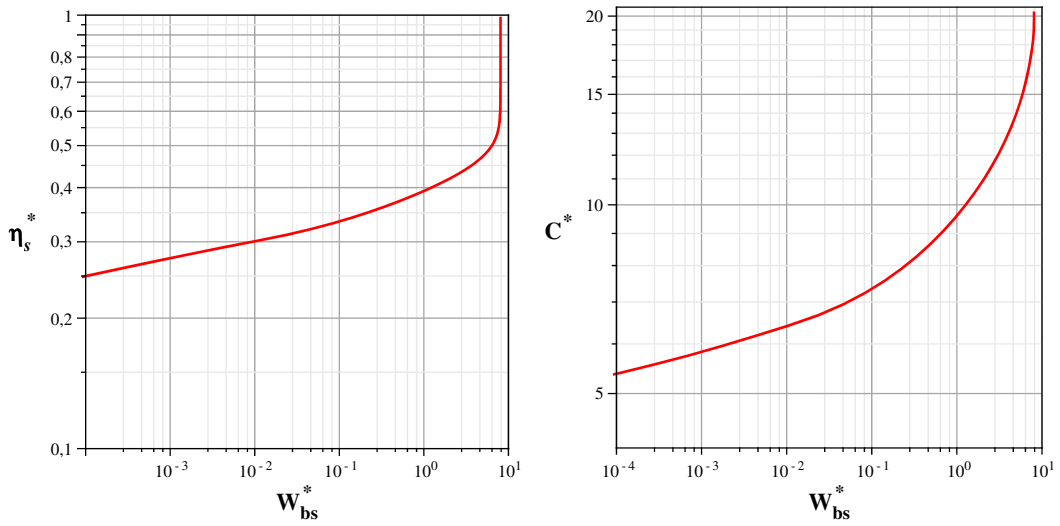

Figure 2.28: Dimensionless transport rate for sand fraction W^*_{bs} (*Wilcock and Kenworthy* (2002)) as a function of $\eta^*_s = \eta_s/(6\sigma_d)$ (left pannel) and of dimensionless Chezy coefficient (right pannel) $C^* = C/\sqrt{g}$ for d_s=0.15 mm and a mean flow velocity $\langle\overline{U}\rangle_s$= 0.66 m/s .

trainment is greater than that of deposition phenomenon, then the sand level η_s decreases, otherwise it increases.

Recently, the Bagnoldean formulation (*Bagnold* (1956)) has been demonstrated to break down when applied to equilibrium bed load transport on beds with transverse slopes above a relatively modest value that is well below the angle of repose (*Seminara et al.* (2002)). According to the Bagnoldean formulation (*Bagnold* (1956)) ,the fluid shear stress at the base of the bed load layer is reduced due to the interparticles forces (*sensu Coleman and Nikora* (2008)) acting between the moving and homoegeneous grains. Specifically, the shear stress at the bottom of bed load layer drops to the critical value for incipient transport condition. In a more general framework for incipient particles motion (*Coleman and Nikora* (2008)) the fluid shear stress at the upper limit of the bed load layer has to be greater than a critical value whatever the way in which it is estimated. In the mixed configuration as depicted in Figure 2.24 the flow energy has to take into account the work done by the drag forces on the contour of the gravel elements.

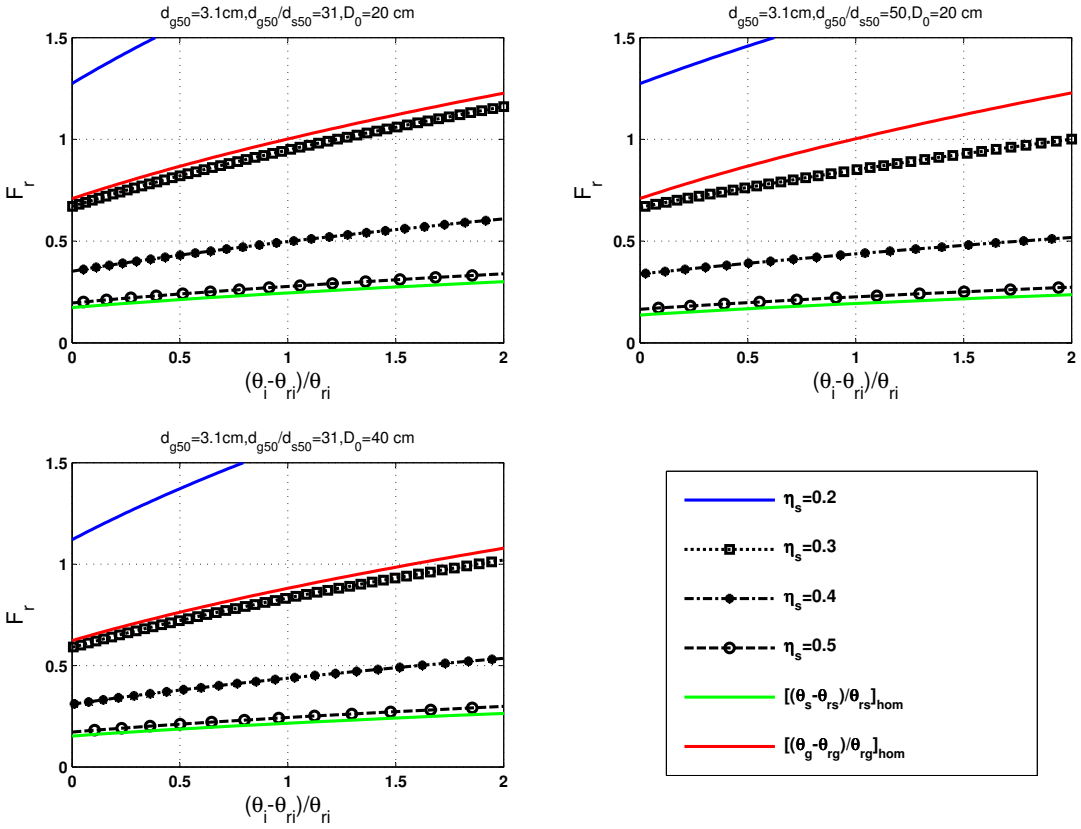

Figure 2.29: Shields stress for different hydraulics conditions for different value of sand level in the gravel matrix. Vertical coordinate refers to Froude number (F_r) and θ_i is the Shields number for i fraction (sand or gravel fraction) and θ_{ri} is the reference Shields number as indicate by *Wilcock and Kenworthy* (2002)

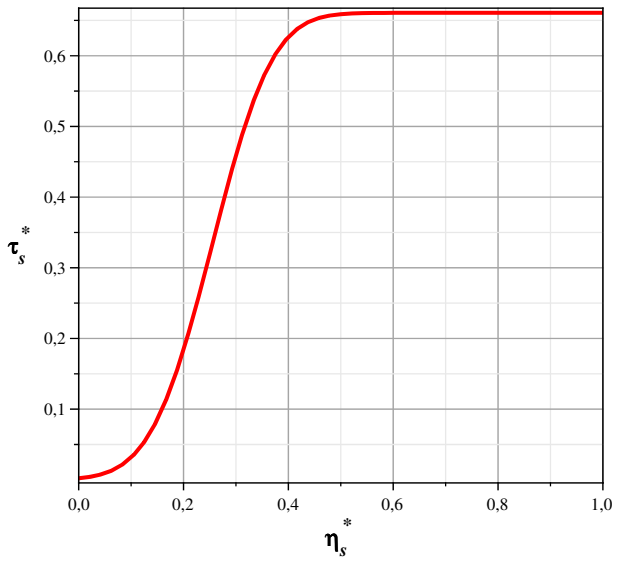

Figure 2.30: Dimensionless shear stress $\tau_s^* = \tau_s/(\rho u_*^2)$ acting of the sand fraction when sand is present in the gravel framework with geometric characteristics as in *Mignot et al.* (2008). $\eta_s^* = \eta_s/(6\sigma_d)$ is the dimensionless sand level.

3 A morphodynamic model for sand bed evolution over an immobile gravel bed

The present Chapter is devoted to the formulation of a morphodynamic model that can be used to predict the temporal and spatial evolution of a sand layer that partially or completely fills the voids beneath an immobile gravel bed.
Coherently with the analysis presented in the previous Chapter 2, the model formulation is two-dimensional, in the streamwise (x) and in the average bed orthogonal (z) directions. Moreover its spatially-averaged character is preserved, therefore "local" values of flow quantities and of the sand bed elevation actually represent the double-averaged quantities resulting from time averaging (especially for flow quantities, Reynolds-averaged over turbulence) and from spatial averaging, performed at the scale comparable to the d_{90} of the gravel grain size distribution, as discussed in the Section devoted the rough bed geometry characterization in Chapter 2.
The vertical subdivision of flow into specific layers, illustrated in Figure 2.1, is adopted for the formulation of the present morphodynamic model. The key ingredients of the model are:

- the momentum conservation equations for the fluid phase in the x and z directions;
- the mass conservation equations for the fluid phase;
- the mass conservation equations for the sand layer within an immobile gravel bed;
- a closure relationship to link the double-averaged Reynolds stresses to the double-averaged flow field;
- a closure relationship to link the double-averaged bedload rate to the double-averaged flow field.

As a first approximation, and having in mind the need of maintaining a reasonable level of simplicity for potential practical applications to real contexts, the momentum and mass

conservation equations for the fluid phase will be formulated referring to the physical balances formally valid only within the logarithmic layer. The physical processes governing the hydrodynamics within the roughness layer and its sublayers are indirectly taken into account according to the relationships proposed in the previous Chapter. Although this might appear a rather crude approximation, it is considered as a reasonable tradeoff between a rigorous model formulation and its practical applicability to real situations; model refinements are relatively straightforward and are not within the main focus of the present Ph.D work.

3.1 Morphodynamic modelling: continuity equation for the sand layer over an immobile gravel bed

In order to predict the morphodynamic evolution of the sand surface, a suitable continuity equation for the mobile sand fraction must be derived. The equation shall account for the

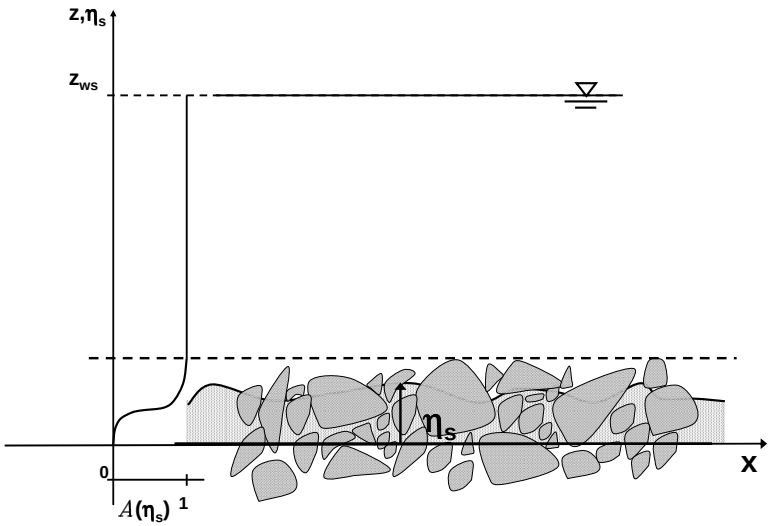

Figure 3.1: Sketch of the bed configuration when sand fraction is present in a gravel framework with relative notation

presence of an immobile gravel bed characterized by a horizontally-averaged vertical distribution of intra-gravel voids (Figure 3.1) that represents the maximum volume available for sand deposition and controls the areal distribution of fine sediments that are available to be entrained by the flow.

Referring to the notations employed in Figure 3.1, the classical sediment continuity balance (*Exner*, 1925) requires that an infinitesimal variation $d\eta_s$ of the local sand surface elevation η_s be locally compensated by a volumetric sand exchange dq between the flow and the bed regions. When the mobile sediment surface develops within an immobile matrix of gravel particles the available space for the evolution of the sand bed surface is limited by the spatial arrangement of the gravel clasts. Therefore the continuity principle shall account for the sand porosity together with the local gravel voids distribution that is described by the roughness geometry funtion $\mathcal{A}(\eta_s)$ and that depends on the local sand surface elevation itself.

The sand continuity equation takes therefore the following modified expression with respect to the homogeneous case:

$$\begin{aligned}(1-\lambda_s)\frac{\partial N\,(t)}{\partial t}+\frac{\partial \widehat{q_{sx}}}{\partial x}=0\\ N(t)=\mathcal{A}(\eta_s(t),t)\eta_s(t)\end{aligned} \tag{3.1}$$

where λ_s denotes the porosity of the sand, t is the time variable and $\hat{q_{sx}}$ is the unit sand bedload rate.
The time dependance in the first term of the left-hand side of (3.1) is, in principle, twofold: the sand surface elevation η_s changes with time and this is reflected also in the function $\mathcal{A}(\eta_s)$, which, in the more general case of mobile gravel bed, can be in principle modified by a variation in the spatial arrangements of the gravel clast. In a general way we may therefore write:

$$(1-\lambda_s)\left\{\mathcal{A}(\eta_s,t)\frac{\partial\eta_s}{\partial t}+\eta_s\left[\frac{\partial\mathcal{A}(\eta_s,t)}{\partial t}+\frac{\partial\mathcal{A}(\eta_s,t)}{\partial\eta_s}\frac{\partial(\eta_s,t)}{\partial t}\right]\right\}+\frac{\partial\widehat{q_{sx}}}{\partial x}=0$$

The assumption of immobile gravel leads to neglect the "direct" temporal variation of the roughness geometry function $\mathcal{A}$. Formally this can be expressed by introducing a "slow" time variable $\tilde{t}$, such that $t=\varepsilon_t\tilde{t}$. The model is indeed intended for applications to streams where most of the time the flow is competent to move only the fine fraction, leaving the coarsest sediments at rest. Henceforth:

$$(1-\lambda_s)\left\{\mathcal{A}(\eta_s,t)\frac{\partial\eta_s}{\partial t}+\frac{\partial\mathcal{A}(\eta_s,t)}{\partial\eta_s}\frac{\partial\eta_s}{\partial t}+\varepsilon_t\eta_s\frac{\partial\mathcal{A}(\eta_s,t)}{\partial t}\right\}+\frac{\partial\widehat{q_{sx}}}{\partial x}=0$$

We note that a time dependence of the function $\mathcal{A}(\eta_s)$ shall be accounted for over the timescales at which also the gravel bed is mobilized in a such way that spatially-averaged gravel particle arrangement is modified. The model formulated in the present paper as-

sumes the gravel bed to be immobile, which implicitly means to refer to shorter timescales, i.e. $\varepsilon_t << 1$ and the eq.(3.2) reads as:

$$(1-\lambda_s)\mathcal{A}(\eta_s,t)\frac{\partial \eta_s}{\partial t}+\frac{\partial \mathcal{A}(\eta_s,t)}{\partial \eta_s}\frac{\partial \eta_s}{\partial t}+\frac{\partial \widehat{q_{sx}}}{\partial x}=0$$

With respect to the classical *Exner* (1925) equation, the above relationship is nonlinear in the sand surface elevation η_s, as shown by the time-derivative term representing the local change in sand elevation. Physically this means that the same volumetric exchange of sand between the evolving bed surface and the flow region can result in different sand level adjustments depending on the local value of the sand level itself. Such nonlinear feedback occurs when the sand surface lies below the top of the gravel crests and is likely to affect the sand bed morphodynamics by contributing to the generation of different patterns with respect to the homogeneous case. The order of magnitude of the time scale of sand bed dynamics can be estimated from (3.2) for the two limit cases, i.e. "homogeneous" and "mixed" case. The morphodynamical time scale T can be expressed as follows from (3.2):

$$T=\frac{l_x l_z(1-\lambda_s)\mathcal{A}(\eta_s)}{d_s\sqrt{(s-1)gd_s}}=\frac{l_x l_z(1-\lambda_s)\mathcal{A}(\eta_s)}{d_s}\frac{\sqrt{\widehat{\theta_s}}}{\widehat{u_*}}=\frac{\widehat{\sqrt{\theta_s}}}{\widehat{u_*}}\frac{l_x l_y(1-\lambda_s)\mathcal{A}(\eta_s)}{\frac{d_s}{l_z}} \tag{3.2}$$

The most evident difference between the homogeneous sand and the mixed (sand - immobile gravel) case is that when the sand available for transport decreases (i.e. $\mathcal{A}(\eta_s)$ tends to vanish), the time scale of sand bed morphodynamic processes tends to be reduced, therefore bed dynamics can be expected to occur more rapidly. This observation is in qualitative agreement with the experimental observation of *Tuijnder* (2010) on the dynamics of supply-limited sand dunes (see Chapter 4 and related text). Moreover the physical condition $\varepsilon_t << 1$ means that:

$$O(t)\gg O\left(\frac{1}{\sqrt{(s-1)gd_s}}\right)O\left(\frac{l_x(1-\lambda_s)\mathcal{A}(\eta_s,\varsigma)}{\frac{d_s}{l_z}}\right) \tag{3.3}$$

where l_x represents the length scale over which $\mathcal{A}$ has been defined. Moreover *Nikora et al.* (2004) showed that $O(l_x) = O(d_{90})$ and $O(l_z) = O(\sigma_z)$. In Eq.(3.2) it has been hypothesized that the roughness geometry function $\mathcal{A}(\eta_s)$ has a different time scale with respect to the sand elevation, concerning its time evolution, so that it has been considered constant regards with the time t in the same equation.
Referring to the DAM-approach and to the partitioning stated by the Eq. (2.1), consid-

ering the Eq.(2.3), the bedload sediment flux $\widehat{q_x}$ in the Eq.(3.2) follows as:

$$\widehat{q_{sx}} = \widehat{f}\left(\frac{\tau}{\tau_{ri}}\right) = \langle\overline{q_{sx}}\rangle + \widetilde{q_{sx}} = \langle\overline{q_{sx}}\rangle\left(1 + \frac{\widetilde{q_{sx}}}{\langle\overline{q_{sx}}\rangle}\right) \tag{3.4}$$

or equivantely

$$\widehat{q_{sx}}^* = \frac{\widehat{q_{sx}}}{\langle\overline{q_{sx}}\rangle} = (1 + \widetilde{q_{sx}}^*) \tag{3.5}$$

where $\langle\overline{q_{sx}}\rangle$ is defined over a spatial length scale as in the Eq.(2.3).
For the "homogeneous" case, i.e. sandy beds, *Jerolmack and Mohrig* (2005) assumed that the shear stress may be regarded as a Taylor expansion depending on the local topography and neglecting terms beyond the 2-order Taylor approximation. This means that within the spatially averaged approach (see *Whitaker* (1999)) the approximation made by *Jerolmack and Mohrig* (2005) is equivalent to considering up to 2-order superficial spatial moments as indicated by the Eqs. (2.19).
Referring to the "mixed" case and considering the bed load transport for the motion of the two fractions composing the bed structure, it follows that the Shields stress reference value is represented by the Eq.(2.54). Moreover, the sand sediment flux in the Eq.(3.4) has been represented by two terms depending on the characteristic length scale that are considered. In fact for bed load transport over immobile gravel bed *Wilcock and Kenworthy* (2002) assume that the spatial fluctuations (see Eq.(2.22)), over the length scale $\sqrt{A_0} = O(\Gamma_0)$ is represented by an exponential function; this means that the different spatial scales shorter than $\sqrt{A_0}$ decay exponentially as the sand level approach to the "homogeneous" case, i.e. the sand elevation buries completely the gravel beds. Physically, this means that as sand elevation approach to the "homogeneous" case, then the "hiding effect" due to the gravel elements approaches to zero and the characteristic length scales associates with the spatial fluctuations of the shear stresses in the Eq.(2.22) decays to the "homogeneous" case.
Different is the "homogeneous" case, where *Jerolmack and Mohrig* (2005) assumed that the shear stress for the morphodynamics modelling is composed by two terms: one refers to the principal spatial scale to which some hydraulics quantities are spatially averaged, the other refers to a different spatial scale that is less than the first and it accounts for the local bed slope.

3.2 Momentum and continuity equations for the fluid phase

Flow model can be grouped in various categories depending on the description accuracy for the shear stress distribution; as proposed by *Colombini* (2004) the following type can be distinguished : potential flow (*Kennedy* (1963); *Coleman and Fenton* (2000)), shallow-water (*Gradowczyk* (1968)) and rotational solutions (*Fredsøe* (1974)). The used flow model affects the value of the phase-lag between sediment transport rate and bed topography and, since the phase-lag controls the mechanism of bed instability, the choice of the flow model become crucial. Specifically, when studying bedform dynamics at different scales, several effects contribute to the bed instability and consequently to the bed evolution depending on the subtle balance between stabilizing and destabilizing effects. Therefore, the description of shear stress distribution is an important ingredient in order to understand the evolving bed, and the rotational flow models provide the most accurate description for the shear stress distribution (*Colombini* (2004)). Since the flow equations presented here will be the mathematical tool for stability analysis of sand dunes in the mixed case (i.e. when the sand fraction is present in a gravel framework), and since the shear stress description is a crucial ingredient for understanding the bedform formation as bed instability mechanism, then in the next section we introduce notations and flow equations for the mixed case when a rotational flow model is adopted. Application of the model to the study of sand dune dynamics in the mixed case will follow in Chapter 4.

3.2.1 Mathematical formulation for the flow field

The governing equations for steady flow field in the domain $z \geq \langle z_c[\eta_s(x)]\rangle_s$ (see Figure 3.2) are the Reynolds equations when the double-averaged operator (in time first and then in space) is applied:

$$\begin{aligned}
\langle\overline{U}\rangle_s\frac{\partial\langle\overline{U}\rangle_s}{\partial x}+\langle\overline{W}\rangle_s\frac{\partial\langle\overline{U}\rangle_s}{\partial z}+\frac{\partial\langle\overline{P}\rangle_s}{\partial x}-gi_f-\frac{\partial\langle\overline{T_{xx}}\rangle_s}{\partial x}-\frac{\partial\langle\overline{T_{xz}}\rangle_s}{\partial z} &= 0 \\
\langle\overline{U}\rangle_s\frac{\partial\langle\overline{W}\rangle_s}{\partial x}+\langle\overline{W}\rangle_s\frac{\partial\langle\overline{W}\rangle_s}{\partial z}+\frac{\partial\langle\overline{P}\rangle_s}{\partial z}+g-\frac{\partial\langle\overline{T_{xz}}\rangle_s}{\partial x}-\frac{\partial\langle\overline{T_{zz}}\rangle_s}{\partial z} &= 0 \\
\frac{\partial\langle\overline{U}\rangle_s}{\partial x}+\frac{\partial\langle\overline{W}\rangle_s}{\partial z} &= 0
\end{aligned} \tag{3.6}$$

where $\mathbf{U} = (\langle\overline{U}\rangle_s, \langle\overline{W}\rangle_s)$ is the local double-averaged velocity vector, $\langle\overline{P}\rangle_s$ is the double-averaged pressure and $\mathbf{T} = \langle\overline{T_{ij}}\rangle_s$ is the two-dimensional double-averaged Reynolds stress tensor. In Eqs. (3.6) it has been assumed that $\sin(i_f) \simeq i_f$ and $\cos(i_f) \simeq 1$, because we

assumed that the rough bed slope is $\ll 1$.

For uniform flow condition in x-coordinate, the friction velocity $\langle u^* \rangle_s$ and the depth-

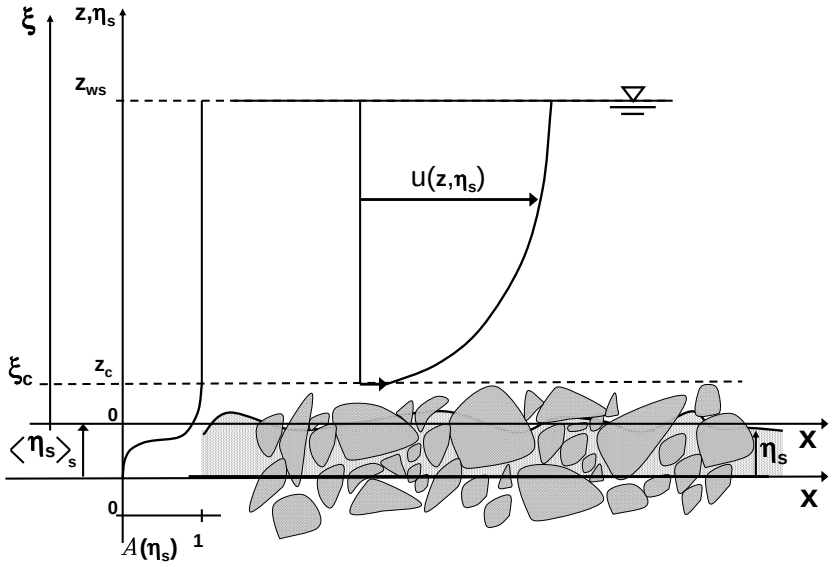

Figure 3.2: Sketch of the flow configuration with relative notation

averaged velocity for the uniform flow $\left\langle \overline{\overline{U}} \right\rangle_s$ are related to the slope i_f and Froude number by the Eq.(2.75), where the dimensionless Chezy coefficient is a function of the sand level η_s.

Referring to a Cartesian coordinate system (x, z) such as the one sketched in Figure 3.2, the curves $z = \eta_s(x) + D(x)$ and $z = z_c(x)$ identify the upper and lower boundaries of the flow domain respectively, where D represents the local flow depth. Furthermore, we stipulate that the latter boundary is set at the reference level, the level at which conventionally and in the homogenous case the mean logarithmic profile vanishes (in the homogeneous case sand elevation $\eta_s^* = \eta_s(x)/(4\sigma_d)$ completely buries the gravel, that is $\eta_s^* = 1$). For the heterogeneous case ($\eta_s^* < 1$)and at the lower boundaries of the flow domain the mean logarithmic velocity is no longer zero, due to the effect of increased gravel roughness on the flow field. The above system is solved with the boundary conditions of vanishing shear stress at the free surface and of velocity at the lower boundary, depending on the value of sand elevation η_s^* .

It is noteworthy that having applying the double-averaged operator in the Eqs.(3.6), we have to specify the reference averaging area A_0 by which the spatial-average operator has been defined. In particular, we assume that the plane length scale $l_x = O(d_{g90})$ as

suggest by *Aberle and Nikora* (2006), while the vertical length scale $l_z = O(\sigma_d) = (4-6)\sigma_d$ (*Nikora et al.* (2001); *Mignot et al.* (2008)) where σ_d is the standard deviation of rough bed elevations and $(4-6)\sigma_d$ represents the all variability of the roughness geometry function $\mathcal{A}(z)$ in the z-coordinate,which can take different forms, depending if the rough bed is a water-worked bed or it has a Gaussian distribution of rough elements elevations as in *Mignot et al.* (2008).
So far, we described what happens to the shear stress distribution and to the double averaged velocity profile when the bed is composed by a gravel matrix and the sand fraction changes the roughness of the rough bed elements. But, how can we link the total shear stress distribution to the double averaged velocity profile as indicate by the Eq.(3.9) where the behavior of double averaged turbulent fluctuations have direct consequences on the double averaged velocity profile?

3.2.2 Closure formulation

In order to close the above mathematical formulation we employ a Boussinesq-type assumption:

$$\langle \overline{T}_{ij} \rangle_s = \nu_t (\langle \overline{U} \rangle_{s,j} + \langle \overline{W} \rangle_{s,i}) \tag{3.7}$$

For the evaluation of the eddy viscosity ν_t, a formulation in terms of a mixing length is adopted:

$$\begin{aligned} \nu_t^* &= \frac{\nu_t}{\langle u_* \rangle_s D} = l_{\nu t}^2 \frac{\partial \langle \overline{U^*} \rangle_s}{\partial z^*},\ z^* = \frac{z}{D},\ D = z_{ws} - \eta_s \\ l_{\nu t} &= k\sqrt{(1-z^*)}(z^* - 0.43 z_c^*) \end{aligned} \tag{3.8}$$

where k is the Von Kármán constant,$\langle u_* \rangle_s$ is the averaged friction velocity at $z = \eta_s$. Figure 3.3 represents the eddy viscosity as indicated by Eq.(3.8) where the function z_c^* is a function of the dimensionless sand level η_s^* and it has been represented by Eq.(2.74) with specified gravel framework characteristics as indicated by Figure 2.17 . The adopted formulation for the flow field rigorously refers to the flow region above the roughness layer, and allow to estimate a "near-bed" shear stress value at the bottom of this region, accounting for the dynamics of the roughness layer in a parameterized way through the relationships expressing the variability of the base level z_c with the flow and sand bed characteristics.
The following considerations can be made concerning the vertical distribution of the shear stress within the roughness layer and its sub-layers.

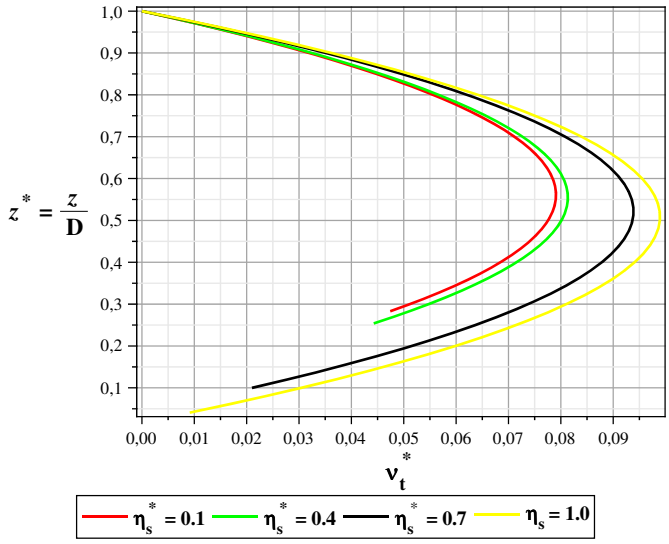

Figure 3.3: Eddy viscosity as indicated by Eq.(3.8) referring to a protrusion $\zeta^* = z_c^*$ as indicated by Eq.(2.74) and represented by Figure 2.17.

The geometrical length scales discussed above have influence on the turbulent properties of the flow over a rough bed, but the length scale as indicate above are not necessarily the same for the turbulence length scales as point out by *Mignot et al.* (2008), in fact:

- the production term P in Eq. (2.33) reaches a maximum value slightly below z_c (see Figure 3.2) at z/z_c=0.88 (*Mignot et al.* (2008));
- in the form-induced layer (i.e. $0.76z_c \leq z \leq 1.47z_c$) the production term P in Eq. (2.33) is larger than the dissipation term, and the turbulent diffusion term F_t is also maximum in this region.

Therefore, the geometrical length scale $l_z = z_c = 6\sigma_d$ (assuming a function $\mathcal{A}(z)$ as in *Mignot et al.* (2008)) represents the order of magnitude of the turbulent characteristics length scales and not the length scale itself, because:

- the production term P in Eq. (2.33) reaches a maximum value at z/σ_d=5.28;
- the form-induced layer is between $4.56\sigma_d \leq z \leq 8.82\sigma_d$.

where σ_d is the standard deviation of rough bed elevations.
Further investigation is required in order to understand which are the longitudinal and transverse length scales for the turbulence properties considering a reference gravel framework only or when sand is present in the porosity of gravel elements measured by the function $\mathcal{A}(z)$ in the roughness layer.
The mathematical formulation stated by Eqs.(3.6) assumed that:

- the production term P in Eq. (2.33) reaches a maximum value at z/σ_d=(4-6);
- the form-induced layer coincides with the roughness layer and the maximum value of the total shear stress $\tau(z)$ is at $z = (4-6)\sigma_d = z_c$.

With the above assumptions, the integration of Eqs.(3.6) for $z \geq z_c$ and steady, uniform, spatially averaged flow (*sensu Nikora et al.* (2001)) , produced the linear behavior of the total stress distribution as follows:

$$\frac{\tau(z)}{\rho} = g i_f (z_{ws} - z) = -\langle\overline{u'w'}(z)\rangle_s = -\overline{u'w'}(z), \quad z \geq z_c \tag{3.9}$$

In general, the total stress $\tau(z)$ accounts for different hydrodynamics contributions depending on the flow layer as depicted in Figure 2.4, specifically:

$$\tau(z) = \underbrace{\overbrace{\underbrace{-\rho\langle\overline{u'w'}(z)\rangle_s}_{logarithmic+outer\,layer} \quad -\rho\langle\widetilde{u}\widetilde{w}(z)\rangle_s}^{form-induced\,layer} + \int_0^{z_c} f_p(z)dz + \int_0^{z_c} f_\nu(z)dz}_{roughness\,layer} \tag{3.10}$$

or

$$\tau(z) = \overbrace{-\rho\langle\overline{u'w'}(z)\rangle_s - \rho\langle\widetilde{u}\widetilde{w}(z)\rangle_s}^{flow\,turbulence\,components} + \underbrace{\int_0^{z_c} f_p(z)dz + \int_0^{z_c} f_\nu(z)dz}_{resultant\,drag\,forces} \tag{3.11}$$

where $f_p(z)$ and $f_\nu(z)$ are the drag forces induced respectively by the pressure and viscous forces integrated on the contours of the roughens elements, also indicated in Eq.(2.32), and having neglecting the viscous stress relating to the derivative of the streamwise velocity with respect to the vertical coordinate. Therefore, the linear behavior of the total stress $\tau(z)$ is recovered only above the level z_c. But, what happens to the function $\tau(z)$ for $z < z_c$ when the sand fraction is present in the gravel framework, as indicate in Figure 3.2?
As pointed out in the Chapter 2, the "flow turbulence components" in Eq.(3.11) behave as stated by Eq. (2.65) and they represent the shear stress available to the sand fraction to be transported by the flow, while the "resultant drag forces" represent the resultant

that acts on the rough bed elements in the averaging area A_0 due to the drag forces. Considering the Figure 3.4, the function $\tau(z)$ depends on the sand level η_s and on the

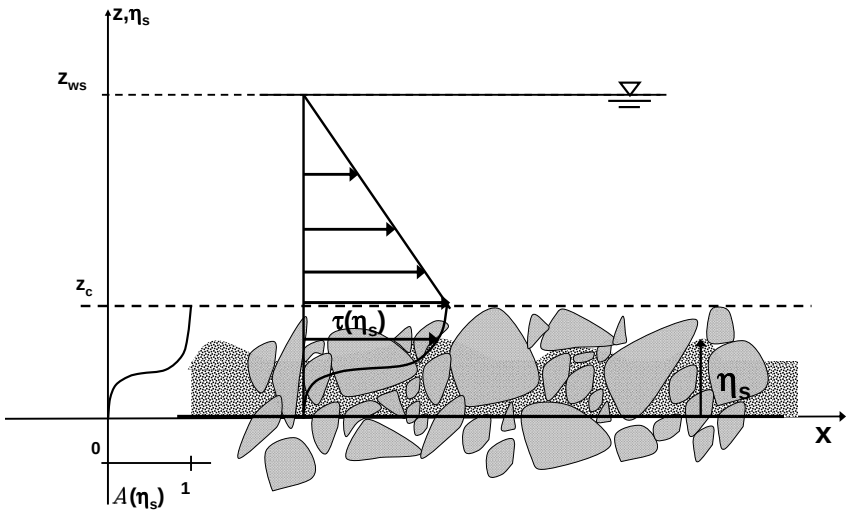

Figure 3.4: Sketch of the double averaged shear stress configuration as a function of the sand level η_s

geometric characteristics of the gravel framework for a given flow depth. Concerning the velocity profile above the level z_c , it depends on the two quantities z_c and λ_0 as indicated by Eq.(2.44) that, in its turn, depend on the sand level η_s.

4 Theory of sand dunes stability in the mixed case

Sand dunes are the most common bedforms encountered in rivers, and their dynamics is crucial in many environmental and river engineering problems (*ASCE* (2002)). From hydraulics point of view, the bedforms, especially dunes, are a primary source of roughness and therefore a major factor in determining water levels (*Tuijnder* (2010)).To this regard, acceleration/deceleration of the flow associated with the sequence of contractions above sand dunes is critical in controlling the shape of the bed surface through nonlinear interactions. Consequently, the local shear stress distributions and the sediment transport are affected by the flow separation behind the crest sand dune with a specific amplitude (*Colombini and Stocchino* (2008)).

Kennedy (1963) showed that bedforms can be interpreted as periodic perturbations of the shape of the river bed that interact with the flow, creating a dynamic system that can experience temporal growth or decay according to an instability mechanism (see *Colombini* (2004) for literature review). From morphological point of view, the phase-lag between flow and bed topography is confirmed to be the mechanism controlling sand dunes formation and nonlinear evolution (*Colombini and Stocchino* (2008)).

Sand dunes occurs in most studies as bedforms related to a flow strength parameter, a grain size parameter and geometrical sand dunes characteristic as the wavenumber. *Colombini* (2004) studied sand dunes formation in the contest of linear stability theory where the shear stress responsible for bed load transport is computed at the top of a specified bedload layer (*sensu Bagnold* (1956)) , so that a new term, which is related to the role of the longitudinal pressure gradient, formally enters in the analysis. The reference level that refers to the top of the specified bedload layer where the shear stress is computed, represents a crucial choice for the delicate balance between destabilizing and stabilizing effects, that in its turn affect the stability of a small bed perturbation,i.e. the existence or not of the sand dunes (*Colombini* (2004)).

It is noteworthy that sand dunes amplitude reaches heights up to one third of the water

depth, while dune length is several times the water depth.Hereinafter, we refer to alluvial sand dunes to that beform formations that are not limited by the amount of available sediment. Different bedform types are reported due to partial mobility and grain size sorting compared to bedforms in uniform sediment and under alluvial conditions. Bedforms types that are typically associated with partial mobility conditions are: sand ribbons, barchanoid dunes, isolated dunes and sediments starved dunes, bedload sheets an low-relif beforms (*Kleinhans et al.* (2002); *Tuijnder et al.* (2009); *Tuijnder* (2010)). These bedforms are observed if the amount of transportable sediment on top of an immobile layer is limited, i.e. the supply-limitation condition is recovered. This condition is typically of a non-uniform bed composition, also know as graded sediment, and if the coarsest part of the non-uniform bed composition cannot be transported, a coarser immobile layer can develop through vertical sorting of grain size fractions. This layer prevents entrainments of underlaying sediments and thus limits the availability of sediment for bedform formation to the volume present on top of the coarse layer. The availability of sediment is a primary control on the bedform development (*Kleinhans et al.* (2002); *Tuijnder et al.* (2009); *Tuijnder* (2010)). *Tuijnder et al.* (2009) investigate how the geometrical sand dune characteristics (i.e. average sand dune wavelength λ and height Δ in Figure 4.1) react to a sediment supply-limitation. Specifically, it can be seen that the average dune dimensions (i.e. λ and Δ in Figure 4.1) increase with an increasing sand layer thickness d for all series of experiments (*Tuijnder et al.* (2009)). Figure 4.2 and Figure 4.3 report how the geometrical sand dunes characteristics change with the average sand layer thickness d assumed as a measure of sand availability. The experimental points represented in the figures refer to the series 5 in *Tuijnder et al.* (2009)'s work. Particularly, the geometrical sand dune characteristics have been represented in dimensionless form using the analogous geometrical sand dune characteristics in the alluvial conditions (i.e. when the supply-limitation condition vanishes). Moreover, the same figures report the dimensionless Chezy coefficient C^* as a function of the ratio Δ/Δ_0 and λ/λ_0, respectively. It can be seen that the Chezy coefficient as a measure of roughness characterization of the sand dunes decrease as the sand dunes approach to the alluvial conditions.
Differently from the previous figures, Figure 4.4 and Figure 4.5 represent the time variable t that has been defined as the equilibrium time so that the sand beform, sediment transport and bed roughness reach the equilibrium conditions. Also in this case the variable t has been represented in the dimensionless for using the analogous equilibrium time t_0 in the alluvial conditions. Specifically, the figures show that when the supply-limitation condition vanishes (i.e. $d/d_0 \to 1$) then the equilibrium time t reaches its maximum value compared to that in the alluvial conditions and the dimensionless Chezy coefficient C^*

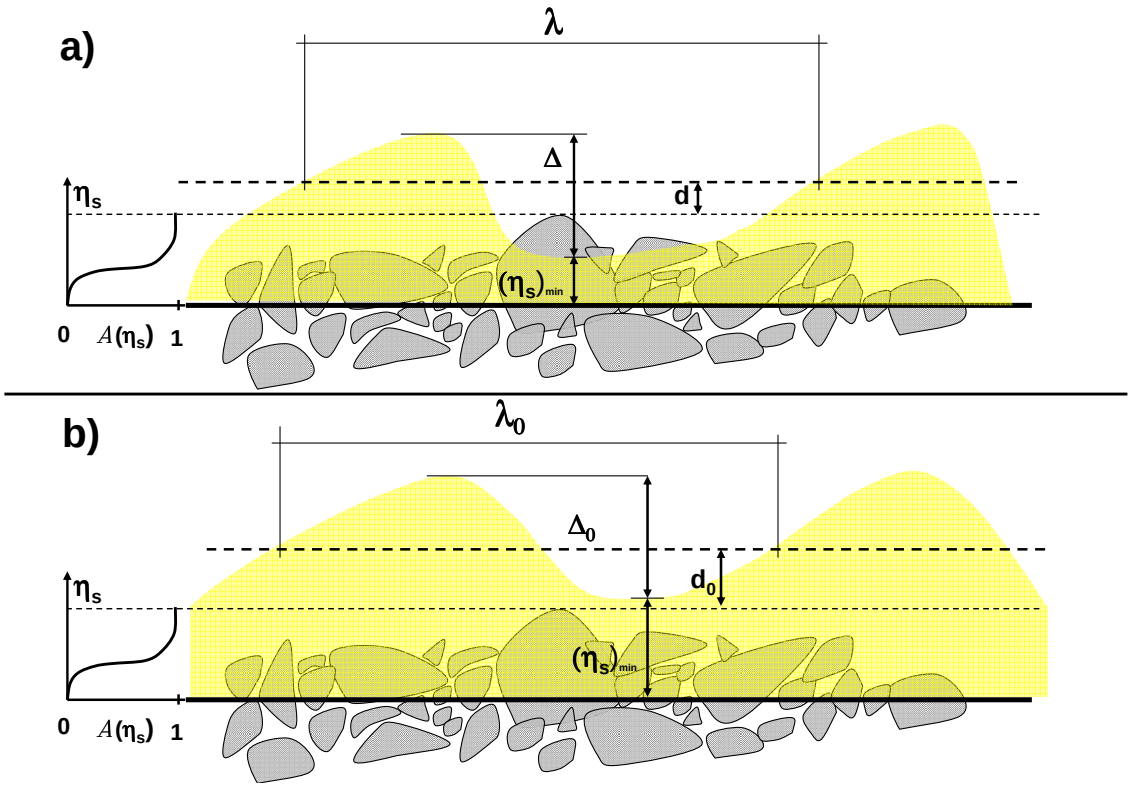

Figure 4.1: Sketch and notation for *Tuijnder et al.* (2009)'s experimental work. Panel a) refers to mixed configuration and panel b) refers to alluvial configuration. λ refers to sand dune wavelength and Δ refers to sand dune height as the height difference between the dune crest and the dune trough on the downstream side. Moreover, d refers to the average sand layer thickness and it was determined by subtracting the measured level of the gravel layer from the measured level of sand bed and averaging over the flume length.

assumes its minimum value.

The present Chapter is devoted to apply the morphodynamic model formulated in Chapter 3 to predict the morphodynamics of sand bedforms over immobile gravel bed. The sand surface elevation is a measure of the sediment supply-limitation that crucially controls the sand bedform development. The model will be solved through a linear stability analysis that incorporates recent developments in the theoretical study of sand dune stability in homogeneous conditions. The specific goals of the present Chapter are:

- predict the hydraulics conditions for sand bedform stability and preferred wavelength selection over an immobile gravel bed;
- understand how the supply-limitation condition (i.e.$0 \leq d/d_0 \leq 1$) can influence the sand bedform stability.

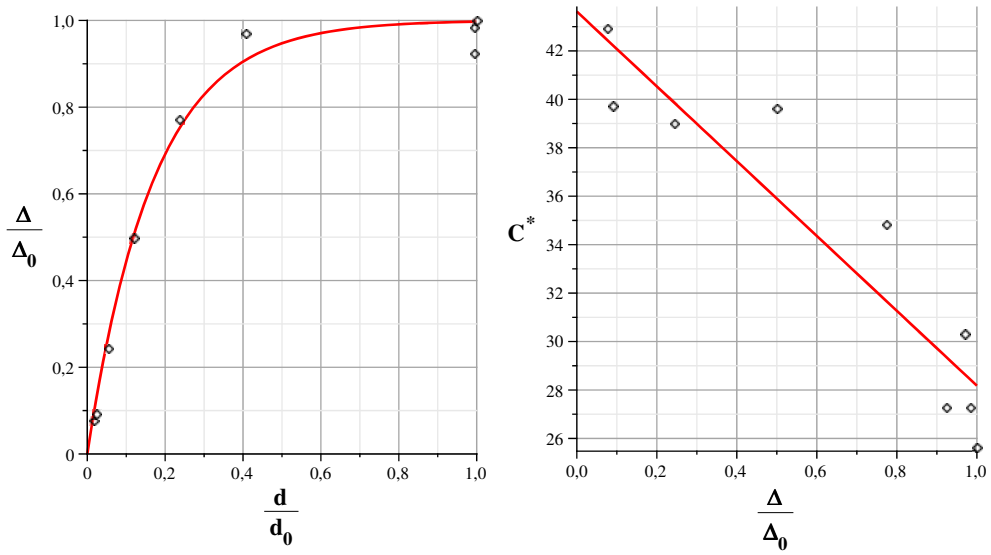

Figure 4.2: Left graph represents ratio between sand dune height Δ in the mixed bed configuration and sand dune height in alluvial condition Δ_0 in the alluvial condition as a function of ratio between average sand layer thickness d in the mixed bed configuration and average sand layer thickness d_0 in the alluvial condition. Right graph represents the dimensionless Chezy coefficient C^* as a function of the ratio between the sand dune height Δ in the mixed bed configuration and sand dune height in alluvial condition Δ_0 (see Figure 4.1 for notation). Circle points refer to the experimental data from *Tuijnder et al.* (2009)'s work, specifically they refer to the series labeled with number 5

Specifically, this stability analysis has been developed in the mathematical context of linear stability analysis where the amplitude of an hypothetical sand bed perturbation of the uniform configuration has been chosen to be small compared to the average sand dune height Δ in the *Tuijnder et al.* (2009)'s work.

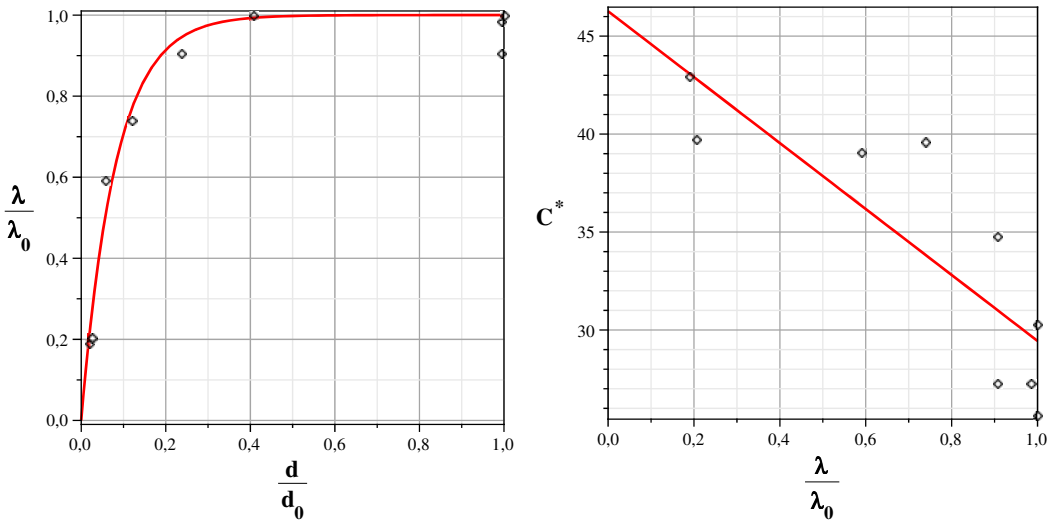

Figure 4.3: Left graph represents ratio between sand dune wavelength λ in the mixed bed configuration and the sand dune wavelength λ_0 in the alluvial condition as a function of ratio between average sand layer thickness d in the mixed bed configuration and average sand layer thickness d_0 in the alluvial condition. Right graph represents the dimensionless Chezy coefficient C^* as a function of the ratio between the sand dune wavelength λ in the mixed bed configuration and sand dune wavelength λ_0 in alluvial condition (see Figure 4.1 for notation).Circle points refer to the experimental data from *Tuijnder et al.* (2009)'s work, specifically they refer to the series labeled with number 5

4.1 Mathematical formulation: notation and scaling for the flow

With the same assumptions made in the paragraph 3.2.1 for the flow field, hereafter a star superscript will denote *dimensional* quantities. We denote by D^*,U^*, η_s^* and l_z^* the uniform values of flow depth, depth-averaged speed, the sand elevation and a geometrical characteristic length scale for the gravel matrix, respectively. Moreover, we assumed that the above quantities represent the spatial-temporal average value, as indicated in Eqs. 3.6 by the operator $\langle\dot{\cdot}\rangle_s$.

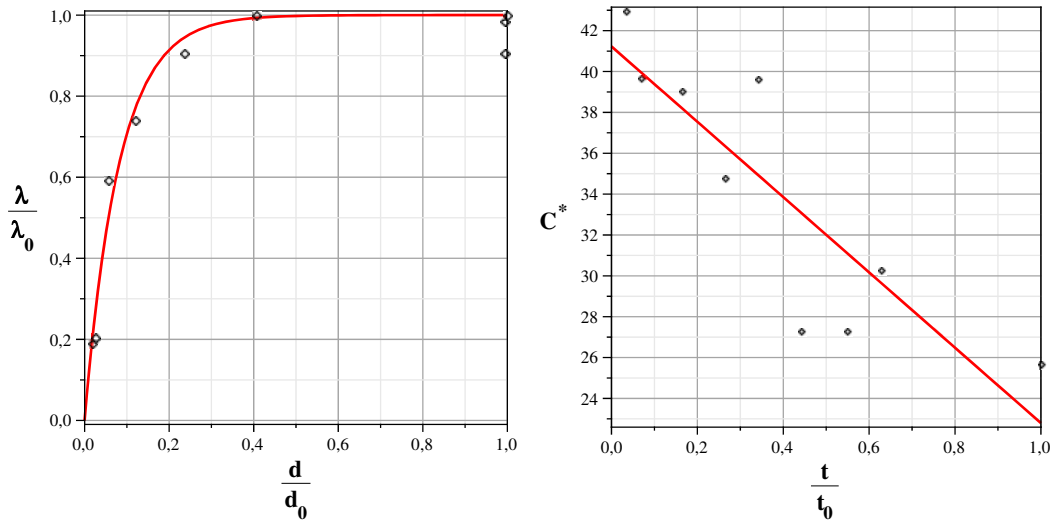

Figure 4.4: Left graph represents ratio between sand dune wavelength λ in the mixed bed configuration and the sand dune wavelength λ_0 in the alluvial condition as a function of ratio between average sand layer thickness d in the mixed bed configuration and average sand layer thickness d_0 in the alluvial condition. Right graph represents the dimensionless Chezy coefficient C^* as a function of the ratio between sand dune equilibrium time t in the mixed bed configuration and the sand dune equilibrium time t_0 in the alluvial condition(see Figure 4.1 for notation). Circle points refer to the experimental data from *Tuijnder et al.* (2009)'s work, specifically they refer to the series labeled with number 5

The approach used to implement the present linear stability analysis is formally analogous to that proposed by *Colombini* (2004); differences are in the governing mathematical problem.

Variables will be made dimensionless using the friction velocity u_f^*, the depth D^* of the unperturbed uniform flow, the fluid density ρ and for the only sand elevation η_s^* we use geometrical characteristic length scale for the gravel matrix $l_z^* = (4-6)\sigma_d^*$, where σ_d^* is the usual standard deviation of the rough bed elements elevations.

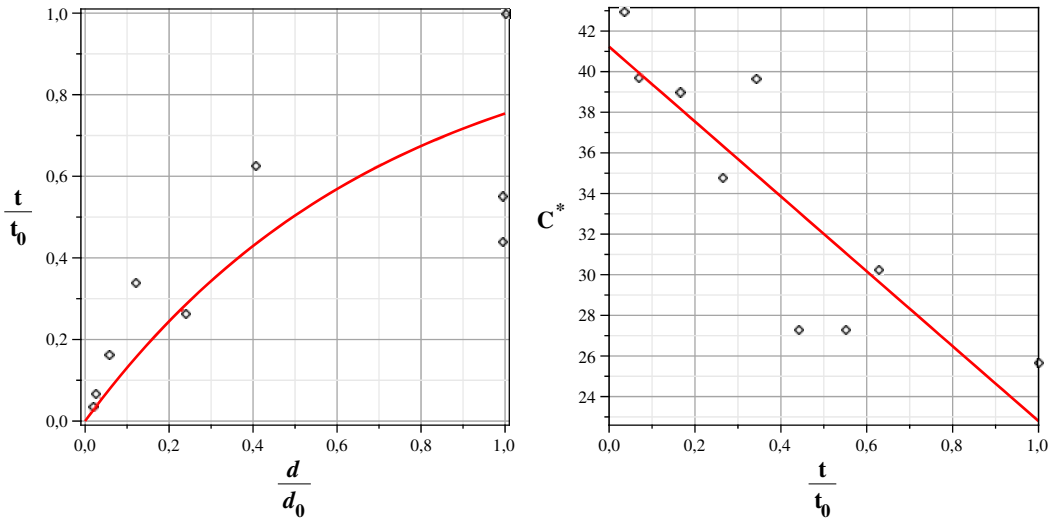

Figure 4.5: Left graph represents ratio between sand dune equilibrium time t in the mixed bed configuration and the sand dune equilibrium time t_0 in the alluvial condition as a function of ratio between average sand layer thickness d in the mixed bed configuration and average sand layer thickness d_0 in the alluvial condition. Right graph represents the dimensionless Chezy coefficient C^* as a function of the ratio between sand dune equilibrium time t in the mixed bed configuration and the sand dune equilibrium time t_0 in the alluvial condition (see Figure 4.1 for notation). Circle points refer to the experimental data from *Tuijnder et al.* (2009)'s work, specifically they refer to the series labeled with number 5

Eqs. 3.6 in dimensionless form and with the above assumption read as:

$$\begin{aligned} UU_{,x} + WU_{,z} + P_{,x} - 1 - T_{xx,x} - T_{xz,z} &= 0 \\ UW_{,x} + WW_{,z} + P_{,z} - 1 - T_{xz,x} - T_{zz,z} &= 0 \\ U_{,x} + W_{,z} &= 0 \end{aligned} \tag{4.1}$$

In order to close the above formulation we employ for the Reynolds stress tensor $\mathbf{T} = T_{ij}$ the closure relationships indicated in the paragraph 3.2.2.
The curves $z_{ws} = \eta_s(x) + D(x)$ and $z = z_c[\eta_s(x)]$ identify the upper and lower boundaries of the logarithmic domain respectively, so that D represents the local flow depth (see

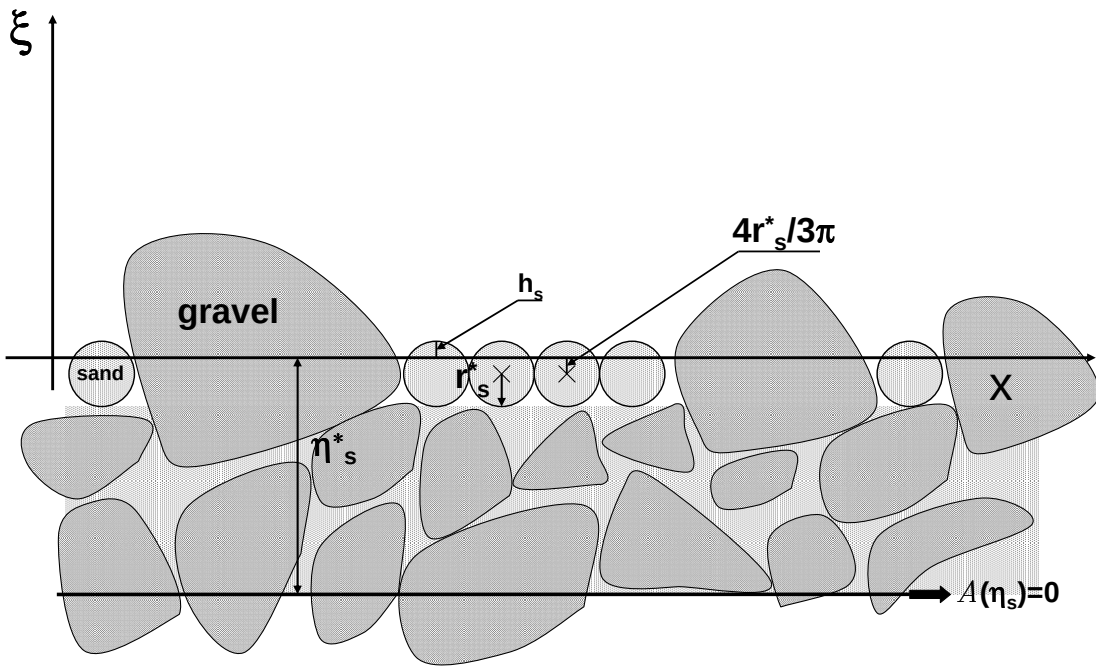

Figure 4.6: Sketch and notation for transformation of variables in (4.2)

Figure 3.2). Furthermore, we stipulate that the latter boundary is set at the reference level, the level at which conventionally and in the homogenous case (when sand elevation $\eta_s(x)$ completely buries the gravel, that is $\eta_s(x) = 1$) the mean logarithmic profile vanishes. For the heterogeneous case ($\eta_s(x) < 1$) and at the lower boundaries of the flow domain the mean logarithmic velocity is no longer zero, due to the effect of increased gravel roughness on the flow field as we can see later. The above system is solved with the boundary conditions of vanishing shear stress at the free surface and of velocity at the lower boundary, depending on the value of sand elevation $\eta_s(x)$.
The transformation of variables

$$\zeta = \frac{z - \eta_s(\chi)}{D(\chi)} = \frac{\xi}{D(\chi)} \tag{4.2}$$

$$\chi = x \tag{4.3}$$

is then employed in Eqs. 4.1, which maps the channel sketched in Figure 3.2 into a rectangular domain.

Referring to Figure 4.6, Eq.(4.2) represents dimensionless vertical coordinate for the entire flow domain. Since in the interfacial sublayer it has been assumed that the streamwise velocity profile is linear (*Nikora et al.* (2001)), consequently, at $z^* = \eta_s^*(x)$ (i.e. $\zeta = 0$) the spatially-averaged streamwise velocity is 0. Since $\eta_s^*(x)$ refers to spatially-averaged sand bed elevation, then $\eta_s^*(x)$ is located just above the center of the sand particles assumed as spheres, specifically spatially-averaged streamwise velocity is 0 at distance $h_s \approx d_s/6$ below of the top of the sand particles (see Figure 4.6).

4.2 Conceptual and mathematical formulation for the bed load sediment transport model

Referring to the Figure 2.24, we assumed that fine sediments move as bedload transport by small jumps (saltation) confined in a region close to the bed whose thickness is equal to ξ_b and defined as "bedload" layer. Above this layer we assumed clear water, inside this layer the shear stress drops according to the Eqs. 3.10 and 3.11. In alluvial or homogeneous configuration the reduction in the shear stress inside the bedload layer is due to the energy loss that has to be spent for the sediment transport, in the mixed configuration the energy flow loss is due to the drag forces applied on the contour of the rough elements in the bedload layer and to the flow energy spent for the sand transport. The energy loss for the drag forces is comparable larger than that for sediments transport because the ratio between the gravel diameters and sand diameters is larger than one. Consequently, the shear stress exerted by the fluid on the fines sediments in the bedload layer should be evaluated at the level ξ_b.
In order to compute the thickness of the bedload layer, and in the absence of any published experimental data on the case of an immobile gravel bed with a partial sand cover, we assume a formal analogy with the relationship proposed by *Colombini* (2004) where the dependence from the sand surface level and from the sand/gravel grain size ratio is accounted for through the computation of local (spatially-averaged) values of the near-bed and of the critical shear stress. Following *Colombini* (2004), the thickness of the bedload layer can be written in the following form:

$$h_b = d_s l_b = d_s \left\{ 1 + A_b \left(\frac{\tau_s - \tau_{rs}}{\tau_{rs}} \right)^m \right\}, \quad \tau_s \geq \tau_{rs} \tag{4.4}$$

where d_s is the dimensionless sand diameter, l_b dimensionless maximum saltation height and the value of the constant A_b and for the exponent m have been set equal to 1.3 and to 0.55 (*Colombini* (2004)). Figure 4.7 represents the curve (4.4) as interpolation curve of experimental data of maximum saltation height (see *Colombini* (2004) for references).
It is noteworthy that *Sekine and Kikkawa* (1992) pointed out that the concept of bedload layer thickness derived from the "averaged saltation height" as a measure of "maximum saltation height over an entire step length" l_b.
In Eq. 4.4 τ_s is the shear stress value at $\eta_s(x)$ level and the critical shear stress for sand fraction τ_{rs} is predicted by Eq. 2.54 where it has been reported the critical Shileds number for sand fraction.
The shear stress that acts on the sand particles τ_s at level η_s depends on the the sand

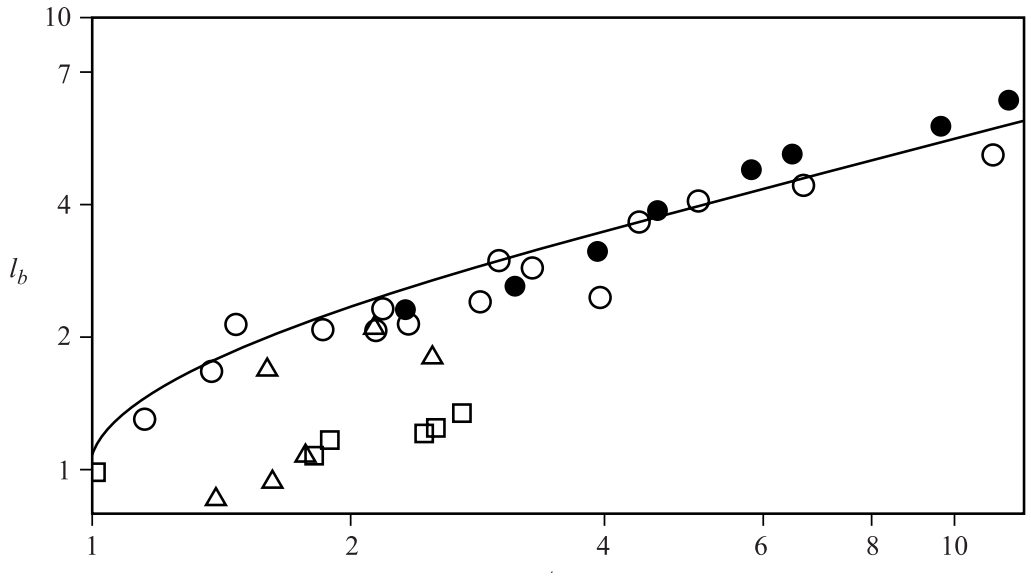

Figure 4.7: Dimensionless maximum saltation height l_b as a function of ratio τ_s^*/τ_c^* in homogeneous condition, i.e. only sand (from *Colombini* (2004)), where τ_c^* is the critical shear stress for incipient motion of the sand. The different points in figure represent experimental values of maximum saltation height (see *Colombini* (2004) for references)

elevation η_s itself as indicated by (2.65).
Accordingly to 4.2, the top level of the bedload layer ζ_b corresponds to :

$$\zeta_b = h_b - \frac{5}{6} d_s \tag{4.5}$$

Figure 4.8 represents the top and the bottom of the bedload layer in two different coordinate systems. In the x-z system B and R located the top and the bottom of the bedload layer, respectively. In the x-ζ system ζ_b and 0 represent, referring to the sand elevation η_s, the local level of the top and the bottom of the bedload layer, respectively. It is noteworthy that

The equation for sand particles mass conservation,neglecting $\partial\mathcal{A}/\partial\eta_s$ with respect to

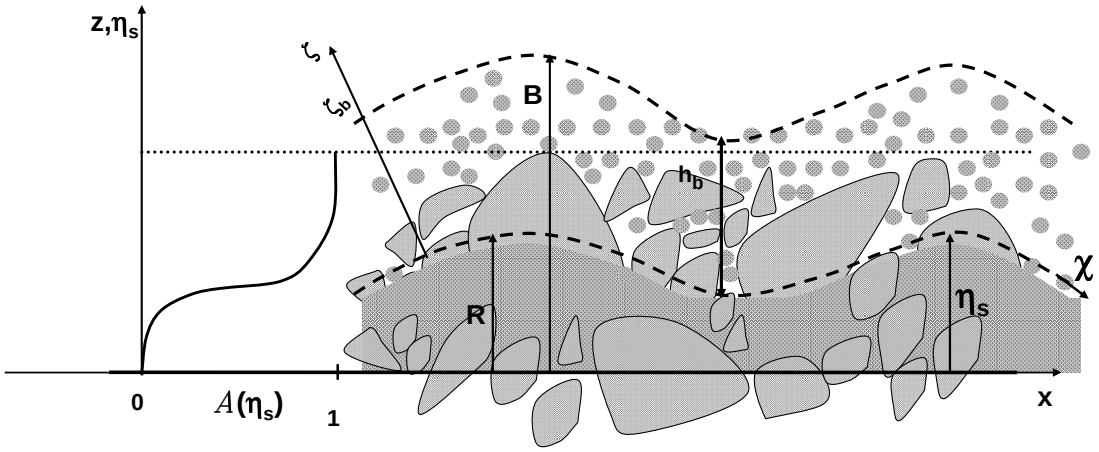

Figure 4.8: Sketch and notations for two different coordinate system: the x-ζ system refers to (4.2), the x-z system contains information on the position of the minimum value of the roughness geometry function $\mathcal{A}(\eta_s)$.

$\mathcal{A}$ as a first approximation, can be written as

$$\mathcal{A}(\eta_s)\eta_{s,t} = -\Phi_{s,x} \tag{4.6}$$

where

$$\Phi_s = \theta_s^{\frac{3}{2}}|_{\zeta_b}\mathcal{A}(\eta_s)W_{bs} \tag{4.7}$$

and $\theta_s|_B$ represents the Shields stress for sand fraction computed at B level (see Figure 4.8). The dimensionless sediment discharge per unit width Φ_s reads as:

$$\Phi_s = \frac{q_s^*}{d_s^*\sqrt{(s-1)gd_s^*}} \tag{4.8}$$

In the (4.7) it has been used, for the sand discharge per unit width in the "mixed" configuration W_{bs}, the relationship indicate by *Wilcock and Kenworthy* (2002) and reported in (2.76). The time in the Equation 4.6 has been made non-dimensional using the sediment

characteristic slow time scale

$$t = \frac{D^{*2}(1-p_s)}{d_s^*\sqrt{(s-1)gd_s^*}} \tag{4.9}$$

where g is the gravitational acceleration, p_s is the porosity of the sand fraction and s is the relative density.

4.3 Sand Bedforms stability:linear analysis

We now assume the following normal-mode representation for the generic perturbed property F:

$$F(\chi,\zeta,t) = F_0(\zeta) + \varepsilon F_1(\chi,\zeta,t), \tag{4.10}$$

$$F_1(\chi,\zeta,t) = f_1(\zeta)\exp[\mathrm{i}(\alpha\chi - \Omega t)] + c.c. \tag{4.11}$$

with the parameter ϵ chosen to be small in accordance with the assumption of small perturbations of the uniform configuration. In the above, α (i.e.$\alpha = \frac{2\pi}{\lambda/D}$)is the wavenumber of the perturbation, Ω the complex growth rate and *c.c.* stands for the complex conjugate of the preceding quantity. The above expansion can then be substituted into the governing equations, boundary conditions and closure assumptions to obtain a sequence of problems at the various orders of approximation in the small parameter ϵ.

4.3.1 $\boldsymbol{O}(\varepsilon^0)$

At leading order the system of differential equations and boundary conditions for the basic uniform flow can be rewritten as

$$T'_{t0} = -1, \qquad T'_{n0} = -i_f^{-1}, \tag{4.12}$$

$$U_0|_{\zeta=\zeta_c} = \widetilde{U_0}, \qquad T_{t0}|_{\zeta=1} = 0, \qquad T_{n0}|_{\zeta=1} = 0, \tag{4.13}$$

where

$$T_{t0} = \nu_{t0}U'_0, \qquad T_{n0} = -P_0 \tag{4.14}$$

are the stresses tangential and normal to surfaces at constant ζ respectively and primes denote differentiation with respect to ζ.

In the (4.13), $\widetilde{U_0}$ refers to (2.45), specifically:

$$\widetilde{U_0} = \widetilde{U_0}(\gamma_i, d_s, \eta_{s0}) \tag{4.15}$$

Linearizing the eddy viscosity reported in (3.8), the above system immediately integrates to yield for $\zeta \geq \zeta_c$:

$$U_0 = \frac{1}{k} ln \left(\frac{\zeta - 0.43\zeta_c}{\lambda_0} \right) \qquad P_0 = i_f^{-1}(1-\zeta) \tag{4.16}$$

where $0.43\zeta_c$ and λ_0 are the zero-plane displacement and the roughness length, respectively.

4.3.2 $\boldsymbol{O}(\varepsilon^1)$

It is convenient to introduce the new variables:

$$T_{t1} = \nu_{t0}(u_1' - U_0' d_1 + \mathrm{i}\alpha v_1 + \frac{\nu_t}{\nu_{t0}} U_0'), \qquad T_{n1} = -p_1 - 2\mathrm{i}\alpha\nu_{t0}u_1, \tag{4.17}$$

which represent the amplitudes of the perturbed stresses tangential and normal to surfaces at constant ζ, respectively. In the above u_1, v_1 are the longitudinal and vertical components of the perturbed velocity, while p_1 and d_1 are the amplitudes of the pressure and flow depth perturbation. The ratio $\frac{\nu_t}{\nu_{t0}}$ follows from 3.8 :

$$\frac{\nu_t}{\nu_{t0}} = (\frac{u_1'}{U_0'} + d_1 + \eta_{s1} C_1), \tag{4.18}$$

$$\begin{aligned} C_1 &= C_1(\chi, d_s, \gamma_i, \eta_{s0}), \\ \nu_{t0} &= \nu_{t0}(\chi, d_s, \gamma_i, \eta_{s0}), \end{aligned} \tag{4.19}$$

where the primes denote differentiation with respect to ζ , η_{s1} is the amplitude of perturbed sand level respect to η_{s0} and C_1 is an appropriate function that takes into account the geometrical information (i.e. the parameter γ_i) of the gravel matrix. After some manipulations, a system of ordinary differential equations is eventually obtained that can be written in the general form:

$$\mathcal{L}\mathbf{Z} = d_1\mathbf{D} + \eta_{s1}\mathbf{H} \tag{4.20}$$

where d_1 is considered as a parameter to be determined. The vector $\mathbf{Z}$ of the unknowns is:

$$\mathbf{Z} = (u_1, v_1, T_{t1}, T_{n1})^T \tag{4.21}$$

The linear differential operator $\mathcal{L}$ in (4.20) is:

$$\mathcal{L} = \begin{pmatrix} d/d\zeta & \mathrm{i}\alpha/2 & -1/(2\nu_{t0}) & 0 \\ \mathrm{i}\alpha & d/d\zeta & 0 & 0 \\ -\mathrm{i}\alpha U_0 - 4\alpha^2\nu_{t0} & -U_0' & d/d\zeta & \mathrm{i}\alpha \\ 0 & -\mathrm{i}\alpha U_0 & \mathrm{i}\alpha & d/d\zeta \end{pmatrix}$$

while the vectors $\mathbf{D}$ and $\mathbf{H}$ are, respectively,

$$\mathbf{D} = \begin{pmatrix} 0 \\ \mathrm{i}\alpha U_0'\zeta \\ (-\mathrm{i}\alpha U_0 U_0' + \mathrm{i}\alpha i_f^{-1} - 2\alpha^2(1-\zeta))\zeta - 1 \\ i_f^{-1} + \mathrm{i}\alpha\zeta - 2\mathrm{i}\alpha(1-\zeta) \end{pmatrix}$$

$$\mathbf{H} = \begin{pmatrix} 0 \\ \mathrm{i}\alpha U_0' \\ -\mathrm{i}\alpha U_0 U_0' + \mathrm{i}\alpha i_f^{-1} - 2\alpha^2(1-\zeta) \\ \mathrm{i}\alpha \end{pmatrix}$$

Linearization of the boundary conditions yields for reference level (ζ=ζ_c):

$$u_1(\zeta_c) = B_u(\eta_{s0}, d_s)\eta_{s1}, \qquad v_1(\zeta_c) = 0, \tag{4.22}$$

where the prime denotes differentiation with respect to ζ and B_u is an appropriate function. At the free surface (ζ=1) we have:

$$v_1(1) = \mathrm{i}\alpha U_0(d_1 + \eta_{s1}), \qquad T_{t1}(1) = 0, \qquad T_{n1}(1) = 0 \tag{4.23}$$

Linearity of the differential system allows us to express its solution in the form

$$\mathbf{Z} = c_1\mathbf{Z}_1 + c_2\mathbf{Z}_2 + d_1\mathbf{Z}_{d1} + \eta_{s1}\mathbf{Z}_{\eta s1} \tag{4.24}$$

Thus $\mathbf{Z}$ is a linear combination of two linearly independent solutions of the homogeneous initial value problem

$$\mathcal{L}\mathbf{Z}_{1,2} = 0 \tag{4.25}$$

each satisfying the boundary conditions at the lower boundary, plus particular solutions of the non-homogeneous differential systems

$$\mathcal{L}\mathbf{Z}_{d1} = \mathbf{D} \qquad \mathcal{L}\mathbf{Z}_{\eta s1} = \mathbf{H}, \tag{4.26}$$

again satisfying the lower boundary conditions. Using the splitting (4.24) on the boundary conditions at the free surface (4.23) , a linear 3×3 non-homogeneous algebraic system in the three unknowns c_1, c_2 and d_1 is found, the solution of which is proportional to η_{s1}. We then readily obtain

$$(c_1, c_2, d_1, \eta_{s1})^T = \eta_{s1}(T_{tr}, T_{nr}, D, 1)^T = \eta_{s1}\mathbf{X} \tag{4.27}$$

where the two linearly independent solutions of the homogeneous problem (4.25) have been chosen so that the unknowns c_1 and c_2 are the values of the perturbation of the tangential and normal stress at the reference level, respectively. The vector $\mathbf{X}$ thus provides the 'forced' response of the flow to a unit reference level perturbation. Linearization of the sand sediment continuity equation yields the following equation:

$$\Omega\eta_{s1} = \alpha\phi \tag{4.28}$$

In the Eq.(4.28) it has been assumed that the amplitude of the perturbation η_{s1} is identical to the amplitude of the perturbation for the top of bedload layer b_1 where it has been assumed to compute the shear stress responsible for the sand transport.
The amplitude ϕ of the perturbation of the bedload discharge Φ defined by 4.7 can be expanded as in 4.24, leading to

$$\phi = \phi_1 c_1 + \phi_2 c_2 + \phi_d d_1 + \phi_{\eta s1}\eta_{s1} = \phi \cdot (c_1, c_2, d_1, \eta_{s1})^T = \phi \cdot Xr \tag{4.29}$$

where

$$\phi_1 = \left[\frac{\partial \Phi}{\partial c_1}\right]_0 = \left[\frac{\partial \Phi}{\partial \theta_{b1}}\frac{\partial \theta_{b1}}{\partial c_1} + \frac{\partial \Phi}{\partial \theta_{rs}}\frac{\partial \theta_{rs}}{\partial c_1}\right]_0 = \left[A_{\Phi b}\frac{\partial \theta_{b1}}{\partial c_1} + A_{\Phi_{rs}}\frac{\partial \theta_{rs}}{\partial c_1}\right]_0 \tag{4.30}$$

where θ_{rs} is the critical Shields stress for sand fraction (*Wilcock and Kenworthy* (2002)), the suffix 0 stands for 'evaluated at base flow condition'and

$$\frac{\partial \theta_{rs}}{\partial c_1} = \frac{\partial \theta_{rs}}{\partial \mathcal{A}_1}\frac{\partial \mathcal{A}_1}{\partial c_1} \qquad A_{\Phi_{b1}} = \frac{\partial \Phi}{\partial \theta_{b1}} \qquad A_{\Phi_{rs}} = \frac{\partial \Phi}{\partial \theta_{rs}} \tag{4.31}$$

Analogous relationships hold for ϕ_2, ϕ_{d1} and $\phi_{\eta s1}$. In 4.31, $\mathcal{A}_1$ represents the approximation of the "roughness geometry function" $\mathcal{A}$ at the ε order of the solution. Expanding also the perturbed shear stress T_{tb1} in (4.30) as in (4.24) we then readily obtain

$$\phi = A_\phi(T_{tb1}, T_{tb2}, T_{tbd_1} + \zeta_b, T_{tb\eta_{s1}}) + B_\phi(0, 0, 0, \frac{\partial \theta_{rs}}{\partial \mathcal{A}_1}\frac{\partial \mathcal{A}_1}{\partial z_{s1}}) \tag{4.32}$$

In the above equation ζ_b refers to (4.5), having assumed that $\eta_{s1} = b_1$.
Moreover, T_{tb1}, T_{tb2}, T_{tbd_1} and $T_{tb\eta_{s1}}$ are evaluated at ζ_b and

$$A_\phi = [A_{\Phi b1}]_0\,\theta_{r_0} \qquad B_\phi = [A_{\Phi rs}]_0 \tag{4.33}$$

where

$$\theta_{r_0} = \frac{i_f}{(s-1)d_s} \tag{4.34}$$

Making use of (4.29) and (4.32), we can rewrite (4.28), obtaining the dispersion relationship

$$\Omega = \alpha\phi \cdot X \tag{4.35}$$

and solving for the imaginary part of the growth rate we finally obtain:

$$\Omega^i = \alpha[A_\phi(T^i_{tb} + \zeta_b D^i) + B_\phi\frac{\partial \theta_{rs}}{\partial \mathcal{A}_1}\frac{\partial \mathcal{A}_1}{\partial \eta_{s1}}] \tag{4.36}$$

The above equation indicates the instability is related to a balance between destabilizing and stabilizing effects. Specifically, the second term, which is associated with the derivative of θ_{rs} with η_{s1}, when negative acts to reduce the instability.

4.4 Discussion of the results

Figure 4.9 represents marginal curves (vanishing growth rate Ω^i) in two configurations: the homogeneous case when sand completely buries the gravel matrix (i.e. η_s=1) indicated in figure as solid blue line and the mixed case ($0 \leq \eta_s <1$) indicate in figure in red solid line for differen values of η_s.In the homogeneous configuration (i.e. panel a) Figure 4.9) two region of instability appear which are bounded by the marginal curves. Specifically, the upper region refers to sand antidunes, the lower one refers to the dunes instability. Referring to the homogenous case, *Colombini* (2004) found a good agreement with experimental data, in fact almost the whole set of measurements fall inside the appropriate region of instability. The marginal curve in the mixed case reports a tendency with the decreasing of the sand content in the gravel matrix. Specifically, at the same Froude number, the less the sand elevation is, the bigger the wavenumber is . This tendency was also pointed out by *Tuijnder et al.* (2009)'s experimental work, in fact Figure (4.3) shows that when the average sand volume represented by the parameter d decreases, then also the sand wavelength decreases, i.e. the sand wavenumber increases. It is noteworthy that with the notations sketched in Figure (4.1), the parameter d is computed above the level at which $\mathcal{A}(\eta_s) = 1$, nonetheless the sand dunes observed by *Tuijnder et al.* (2009) interact with the gravel matrix as indicated by sand dune height Δ in Figure (4.2).
Figure 4.10 and 4.11 remark the different behavior in term of growth rate Ω^i for the two different configurations (i.e. homogeneous and mixed case) for two specified Froude number: Fr=1.2 for Figure 4.10 and Fr=0.6 for Figure 4.11. Moreover, the sand level η_s controls the extent of the instability region of the perturbation, in fact in the mixed case when the sand level decrease, the sand bed instability appears also for Froude number greater then the homogeneous case.

Figure 4.12 shows the behaviour of the imaginary part of the perturbation of the tangential shear stress in a neighbourhood of the reference level R (see Figure 4.8) for the two specified Froude value indicated above. The vertical coordinate is scaled by the thickness of the bed load layer ζ_b and wavenumber is set equal to 1. The imaginary component of the shear stress is associated with the growth or decay of the perturbation as indicated by (4.36).It is noteworthy that in the homogeneous condition disturbances that are stable at reference level R, become unstable at the top of the bedload layer. In the mixed case the variability of the instability behaviour of the perturbation is more complex due to the sand elevation η_s that appears to control the stability of the perturbation.

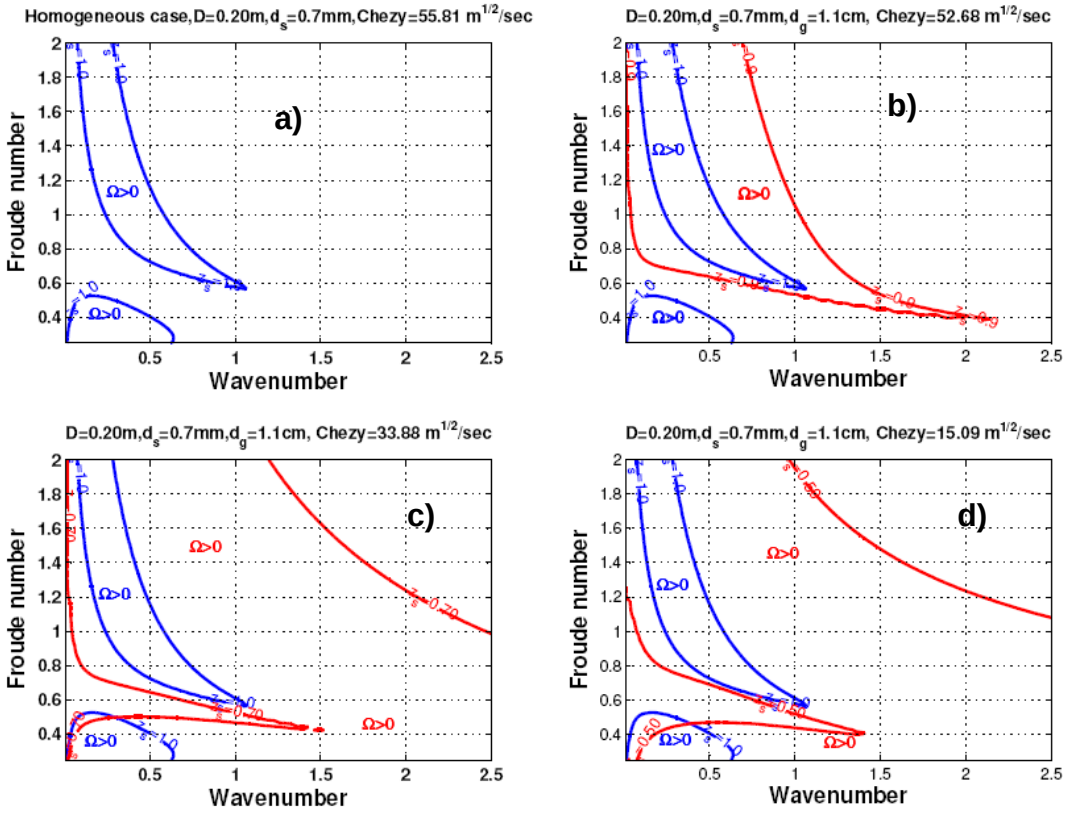

Figure 4.9: Growth rate plot for homogeneous case (blue solid line) and for mixed case (red solid line) with different sand bed elevation. Panel a) refers to homogeneous condition and with specific hydraulics conditions: water depth D=0.20 cm, d_s=0.7 mm, Chezy=C=55.81 $m^{1/2}/s$. Panel b),c),d) show both case when sand bed elevation is $\eta_s = 0.9$,$\eta_s = 0.7$ and $\eta_s = 0.5$, respectively. The specified hydraulics conditions for each case are reported above each panel.

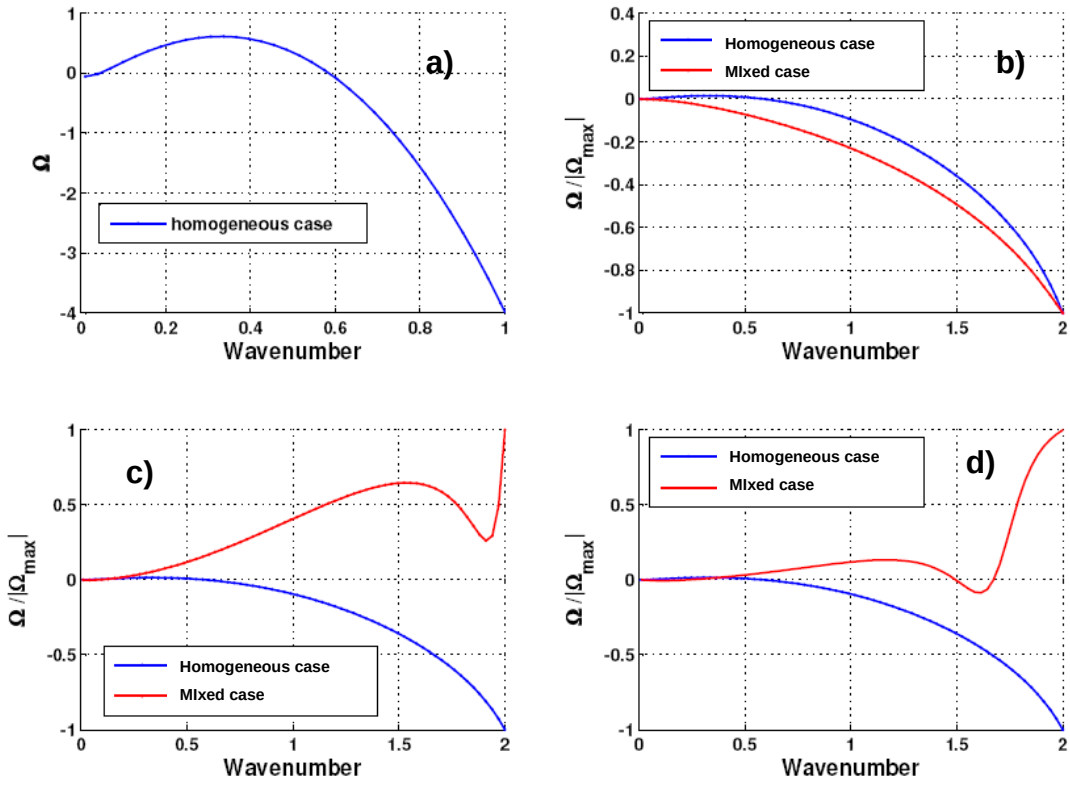

Figure 4.10: Dimensionless grow rate plot for homogeneous case (blue solid line) and for mixed case (red solid line) with different sand bed elevation and with specified Froude number equals to 1.2.Panel b),c),d) show both case when sand bed elevation is $\eta_s = 0.9$,$\eta_s = 0.7$ and $\eta_s = 0.5$, respectively. The specified hydraulics conditions are the same indicated in Figure 4.9 for each panel.

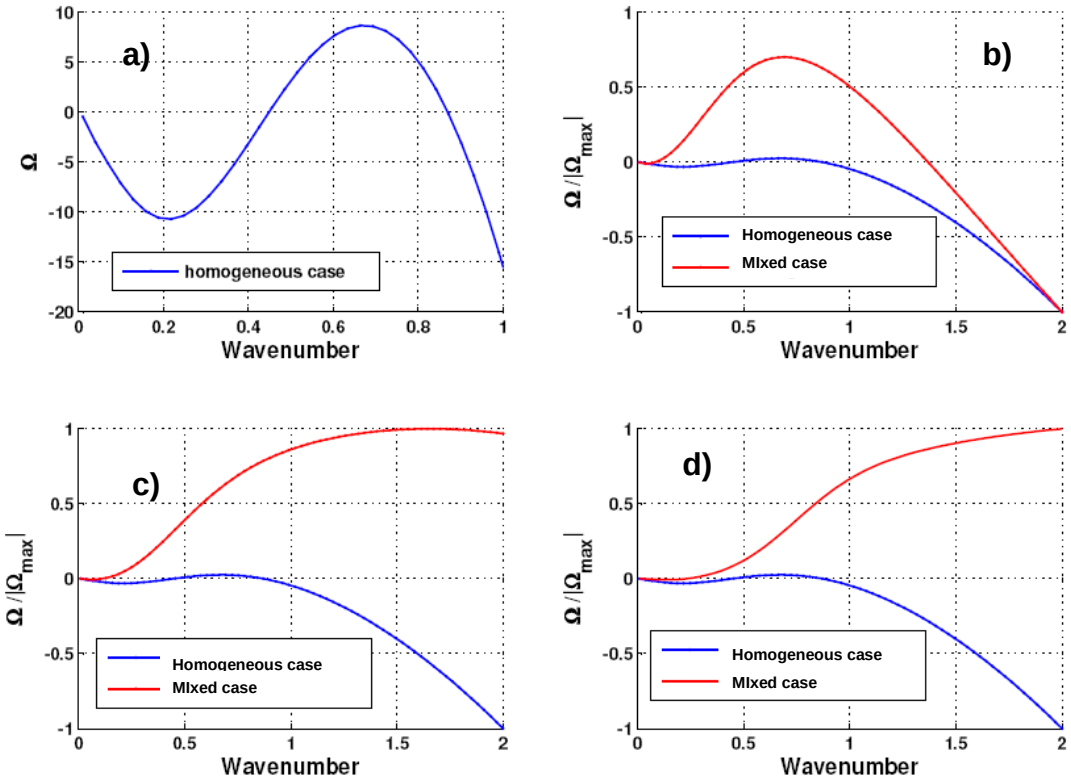

Figure 4.11: Dimensionless grow rate plot for homogeneous case (blue solid line) and for mixed case (red solid line) with different sand bed elevation and with specified Froude number equals to 0.6.Panel b),c),d) show both case when sand bed elevation is $\eta_s = 0.9$,$\eta_s = 0.7$ and $\eta_s = 0.5$, respectively. The specified hydraulics conditions are the same indicated in Figure 4.9 for each panel.

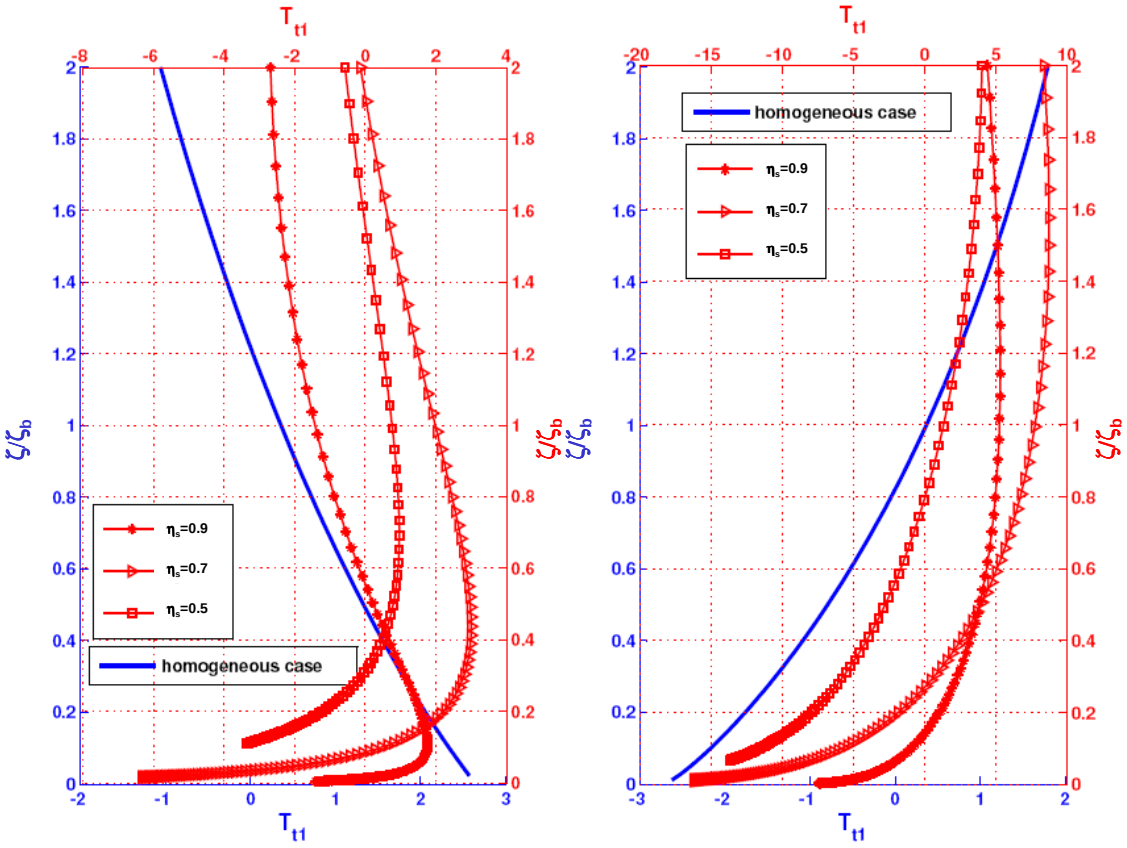

Figure 4.12: Imaginary parts of the amplitude of the shear stress perturbation as a function of vertical distance in the neighbourhood of the reference level R for two different specified Froude number: the left panel refers to Fr=0.6, the right one refers to Fr=1.2.

5 Conclusions and perspectives

The transport of fine sediments over immobile gravel beds is a key and yet relatively unexplored process of many coarse-bed river systems with strong management and ecological implications.
The present study has addresses the dynamics of fine sediment transport in gravel-bed rivers, with the aim to propose a morphodynamic modelling approach for sand transport over a gravel bed that is assumed at rest. The following research questions have been addressed:

- Which are the key physical processes associated with near bed turbulence properties over rough beds, and how do they change when sand is present in variable proportion within the gravel bed? (Chapter 2)
- Which can be an appropriate form of a mathematical model for sand beform dynamics over immobile gravel? How do the continuity and momentum equations, as well as the closure relationships for friction and bedload transport change when the gravel bed is partially sand-covered? (Chapter 3)
- Which are the implications of such model when solved in the form of a stability analysis that aims to predict the conditions for sand bedform stability and preferred wavelength selection over an immobile gravel bed? (Chapter 4)

First, a theoretical approach is developed to the most relevant processes that determine the properties of near-bed turbulent flow and of sand transport when a rough gravel bed is partially covered with sand. This has lead to propose physically-based closure relationships for friction and bedload transport, which are key ingredients, although still to be improved, for a morphodynamic model of sand bedform evolution over immobile gravel beds. The theoretical analysis has been developed at three levels. After reviewing the spatial averaging approach, which underlies all the present work, the geometrical properties of a rough gravel bed have been reviewed and the implications associated with the presence of a sand cover with variable height have been discussed. Second, the near-bed

hydrodynamic properties relevant for sediment transport over rough beds in general have been reviewed and a novel theoretical approach is proposed to account for the effect of a variable sand cover on the near-bed shear stress and related spatially averaged turbulence properties. Third, the implications of varying sand surface level for threshold condition for sand bedload motion as well as for the rate of bedload transport have been discussed and existing relationships, derived on an empirical basis, are integrated within the proposed theoretical approach.

The theoretical approach is based on (i) a two-fraction assumption for the bed composition (sand and gravel) and (ii) a spatially-averaged description of bed roughness geometry, near bed turbulence properties and closure relationships for bedload and suspended load. The reach-averaged sand surface elevation and the relative size ratio between the sand and gravel diameter emerge as the key parameters that distinguish between different types of mixed bed configurations. A key distinction can be made between "gravel-clast framework" and "sand matrix" types of bed; these configurations are discriminated by a relatively sharp transition region in the sand surface elevation. Moreover, the near-bed shear stress and bedload transport of sand depend on a dynamic balance between a "hiding" and a "bridge" effect, which in turn are related to the sand surface level and to the grain size ratio between the two fractions. Application to spatially-averaged uniform flow conditions shows satisfactory agreement with the few available experimental data and has allowed to make a preliminary quantifcation of the effect of the two key parameters describing different types of mixed bed configuration. The limits of validity of the model have been also discussed.

A morphodynamic model that can be used to predict the temporal and spatial evolution of a sand layer that partially or completely fills the voids beneath an immobile gravel bed has been then formulated. The mathematical formulation is two-dimensional, in the streamwise (x) and in the average bed orthogonal (z) directions. Moreover it is spatially-averaged, therefore "local" values of flow quantities and of the sand bed elevation actually represent double-averaged quantities resulting from time averaging and from spatial averaging, performed at the scale comparable to the d_{90} of the gravel grain size distribution. A vertical subdivision of flow into specific layers has been adopted for the formulation of the morphodynamic model. The key ingredients of the model are:

- the momentum conservation equations for the fluid phase in the x and z directions;
- the mass conservation equations for the fluid phase;
- the mass conservation equations for the sand layer within an immobile gravel bed;
- a closure relationship to link the double-averaged Reynolds stresses to the double-averaged flow field;

- a closure relationship to link the double-averaged bedload rate to the double-averaged flow field.

Momentum and mass conservation equations for the fluid phase will be formulated referring to the physical balances formally valid only within the logarithmic layer. The physical processes governing the hydrodynamics within the roughness layer and its sublayers are indirectly taken into account according to the closure relationships proposed above. The novel formulation of the sediment continuity equation reveal an intrinsic nonlinearity in the time-derivative term and is able to reproduce the experimentally observed reduction in the morphodynamical time scale at increasing levels of sand supply limitation.

The morphodynamic model has been finally used to predict the sand bed morphodynamics under supply-limited conditions. The sand surface elevation is a measure of the sediment supply-limitation that crucially controls the sand bedform development. The model has been solved through a linear stability analysis that incorporates recent developments in the theoretical study of sand dune stability in homogeneous conditions. The theoretical outcomes have allowed to focus on the physical phenomena controlling the development of sand bedforms when sand is transported over an immobile gravel bed and to determine the hydraulic conditions under which sand dunes formation can be expected to develop within immobile gravel beds. Results also indicate a consistent effect of supply limitation to extend the instability region towards shorter bedforms, as observed by recent experimental investigations.

The present theoretical work shall be considered as a first step in the attempt of developing a comprehensive morphodynamic modelling framework for the sand fraction over immobile gravel beds. Some of the most relevant related issues that will deserve attention in future research are listed below.

1. There's the need of a direct experimental testing of the physically-based relationships that have been proposed to link the near-bed turbulence properties with the sand surface level and the sand-gravel grain size ratio. This will require detail measurements of turbulence properties with high vertical and horizontal resolution in the vicinity of the rough bed.

2. Relatively few experimental observations are available on the geometry of sand supply-limited dunes. It would be important that the valuable dataset of *Tuijnder* (2010) could be extended to assess the effect of different sand/gravel grain size ratios on the stability properties of the sand dunes.

3. The stability analysis proposed in the present research work to study the stability of supply-limited sand dunes is linear, and as such it cannot be used to predict any

information related to the time evolution and to the finite-amplitude geometry of the sand bedforms. An extension of the present theoretical work would be desirable in the weakly nonlinear regime, following the approach of *Colombini and Stocchino* (2008) under homogeneous sand conditions.

References

Aberle, J., and V. Nikora (2006), Statistical properties of armored gravel bed surfaces, *Water Resour. Res.*, *42*(11), doi:10.1029/2005WR004674.

Aberle, J., K. Koll, and A. Dittrich (2008), Form induced stresses over rough gravel-beds, *Acta Geophysica*, *56*, 584–600, 10.2478/s11600-008-0018-x.

ASCE (2002), Flow and transport over dunes, *J. Hydr. Engrg.*, *128*(8), 726–728, Task committee on flow and transport over dunes.

Bagnold, R. A. (1956), The flow of cohesionless grains in fluids, *Philosophical Transactions of the Royal Society of London. Series A, Mathematical and Physical Sciences*, *249*(964).

Beschta, R., and W. Jackson (1979), The intrusion of fine sediment into a stable gravel bed, *Journal Fis. Res. Board Can.*, *36*, 204–210.

Buffin-Bélanger, T., S. Rice, I. Reid, and J. Lancaster (2006), Spatial heterogeneity of near-bed hydraulics above a patch of river gravel, *Water Resour. Res.*, *42*(4), W04,413–, doi:10.1029/2005WR004070.

Buffington, J., and D. Montgomery (1999), Effects of sediment supply on surface textures of gravel-bed rivers, *Water Resour. Res.*, *35*(11), 3523–3530, doi:10.1029/1999WR900232.

Buffington, J., W. Dietrich, and J. Kirchner (1992), Friction angle measurements on a naturally formed gravel streambed: Implications for critical boundary shear stress, *Water Resour. Res.*, *28*(2), 411–425, doi:10.1029/91WR02529.

Carling, D. (1984), Deposition of fine and coarse sand in open-work gravel bed, *Can. J. Fish. Aquatic Sci.*, *41*, 263–270.

Carling, P., and R. Breakspear (2006), Placer formation in gravel-bedded rivers: A review, *Ore Geology Reviews*, *28*, 377–401.

Carling, P., and N. Reader (1982), Structure, composition and bulk properties of upland stream gravels, *Earth Surf. Process. Landforms*, *7*(4), 349–365.

Coleman, S., and J. Fenton (2000), Potential−flow instability theory and alluvial stream bed forms, *Journal of Fluid Mechanics*, *418*, 101–117.

Coleman, S., and V. Nikora (2008), A unifying framework for particle entrainment, *Water Resour. Res.*, *44*(4), W04,415–.

Colombini, M. (2004), Revisiting the linear theory of sand dune formation, *J.Fluid Mech*, *502*, 1–16.

Colombini, M., and A. Stocchino (2008), Finite-amplitude river dunes, *Journal of Fluid Mechanics*, *611*, 283–306, doi:10.1017/S0022112008002814.

Cui, Y., J. Wooster, P. Baker, S. Dusterhoff, S. Sklar, and W. Dietrich (2008), Theory of fine sediment infiltration into an immobile gravel bed, *J. of Hydr. Eng. ASCE*, *134*(10).

Diplas, P., and G. Parker (1992), *Deposition and removal of fines in gravel*, in: P. Billi, R. D. Hey, C. R. Thome, and P. Tacconi (eds.),Dynamics of gravel-bed rivers. J. Wiley & Sons, Ltd.Chichester, U.K.

Einstein, H. (1968), Deposition of suspended particles in a gravel bed, *Journal of Hydraulics Division, ASCEE*, *94*(HY5), 1197 – 1205.

Exner, F. M. (1925), Uber die Wechselwirkung zwischen Wasser und Geschiebe in Flüssen, *Sitzungsber. Akad. Wiss. Wien Abt. IIa*, (134), 166 – 204.

Franca, M. J., R. M. Ferreira, and U. Lemmin (2008), Parameterization of the logarithmic layer of double-averaged streamwise velocity profiles in gravel-bed river flows, *Advances in Water Resources*, *31*(6), 915 – 925, doi:DOI: 10.1016/j.advwatres.2008.03.001.

Fredsøe, J. (1974), On the development of dunes in erodible channels, *Journal of Fluid Mechanics*, *64*(01), 1–16.

Garcia, M., and G. Parker (1991), Entrainment of bed sediment into suspension, *J. Hydraul. Eng. ASCE*, *117*(4), 414– 435.

Gradowczyk, M. H. (1968), Wave propagation and boundary instability in erodible-bed channels, *Journal of Fluid Mechanics*, *33*(01), 93–112.

Grams, P. (2006), Sand transport over a coarse and immobile bed, Ph.D. thesis, Johns Hopkins University, 163 pp.

Grams, P., and P. Wilcock (2007), Equilibrium entrainment of fine sediment over a coarse immobile bed, *Water Resour. Res.*, *43*.

Hesse, L., and W. Sheets (1993), The missouri river hydrosystem, *Fisheries*, *18*(5), 5–14.

Jackson, P. (1981), On the displacement height in the logarithmic velocity profile, *Journal of Fluid Mechanics*, *111*, 15–25, doi:10.1017/S0022112081002279.

Jerolmack, D. J., and D. Mohrig (2005), A unified model for subaqueous bed form dynamics, *Water Resour. Res*, (41), W12,421.

Jiménez, J. (2004), Turbulent flows over rough walls, *Annual Review of Fluid Mechanics*, *36*(1), 173–196, doi:10.1146/annurev.fluid.36.050802.122103.

Jobson, H., and W. Carey (1989), Interaction of fine sediment with alluvial streambeds, *Water Resour. Res.*, *25*(1), 135–140.

Johnston, C., E. Andrews, and J. Pitlick (1996), In situ determination of particle friction angles of fluvial gravels, *Water Res. Research*, *34*(8), 2017–2030.

Kennedy, J. F. (1963), The mechanics of dunes and antidunes in erodible-bed channels, *Journal of Fluid Mechanics*, *16*(04), 521–544.

Kirchner, J. W., W. Dietrich, F. Iseya, and H. Ikeda (1990), The variability of critical shear stress, friction angle, and grain protrusion in water-worked sediments, *Sedimentology*, *37*(4), 647–672.

Kleinhans, M., A. Wilbers, A. De Swaaf, and J. Van Den Berg (2002), Sediment supply-limited bedforms in sand-gravel bed rivers, *J. Sed. Res.*, *75*(5), 629–640.

Kondolf, G., and P. Wilcock (1996), The flushing flow problem: Defining and evaluating objectives, *Water Res. Research*, *32*(8), 2589–2599.

Koski, K. (1966), The survival of coho salmon egg deposition to emerge in three oregon coastal streams, Master's thesis, Oregon State University, Corvallis, OR, USA.

Lisle, T., and S. Hilton (1991), Fine sediment in pools: an index of how sediment is affecting a stream channel.R-5 fish habitat relat. tech. bull., *Tech. Rep. 6*, USDA Forest Service Pacific southwest Region.

Mignot, E., E. Barthelemy, and D. Hurter (2008), Double-averaging analysis and local flow characterisation of near-bed turbulence in gravel-bed channel flow, *J.Fluid Mech.*, *618*, 279–303.

Mignot, E., E. Barthelemy, and D. Hurter (2008a), Turbulent kinetic energy budget in a gravel-bed channel flow, *Acta Geophysica*, *56*(3), 601–613.

Nezu, I., and H. Nakagawa (1993), *Turbulence in open-channel flows*, IAHR Monograph Series, A.A.Balkema.

Nikora, V. (2008), Hydrodynamics of gravel-bed rivers:scale issue, in *Gravel-Bed Rivers VI:From Process Understanding to River Restoration*, edited by H. Habersack, H. Piégay, and M. Rinaldi, Elsevier B.V.

Nikora, V., D. Goring, and B. Biggs (1998), On gravel-bed roughness characterisation, *Water Resour. Res.*, *34*(3), 517–527.

Nikora, V., D. Goring, I. McEwan, and G. Griffiths (2001), Spatially averaged open-channel flow over rough bed, *J. Hydr. Eng. ASCE*, *127*(2), 123–133.

Nikora, V., K. Koll, S. McLean, A. Dittrich, and J. Aberle (2002), Zero-plane displacement for rough-bed open-channel flows, in *Proceedings of the international conference on fluvial hydraulics, River Flow 2002*, vol. 1, edited by D. Bousmar and Y. Zech, A.A. Balkema Publishers.

Nikora, V., K. Koll, I. McEwan, S. McLean, and A. Dittrich (2004), Velocity distribution in the roughness layer of rough-bed flows, *J. Hydr. Eng. ASCE*, *130*(10), 1036–1042, doi 10.1061/(ASCE)0733-9429(2004)130:10(1036).

Nikora, V., I. McEwan, S. McLean, S. Coleman, D. Pokrajac, and R. Walters (2007a), Double-averaging concept for rough-bed open-channel and overland flows: Theoretical bachground, *J. Hydr. Eng. ASCE*, *133*(8), 873–883.

Nikora, V., S. McLean, S. Coleman, D. Pokrajac, I. McEwan, L. Campbell, J. Aberle, D. Clunie, and K. Koll (2007b), Double-averaging concept for rough-bed open-channel and overland flows: Applications, *J. Hydr. Eng. ASCE*, *133*(8), 884–895, doi 10.1061/(ASCE)0733-9429(2007)133:8(884).

Parker, G., and A. Anderson (1977), Basic principles of river hydraulics, *J. Hydraul. Div. Am. Soc.Civ.Eng.*, *103*(9), 1077–1087.

Petticrew, E., A. Krein, and D. Walling (2007), Evaluating fine sediment mobilization and storage in a gravel-bed river using controlled resevoir releases, *Hydrological Processes*, *21*, 198–210.

Poggi, D., A. Porporato, L. Ridolfi, J. Albertson, and G. Katul (2004), The effect of vegetation density on canopy sub-layer turbulence, *Boundary-Layer Meteorology*, *111*(3), 565–587.

Schälchli, U. (1992), The clogging of coarse gravel river beds by fine sediment, *Hydrobiologia*, *235/236*, 189–197.

Sekine, M., and H. Kikkawa (1992), Mechanics of saltating grains, *J. Hydraulic Eng.*, *118*, 536–558.

Seminara, G., L. Solari, and G. Parker (2002), Bed load at low shields stress on arbitrarily sloping beds: Failure of the bagnold hypothesis, *Water Resour. Res.*, *38*(11), 1249.

Tuijnder, A. (2010), Sand in short supply - Modelling of bedforms, roughness and sediment transport in rivers under supply-limited conditions, Ph.D. thesis, University of Twente,the Netherlands, 148 pp.

Tuijnder, A., J. Ribberink, and S. Hulscher (2009), An experimental study into the geometry of supply-limited dunes, *Sedimentology*, *56*(6), 1713–1727.

Weigelhofer, G., and J. Waringer (2003), Vertical distribution of benthic macroinvertebrates in riffles versus deep runs with differing contents of fine sediments (weidlingbach, austria), *Int. Review of Hydrobiology*, *88*(3-4), 304–313.

Wentworth, C. (1922), A scale of grade and class terms for clastic sediments, *The Journal of Geology*, *30*(5), 377–392.

Whitaker, S. (1999), *The method of volume averaging*, vol. 13, Kluwer Academic Publishers.

Wilcock, P. (1998), Two-fraction model of initial sediment motion in gravel-bed rivers, *Science*, *280*(5362), 410 – 412.

Wilcock, P., and S. Kenworthy (2002), A two-fraction model for the transport of sand/gravel mixtures, *Water Res. Res.*, *38*(10), doi:10.1029/2001WR000684.

Wooster, J., S. Dusterhoff, Y. Cui, L. Sklar, W. Dietrich, and M. Malko (2008), Sediment supply and relative size distribution effects on fine sediment infiltration into immobile gravels, *Water Res. Res.*, *44*.

Wren, D., E. Langendoen, and R. Kuhnle (2011), Effects of sand addition on turbulent flow over an immobile gravel bed, *J. Geophys. Res.-Earth Surface*, *116*, F01,018, doi:10.1029/2010JF001859.

Yager, E. M., J. W. Kirchner, and W. E. Dietrich (2007), Calculating bed load transport in steep boulder bed channels, *Water Resour. Res.*, (43), W07,418.